

ESTIMATING REGIONAL REFERENCE
EVAPOTRANSPIRATION FROM MESO-RESOLUTION
ZERO-DIMENSIONAL METEOROLOGICAL DATA

By

OI-MING DANIEL YUEN

Bachelor of Science

Bemidji State University

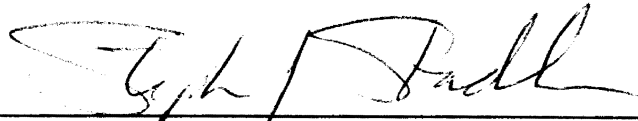
Bemidji, Minnesota

1991

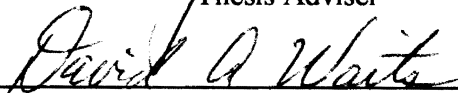
Submitted to the Faculty of the
Graduate College of the
Oklahoma State University
in partial fulfillment of
the requirements for
the Degree of
MASTER OF SCIENCE
December, 1994

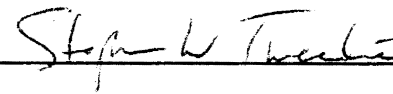
ESTIMATING REGIONAL REFERENCE
EVAPOTRANSPIRATION FROM MESO-RESOLUTION
ZERO-DIMENSIONAL METEOROLOGICAL DATA

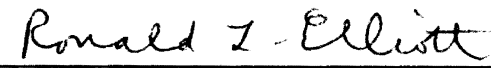
Thesis Approved:



Thesis Adviser









Dean of the Graduate College

ACKNOWLEDGEMENTS

I wish to express my sincere appreciation to my major advisor, Dr. Stephen Stadler for his intelligent supervision, constructive guidance, inspiration and friendship. My sincere appreciation extends to my other committee members Dr. Ronald Elliott, Dr. Stephen Tweddle, and Dr. David Waits, whose guidance, assistance, encouragement, and friendship are also invaluable. I would like to thank the Department of Geography, the National Science Foundation, and State of Oklahoma EPSCoR funds for providing me with this research opportunity and their financial support.

Moreover, I wish to express my sincere gratitude to those who provided suggestions and assistance for this study: Dr. Michael Kizer and Dr. Mark Payton. My sincere gratitude extends to Dr. Michael Garrett, Dr. Charles Parsons, and my fellow students for their encouragement and friendship.

I would also like to give my thanks to my grandmother, my parents and other family members for their support and encouragement. I would like to give my special appreciation to my fiancée, Man-ling, for her encouragement at times of difficulty, love and understanding throughout this whole process.

Last but not least, I would like to thank the Department of Geography for support during these two years of study.

TABLE OF CONTENTS

Chapter	Page
I. INTRODUCTION	1
The Statement of Purpose	3
II. LITERATURE REVIEW	5
Properties of Space	5
Methods of Interpolation	7
Properties of Interpolation Methods	7
Approximate Methods	10
Exact Methods	13
Kriging	16
Evapotranspiration Estimation	26
Hydrologic Cycle and Evapotranspiration	26
Estimation of Evapotranspiration	30
Combination Method	34
Problems of the Combination Method	40
Meteorological Data	40
Oklahoma Mesonetnetwork	41
Conclusions	44
III. METHOD	46
Design	46
Objectives	46
Study Area	47
Map Projection	48
Study Dates	50
Units of Measurement	51
Spatial and Temporal Resolution	51
Equipment and Tools	52
Procedures	55
Preparing Daily Meteorological Data	55
Estimating Alfalfa-Reference Evapotranspiration	58
Interpolating Zero-Dimensional Data to a Surface	58
Preparing Data for Statistical Test	61

Chapter	Page
Method of Investigation	65
Difference between Resolutions	65
Best Resolution	67
Difference between Interpolation Methods	67
Point and Surface Meteorological Data	69
Conclusions	69
 IV. RESULTS	 70
Alfalfa-Reference Evapotranspiration	70
Summary of Weather	70
Reference Evapotranspiration	73
Difference between Resolutions	77
Original Lattice	77
Resampled Lattice	81
Best Resolution	84
Estimation Variance of Kriging	84
Jack-Knife Procedure	86
Difference between Interpolation Methods	86
Inverse Distance Weighting	86
Thiessen Polygons	90
Point and Surface Meteorological Data	94
 V. CONCLUSIONS AND DISCUSSION	 97
Conclusions	97
Difference between Resolutions	97
Best Resolution	98
Difference between Interpolation Methods	99
Point and Surface Meteorological Data	100
Problems and Discussion	100
Designs	100
Limitation of ARC/INFO	101
Kriging	102
Accuracy of Interpolation	106
Practicality of Interpolating E_r with Kriging	110
Spatial Pattern of Interpolation	113
Further Studies	115
Daily Variations	115
Regional Variations	115
Density of Data Collection	116
Kriging Parameters and Other Interpolation Methods	116
Evapotranspiration Estimation	116
Summary	117

Chapter	Page
REFERENCES	120
APPENDIXES	123
APPENDIX A—ADDITIONAL DATA ON OKLAHOMA MESONETWORK	124
APPENDIX B—MAP PROJECTION AND PROGRAMS	130
APPENDIX C—METEOROLOGICAL ELEMENTS ON STUDY DAYS	138
APPENDIX D—SEMIVARIOGRAMS	145
APPENDIX E—CORRELATION ANALYSIS	158
APPENDIX F—DIFFERENCES BETWEEN VARIOUS SURFACES	164
APPENDIX G—SPATIAL PATTERN OF DIFFERENCES BETWEEN SURFACES	177

LIST OF TABLES

Table	Page
I. Monthly Potential Evapotranspiration of Oklahoma City Using the Thornthwaite Method	33
II. Variables Measured at Mesonet Sites	43
III. Interpolated Lattices and Variance Lattices of Different Attributes Created by Kriging	62
IV. Configuration of Different Spatial Resolutions	64
V. Summary of Study Days	71
VI. Kriging Error of Jack-Knife Procedure	87
VII. Interpolation Errors of Kriging, Inverse Distance Weighting and Thiessen Polygons Using Jack-Knife Procedure	91
VIII. Nugget Variance, Sill Variance and Range of Reference Evapotranspiration	103
IX. Correlations between Results of Interpolation Methods Using Jack-Knife Procedure	112
X. List of Mesonet Stations	125
XI. Albers Conic Equal Area Projection Used in the Study	131
XII. Differences between Interpolation Results Using Various Resolutions (Original Lattice)	165
XIII. T Scores of Difference between Resolutions by Distance From Mesonet Sites (Original Lattice)	167
XIV. Differences between Interpolation Results Using Different Resolutions (Resampled Lattice)	168

Table	Page
XV. T Scores of Difference between Resolutions by Distance From Mesonet Sites (Resampled Lattice)	170
XVI. Difference between Interpolation Results of Kriging and Inverse Distance Weighting	171
XVII. T Scores of Difference between Kriging and IDW by Distance from Mesonet Sites	172
XVIII. Differences between Interpolation Results of Kriging and Thiessen Polygons	173
XIX. T Scores of Difference between Kriging and Thiessen Polygons by Distance from Mesonet Sites	174
XX. Difference between Interpolation Results Using Point and Surface Meteorological Data	175
XXI. T Score of Difference between Using Point and Surface meteorological Data by Distance from Mesonet Sites	176

LIST OF FIGURES

Figure		Page
1.	The Geographic Matrix	6
2.	Spatial Interpolation Methods.	9
3.	Relationship between Semivariance and Covariance	20
4.	Bounded and Unbounded Models for Semivariograms	23
5.	A Qualitative Representation of the Hydrologic Cycle	27
6.	Water Balance on Land According to Difference Authors	29
7.	Generalized Crop Curves Showing the Effects of Growth Stages, Wet Soil Surface, and Limited Available Soil Water	39
8.	Oklahoma Mesonetnetwork	42
9.	The Extent of the Study Area, Test Area and Main Body of Oklahoma ...	49
10.	Relationship between Lattices of Various Resolutions.	53
11.	Procedures of Deriving Reference Evapotranspiration Lattices from Point and Surface Meteorological Data	59
12.	Thiessen Polygons Created from Mesonet Stations, May 6, 1994	63
13.	The Procedures of Comparing Original Lattice and Resampled Lattice ...	66
14.	Oklahoma Mesonetnetwork Stations Used to Calculate Daily Reference Evapotranspiration of the Three Study Days	74
15.	Daily Reference Evapotranspiration at Mesonet Sites, March 3, 1994	75
16.	Daily Reference Evapotranspiration at Mesonet Sites, May 5, 1994	76

Figure	Page
17. Daily Reference Evapotranspiration at Mesonet Sites, June 16, 1994	78
18. Positive and Negative Differences between Interpolation Results of Reference Evapotranspiration Using Various Resolutions in Kriging (Original Lattice)	80
19. Positive and Negative Differences between Interpolation Results of Reference Evapotranspiration Using Various Resolutions in Kriging (Resampled Lattice)	83
20. Estimation Variance of Kriging and Percent Error of Kriging	85
21. Positive and Negative Differences between Interpolation Results of Reference Evapotranspiration Using Kriging and Inverse Distance Weighting	89
22. Positive and Negative Differences between Interpolation Results of Reference Evapotranspiration Using Kriging and Thiessen Polygons . . .	93
23. Positive and Negative Difference between Reference Evapotranspiration Surfaces Resulting from Point and Surface Meteorological Data	95
24. Comparison of Average CPU time Used by Different Interpolation Methods in ARC/INFO	105
25. A Schematic Relationship between Reference Evapotranspiration Lattices of Various Resolutions (Original Lattice), June 16, 1994 . . .	114
26. Thiessen Polygons Created from Mesonet Stations, March 3 and June 16, 1994	128
27. The Subsets of the Test Area by Distance from Mesonet Stations	129
28. Daily Air Temperature at Mesonet Stations	139
29. Daily Solar Radiation at Mesonet Stations	140
30. Daily Relative Humidity at Mesonet Stations	141
31. Daily Vapor Pressure Deficit at Mesonet Stations	142
32. Daily Wind Speed at 2 m (Extrapolated from 10 m) at Mesonet Stations .	143

Figure	Page
33. Daily Station Air Pressure at Mesonet Stations	144
34. Actual and Fitted Variograms of Reference Evapotranspiration (Resolution = 1 km), May 6, 1994	146
35. Actual and Fitted Variograms of Reference Evapotranspiration (Resolution = 3 km), May 6, 1994	147
36. Actual and Fitted Variograms of Reference Evapotranspiration (Resolution = 9 km), May 6, 1994	148
37. Actual and Fitted Variograms of Reference Evapotranspiration (Resolution = 27 km), May 6, 1994	149
38. Actual and Fitted Variograms of Reference Evapotranspiration (Searching Radius = 120 km), March 3, 1994	150
39. Actual and Fitted Variograms of Reference Evapotranspiration (Searching Radius = 120 km), June 16, 1994	151
40. Actual and Fitted Variograms of Air Temperature (Searching Radius = 120 km)	152
41. Actual and Fitted Variograms of Solar Radiation (Searching Radius = 120 km)	153
42. Actual and Fitted Variograms of Vapor Pressure Deficit (Searching Radius = 120 km)	154
43. Actual and Fitted Variograms of Vapor Pressure Deficit at Dew Point (Searching Radius = 120 km)	155
44. Actual and Fitted Variograms of Wind Speed at 2 m—Extrapolated from 10 m (Searching Radius = 120 km)	156
45. Actual and Fitted Variograms of Station Air Pressure (Searching Radius = 120 km)	157
46. Correlation between Interpolation Results of Reference Evapotranspiration Using Various Resolution in Kriging (Original Lattice)	159
47. Correlation between Interpolation Results of Reference Evapotranspiration Using Various Resolution in Kriging (Resampled Lattice)	160

Figure	Page
48. Correlation between Interpolation Results of Reference Evapotranspiration Using Kriging and Inverse Distance Weighting	161
49. Correlation between Interpolation Results of Reference Evapotranspiration Using Kriging and Thiessen Polygons	162
50. Correlation between Reference Evapotranspiration Surfaces Resulting from Point and Surface Meteorological Data	163
51. Spatial Pattern of the Difference between Interpolation Results of Various Resolutions (Original Lattice), March 3, 1994	178
52. Spatial Pattern of the Difference between Interpolation Results of Various Resolutions (Resampled Lattice), March 3, 1994	179
53. Spatial Pattern of the Difference between Interpolation Results of Various Resolutions (Original Lattice), May 6, 1994	180
54. Spatial Pattern of the Difference between Interpolation Results of Various Resolutions (Resampled Lattice), May 6, 1994	181
55. Spatial Pattern of the Difference between Interpolation Results of Various Resolutions (Original Lattice), June 16, 1994	182
56. Spatial Pattern of the Difference between Interpolation Results of Various Resolutions (Resampled Lattice), June 16, 1994	183
57. Spatial Pattern of the Difference between Interpolation Results Using Kriging and Inverse Distance Weighting, May 6, 1994	184
58. Spatial Pattern of the Difference between Interpolation Results Using Kriging and Thiessen Polygons, May 6, 1994	185
59. Spatial Pattern of the Difference between Interpolation Results Using Point and Surface Meteorological Data, May 6, 1994	186

NOMENCLATURE

γ	Psychrometric constant, kPa °C ⁻¹
$\gamma(0)$	Semivariance at lag 0, nugget variance
$\gamma(h)$	Semivariance at lag h
Δ	Slope of the saturation vapor pressure-temperature curve, kPa °C ⁻¹
ΔST	Change of surface storage
λ	Latent heat of vaporization, MJ kg ⁻¹
λ	Weights used by an interpolation method
$\rho(h)$	Autocorrelation coefficient at lag h
σ^2	Estimation variance of kriging
ψ	Lagrange multiplier
a	Range
c	Sill variance
$C(0)$	Covariance at lag 0
$C(h)$	Covariance at lag h
$c0$	Nugget variance
CNSD	Conditional negative semi-definite
d_a	Vapor pressure deficit, kPa
Derror	IDW-error, jack-knife procedure, interpolated E_r using IDW minus estimated E_r
DEtr	Interpolated E_r using IDW, jack-knife procedure
E	Evaporation
e^0	Saturation vapor pressure, kPa
e_d	Saturation vapor pressure at dew point, kPa
ELD	E_r surface interpolated from point meteorological data using inverse distance weighting
ELE	E_r surface interpolated from surface meteorological data using kriging
ELI	E_r surface interpolated from point meteorological data using kriging
ELT	E_r surface interpolated from point meteorological data using Thiessen polygons
E_o	Evaporation from water surface, mm
E_t	Evapotranspiration, mm
E_{to}	Grass reference evapotranspiration, mm

E_{tp}	Potential evapotranspiration, mm
E_{tr}	Alfalfa reference evapotranspiration, mm
e_z	Vapor pressure at height z
e_z^0	Saturation vapor pressure at height z
$f(u)$	Wind function in the Dalton-type equation
FAO	Fishing and Agriculture Organization
G	Heat flux density to the ground, MJ m ⁻²
GW	Change of ground water
h	Lag
h_c	Height of crop canopy, cm
I	Interception
IDW	Inverse distance weighting
K_c	Crop coefficient
K_{cb}	Basal crop coefficient
K_{cm}	Mean crop coefficient
Kerror	Kriging-error, jack-knife procedure, interpolated E_{tr} using kriging minus estimated E_{tr}
KEtr	Interpolated E_{tr} using kriging, jack-knife procedure
Mesonet	Oklahoma Mesonet
Nerror	Proximal-error, E_{tr} of the nearest Mesonet station minus E_{tr} of the station
NEtr	E_{tr} of the nearest station, jack-knife procedure
P	Precipitation
P	Station atmospheric pressure, kPa
p	Probability
r	Pearson's product moment correlation
RH	Relative Humidity, %
R_n	Net radiation, MJ m ⁻²
RO	Runoff
R_s	Solar radiation at the earth's surface, MJ m ⁻²
SW	Change of soil moisture
T	Air Temperature, °C
T	Transpiration
u_{10}	Wind speed at 10 m, m s ⁻¹
u_2	Wind speed at 2 m, m s ⁻¹
USDA	United States Department of Agriculture
W_f	Wind function, $W_f = a_w + b_w u_2$
Z	Regionalized variable
$z(x)$	Value of regionalized variable, Z , at location x

CHAPTER I

INTRODUCTION

If Earth is not the only place that life has developed, it is the only planet in the Universe that living organisms are known to exist. With the coming of the space era, for the first time, we can see our own planet with a glance. The beauty of our home is a source of wonder for us and we have given her a name—the Blue Planet. To the best of our knowledge, what makes Earth so special is the existence of one substance—water.

Not only is water found here, it occurs in abundance; most important of all is that water occurs in all three states of matter naturally. The conversion of water from one state to another involves a great amount of energy. The processes facilitate energy exchange which brings the excess heat from the tropics to the energy deficit poles. The constantly changing conditions of the atmosphere, resulting from the energy exchange, is weather. Although the atmosphere changes every moment, there is a pattern, both temporally and spatially.

Agriculture is a fundamental part of our society and economy. In the United States, only small fractions of people work in agricultural production, yet all people rely on a stable food supply. In addition, if there was no excess agricultural production, there would not be industries that use agricultural products as raw materials and there would not be manpower for the secondary and tertiary industries.

Water is an indispensable input for agriculture. Most water on Earth is stored in the great depressions on the crust—oceans; unluckily, it is not readily usable for agriculture. The main supply of fresh water on land surfaces is precipitation from the sky. Back at the dawn of civilization, people in the desert regions of Mesopotamia and Egypt developed irrigation systems to bring the precious water from the life-giving rivers to the fields. Today, in the arid western United States, where solar energy is abundant but water is scarce, farmers pump underground water or bring water from far away to irrigate large agricultural tracts. In this setting, it is vital to be conservative with the use of water.

Of course, not all water is used by plants. If the rate of adding water is faster than the rate plants can use it, the excess seeps through the soil. It is a waste to put more water than needed on a field, for both water and energy used to transport water are scarce. On the other hand, if there is not enough water, the crops will fail. Most water added to the land surface through precipitation and irrigation goes back to the atmosphere through evaporation from the soil surface and transpiration of plants. These combined processes are called evapotranspiration. It is imperative that this translocation of water be thoroughly understood.

Evaporation, E , is the "process by which water is changed from the liquid or solid state into the gaseous state through the transfer of heat energy" (Veihmeyer, 1964, p. 2). Transpiration is the "evaporation of water absorbed by the crop and transpired and used directly in the building of plant tissue, in a specified time. It does not include soil evaporation" (Veihmeyer, p.2). Evapotranspiration, E_e , is the "combined process by which water is transferred from the earth's surface to the atmosphere; evaporation of liquid water

from the soil surface and water intercepted by plants, plus transpiration by plants" (Jensen, Burman, & Allen, 1990, p. 42) .

In order to decide whether to irrigate and how much water to put on a field, it is important to know the amount of water the plants and the atmosphere require. Besides agriculture, the studies of hydrology, soil moisture and land-atmospheric interaction also require a knowledge of evapotranspiration.

There have been numerous efforts in estimating and measuring evapotranspiration in different environments. However, it is both impossible and impractical to measure at every location on earth. Therefore, it is important to understand evapotranspiration as a two dimensional phenomenon and how to represent it by measurement at different point locations. This study will combine previously unobtainable regional data with a geographical information system to estimate regional evapotranspiration.

The Statement of Purpose

The purpose of this research is to investigate the effectiveness of using kriging on deriving evapotranspiration, particularly regional evapotranspiration, from the Oklahoma Mesonet network. Kriging is gaining attention among geographers, and the method is readily available to users through geographical information system. This study will examine if there is any difference as a result of using different resolutions in kriging. If there is any difference found, then the best resolution will be determined. To investigate the comparative advantage of using kriging, the method will be compared with two commonly used interpolation methods—inverse distance weighting and Thiessen polygons.

Furthermore, the study will compare the difference between interpolating derived evapotranspiration and deriving evapotranspiration from interpolated meteorological data.

CHAPTER II

LITERATURE REVIEW

Properties of Space

Geography is the study of space, of the distribution of phenomena on the earth surface. The stage of geographic study is obviously a three dimensional space.

Nevertheless, it is quite often necessary to reduce the three dimensional space to a two dimensional surface. Furthermore, to facilitate study, some phenomena are normally viewed as line (one-dimensional) features, e.g. roads and rivers, and point (zero-dimensional) features, e.g. weather stations.

It is possible to organize the objects of geographical studies as a geographic matrix (see Figure 1), with different phenomena in rows and different areal units in columns. In database terminology, every areal unit is a record and different phenomena form the fields. Some geographers study individual areal units, some group units together, while some differentiate between different units. On the other hand, some geographical studies orient towards the spatial variation of a phenomenon, or the areal association of a few phenomena (Griffith, 1987).

Based on the properties of the phenomena under study, their distribution on the earth surface can be either discrete or continuous. For instance, the distribution of temperature is continuous while that of thermometers which measure temperature is

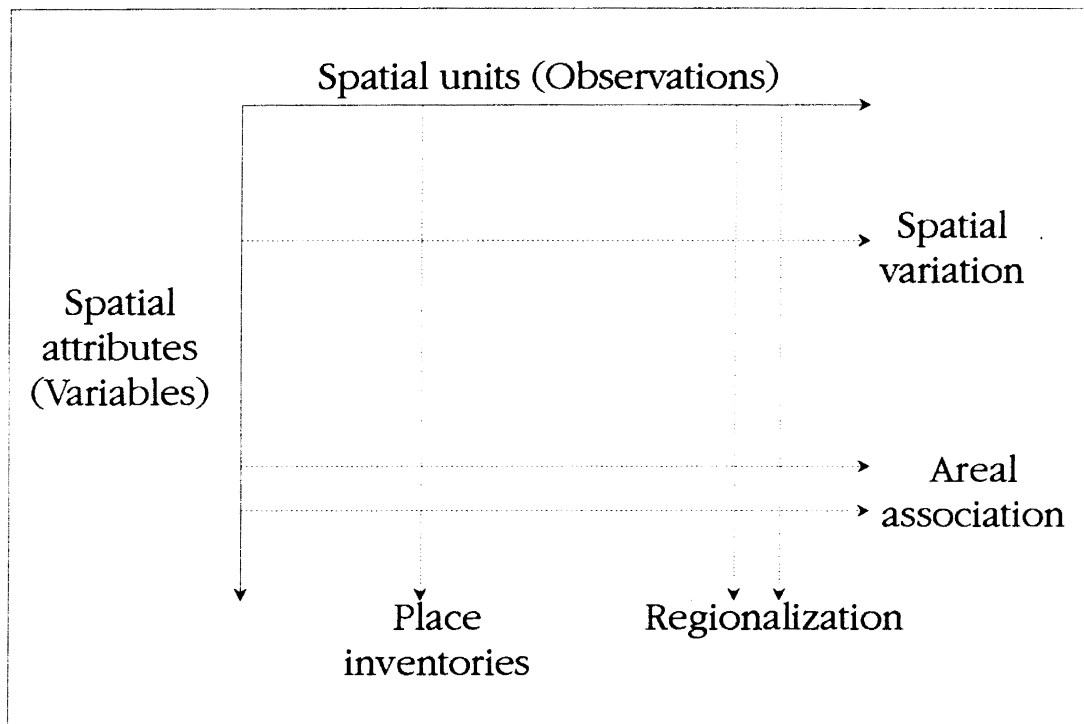


Figure 1. The Geographic Matrix (Griffith, 1987).

discrete. It may not make much sense to represent discrete features as a continuous surface; however, continuous variables can be measured at discrete points on the surface, and then used to describe the continuous surface.

Geographical attributes vary continuously through space; however, observations of these attributes are frequently fragmentary. There are infinite locations on a surface but only finite observations are possible. Interpolation is a necessary operation in geography in order to characterize the continuous surface using the discrete observations (Oliver & Webster, 1990).

Methods of Interpolation

Oliver and Webster (1990) indicated that positive spatial autocorrelation is the underlying quality making interpolation of spatial data possible. Observations closer to each other are more likely to have similar values than those farther apart. In other words, observations closer together spatially have higher correlation than those far apart. Interpolation finds the function that best describes the surface and use it to predict values at locations other than the observations (Lam, 1983). As there is always more than one function to describe a set of points, the problem of interpolation is to find a "plausible model" which fits the observations (Burrough, 1986). In terms of this thesis, there is a question of which plausible model is the "best".

Properties of Interpolation Methods

Burrough indicates that "interpolation is a problem that has occupied the geographers and earth scientists for a long time, and is one that still commands a great

deal of attention." Different methods of interpolation have been developed for different applications. A list of interpolation methods is shown in Figure 2. To compare the performance of different methods of interpolation, one can apply them directly to some actual data as done by Laslett, McBratney, Pahl and Hutchinson (1987). Nevertheless, the review of Lam in 1983 "has shown that various methods have individual advantages and disadvantages, and the choice of an interpolation model depends largely on the type of data, the degree of accuracy desired, and the amount of computational effort afforded." Any data set may have a bias towards certain kinds of methods.

In order to compare different methods of interpolation, it is important to set up some qualitative criteria. Different authors use various terminology and different taxonomies to classify the interpolation methods. In this thesis, five measures of classifying interpolation methods are identified. The first one is global versus local interpolation. Global interpolation uses all observations in the study area for calculation while local interpolation only uses the neighboring points (Burrough, 1986).

Another way of classification is exact methods versus approximate methods. The exact methods preserve the value of the original observations on the interpolated surface, while others only approximate the value at points of observation. Although the values of observation are preserved, the interpolation may not preserve the points of observations. If the observations are interpolated into a mesh of grids, the grids may not coincide with the original observations. On the contrary, if Delaunay triangulation is used, the interpolated surface will contain the original observations (Lam, 1983).

The third classification is stochastic versus deterministic. Deterministic methods use a mathematical function and do not provide a degree of confidence of the result. The

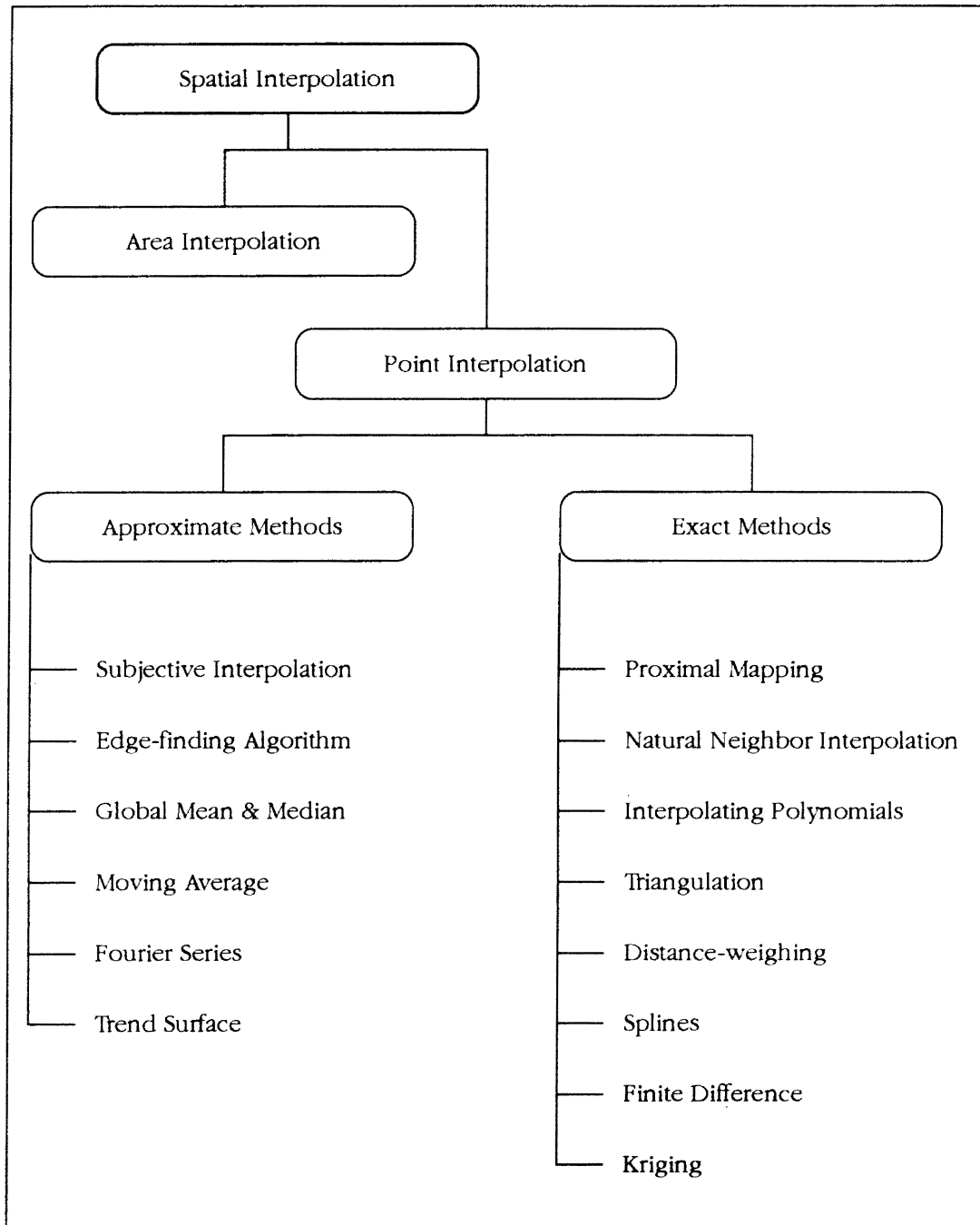


Figure 2. Spatial Interpolation Methods (Burrough, 1986; Lam, 1983; Laslett et al., 1987).

stochastic methods, on the other hand, can estimate the probable errors of the result (Oliver & Webster, 1990).

Laslett et al. (1987) include another property—smooth or non-smooth, which Burrough (1986) describes as gradual or abrupt transitions. However, the definitions used in the two works are different. The former research defined smooth as a continuous predicted surface with a continuous first partial derivatives. The latter one described a smooth mathematically defined surface as smooth.

Lam (1983) distinguished between point and areal interpolation. Point interpolation deals with observations at points. If the original data are the aggregate of an area, then the interpolation is areal. Although point interpolation can be used for areal interpolation, there are also area-based interpolation methods.

Any method of interpolation will have the properties described above. For instance, a moving average is a deterministic, local, exact, and non-smooth interpolation. However, not all cases are so clear cut for some methods can have two sides of a property. While Laslett et al. (1987) described inverse squared distance interpolation as "global, interpolating, smooth", the research used "a local version" of the method.

Approximate Methods

Interpolation methods of this category include subjective interpretation, edge-finding algorithms, global mean and median, moving average, Fourier series, and trend surface. The trend surface method can be further divided into ordinary least-squares polynomials, distance-weighted least-squares, and least-squares fitting with splines.

Subjective Interpretation. Another name for this method would be "eyeball". This is a deterministic, global method. External landscape features are used to delineate "landscape units". The analyst draws isolines or isopleths (choropleth for nominal spatial attributes) based on the observations. The method relies on the intuitive understanding of the analyst on the spatial process and study area. If the product is an isoline map, then the transition will be gradual. If the product is a choropleth map, then the transition is abrupt and homogeneity is assumed within boundaries. The major limitation of this method is that it is subjective and the result is non-reproducible. This method is suited for field data and aerial photo interpretation (Burrough, 1986).

Edge-finding Algorithms. Like the previous one, this is a deterministic global method. Instead of subjective interpretation, edge-seeking algorithms are used to find the boundaries. The assumption is that all important variation occurs at boundaries. The product is a choropleth map with abrupt transition at the boundaries. In general, the method works best for man-made features. Digital images from remote sensing devices are also suited to this method (Burrough, 1986).

Global Mean and Median. The global mean method uses the arithmetic mean of the observations to represent the entire study area, while global median uses the median. The assumption of global mean is that the observed attribute is an independent, identically distributed, normal random variable. Global median is used if the statistical distribution of observed values has a long tail. However, the assumption neglects the existence of autocorrelation (see Chapter I) between observations. As spatial autocorrelation is an

intrinsic part of geography, the methods are usually not applicable for spatial data (Laslett et al., 1987).

Moving Average. This is a deterministic, local variation of the global mean. Instead of using all observations, a local neighborhood or window is used to limit the input for the interpolation. The interpolated result depends on the size of window used and configuration of observation locations. While the number of observations used may range from 4 to 12, usually 6 to 8 points are used. It is best for quick contour plots of moderately smooth data (Burrough, 1986). Although a continuous surface is assumed, the interpolated surface and the first partial derivatives may not be smooth. As an averaging method, it underestimate peaks and overestimate valleys (Laslett et al., 1987).

Fourier Series. This is a stochastic global method. The assumption is that the surface has some recurring or cyclical form. The model uses a linear combination of trigonometric functions. This model has been used to describe and compare physical surfaces, as well as to enhance patterns in image processing. Fourier series are, therefore, applicable to spatial attributes with periodicity. While features such as sand dunes, ripple marks with periodic variation and man-made features can be described by this method, it would be better to use other methods to interpolate spatial features with no periodic variation (Burrough, 1986).

Trend Surface. This is a stochastic, global method with many variations. The basic form is using least-squares polynomials to model a surface, to simplify it into a major trend and associated residuals. Like all regression, the assumption is that the residuals are

independent normally distributed errors, which is unlikely in most cases concerning spatial data. The residuals of a trend surface are usually spatially dependent. Moreover, the method is very sensitive to extreme values and uneven distribution of observation locations. Towards the edge of the map, the predicted value is unreliable. Trend surface is best used to show broad features and to remove them, leaving the residuals for other interpolation (Burrough, 1986).

"Least-squares fitting with splines" and "distance-weighted least-squares" are two variations of trend surface. The distance-weighted variation places more weight on the nearby observations than on observations farther away (Lam, 1983).

Exact Methods

Exact methods of interpolation retain the original values of observations on the interpolated surface. Methods falling into this category include proximal mapping, natural neighbor interpolation, interpolating polynomials, triangulation, distance-weighting, splines, finite difference, and kriging. Kriging will be discussed in the next section (Optimal Interpolation).

Proximal Mapping. This method is also known as Thiessen polygons, Voronoi polygons or Dirichlet cells. It is a deterministic, local interpolation. The assumption is that the nearest observation has the best information for any unobserved place. The result is a choropleth map. However, the arrangement of the observation points will affect the shape of polygons. While this method uses the closest observation, it does not apply the principle of spatial autocorrelation. For any polygon, only the information contained in one

observation is considered. The autocorrelation between observations is not used for the interpolation. The method works best for nominal attributes (Burrough, 1986).

Natural Neighbor Interpolation. This is a variation of Thiessen polygons and is a deterministic, local method. A Thiessen polygon is drawn for the prediction location. Then the polygon is overlaid on the original proximal map. The proportions of different original polygons in the polygon are used as weights for the corresponding observation. It takes the spatial autocorrelation of observations into account. However, neighborhood instead of distance is used. If the pattern of observation is irregular, strange results may occur (Laslett et al., 1987).

Interpolating Polynomials. This is a deterministic, global method. A polynomial of the lowest order is fitted so that a surface passes through all observations. This is similar to the regression with no residual. However, the resulting surface could have a very strange shape. Although the surface passes through all observations, the values between them could be drastically different. Sometimes, there is more than one solution. It is possible to use a local window instead of all observations. However, smooth matching between different pieces is difficult. This method is not generally recommended, particularly when the number of observations is large (Lam, 1983).

Triangulation. This is a deterministic, local method. Delaunay triangulation is used to create triangles. Akima's method is then used to fit restricted quintic surfaces to each Delaunay triangle. One problem with this method is that there is always more than one way to form Delaunay triangulations for a set of observations (Laslett et al., 1987)).

Distance-weighting. It is also known as "inverse distance weighted". This is a deterministic method with local and global variations. The idea of distance decay is employed; observations are assigned with weights according to their distance to the interpolation point. One problem is that the choice of weighing function is arbitrary. Another drawback is that the interpolated value is bounded by the observed values. Uneven distribution of observation points will affect the interpolation results. If a negative exponential weighting function is used, the interpolation will be an approximate method (Lam, 1983). A local window can be used instead of all observations; it is similar to moving average with distance-weighting.

Splines. This is a deterministic, local method. The method is similar to fitting a flexible ruler to points to draw a smooth line. In a three-dimensional situation, the splines are called bicubic. The assumption of this method is absolute smoothness of variation. As it is not easy to extend splines to the three-dimensional case, B-spline is often used instead. While splines split data into intervals, using observations as break points or not will produce different results. Splines always create a smooth surface even if they are not valid. Besides of exact interpolation, it is always used for smoothing data to create contours (Burrough, 1986).

Finite Difference. This is another deterministic method. The assumption is that the surface is differentiable. The equations are then approximated by finite differences and solved iteratively. A drawback is that the relative and absolute extremes always locate at

observations or boundaries. Sometimes, there may be no value assigned to some locations (Lam, 1983).

Kriging

Kriging is often known as "optimal interpolation" (Burrough, 1986) or *geostatistics* (Oliver, Webster, & Gerrard, 1989). It is optimal because its value estimates are unbiased and have minimum variances (Oliver et al., 1989). It is similar to local moving average using weights, but is stochastic. Oliver and Webster (1990) summarize the disadvantages of other interpolation methods. It is impossible to determine the assumption of spatial dependence; the form of spatial variation is not considered; there is no way to estimate the error of interpolation. Although some interpolation methods are also stochastic, e.g. trend surface, they cannot provide the estimation variances like kriging, which can be used with known confidence.

Kriging is based on regionalized variable theory, which was developed by Matheron and his colleagues at the Paris School of Mines in the 1960s. Similar methods have been used by Russian meteorologists in meteorology and Krige in gold mining. Matheron brought together interpolation methods developed by Kolmogorov, Krige, Matérn, and Yaglom to describe comprehensively and quantitatively the variation of geological deposits. The application of regionalized variable theory is often known as geostatistics (Oliver et al., 1989).

Regionalized Variable Theory. Journel and Huijbregts (1978) define *regionalized variables* as variables that "[distribute] in space" (p. 27). A regionalized variable is any

spatial attribute in one, two, or three dimensions. The value of a regionalized variable varies through space so drastically that it is usually impossible to find a mathematical function to describe the variable. Nevertheless, spatial autocorrelation does and is expected to exist. It is possible to view the spatial attribute as containing two components: a deterministic, general (or average) structural component and a local, random, erratic component. As the second component is a random function, it provides probabilistic interpretation. Oliver et al. (1989) indicate that the random part is usually the larger of the two, so large that it masks the deterministic variation.

Given a spatial attribute Z , the predicted value z at location x can be expressed mathematically as:

$$z(x) = \sum a_k f_k(x) + \varepsilon(x) \quad (1)$$

where the first term, $f_k(x)$, is the deterministic component and the second term, $\varepsilon(x)$, is the stochastic component (Oliver et al., 1989).

Intrinsic Hypothesis. The regionalized variable theory is based on the *intrinsic hypothesis*, which has two conditions (Burrough, 1986; McBratney & Webster, 1986; Webster & Oliver, 1990). The first condition is that the expected difference of z between two locations separated by a distance h (x and $x+h$) is zero. In other words, at all location x , the predicated value z equals the mean of Z , μ . In other words, the mean of the stochastic component, ε , is expected to be zero,

$$\begin{aligned}
z(x) &= \mu_v + \varepsilon(x) \\
E [z(x) - z(x + h)] &= 0 \\
E [z(x)] &= \mu_v \\
E [\varepsilon(x)] &= 0
\end{aligned} \tag{2}$$

The second condition is that the variance of the differences in Z depends on h , the distance between the two locations, instead of x , the spatial location. The distance between the two locations, h , is called the *lag*. In a strict sense, it is a vector with distance and direction. The variance of the differences is the expected squared difference of Z separated by the lag h ,

$$\begin{aligned}
\text{var} [\varepsilon(x) - \varepsilon(x + h)] &= E [\{\varepsilon(x) - \varepsilon(x + h)\}^2] \\
&= 2\gamma(h)
\end{aligned} \tag{3}$$

The expected squared difference of Z separated by the lag h is two times the expected variance at lag h , $2[s^2(h)]$. As a result, half of the expected squared difference at lag h is known as the *semivariance*, $\gamma(h)$.

Semivariance and Autocorrelation. It is possible to describe the autocorrelation of two locations using their *covariance*. The autocorrelation coefficient, $\rho(h)$, of attribute Z at lag h , equals the covariance at lag h , $C(h)$ divided by the covariance at lag 0, $C(0)$ (see Figure 3). If Z is *second-order stationary*, i.e. the variance is constant, the relation between covariance and semivariance is:

$$\begin{aligned}
\gamma(\mathbf{h}) &= C(0) - C(\mathbf{h}) \\
&= C(0) \{1 - \rho(\mathbf{h})\} \quad .
\end{aligned} \tag{4}$$

As the lag increases, the covariance decreases to zero, and the autocorrelation has no meaning beyond this range. However, in reality, the semivariance can continue to increase without limit. Therefore, the semivariance is more useful than the covariance or autocorrelation (Webster & Oliver, 1990).

Semivariance and Kriging. As described earlier, kriging is a local distance-weighted interpolation method. The main difference of kriging from other distance-weighted methods is that the weights are calculated from the regionalized variable theory, which provides the stochastic nature of the method. The predicted value at location x_0 is

$$\hat{z}(x_0) = \sum_{i=1}^n \lambda_i z(x_i), \tag{5}$$

where λ_i are weights of corresponding observation points x_i . The sum of weights, $\lambda_1 \dots \lambda_n$, is one so that the estimates are unbiased. The *estimation variance*, σ^2 , for the predicted value of z at x_0 is

$$\begin{aligned}
\sigma^2 &= E [\{\hat{z}(x_0) - z(x_0)\}^2] \\
&= 2 \sum_{i=1}^n \lambda(x_i - x_0) - \sum_{i=1}^n \sum_{j=1}^n \lambda_i \lambda_j \gamma(x_i - x_j),
\end{aligned} \tag{6}$$

where $(x_i - x_0)$ and $(x_i - x_j)$ are vectors in lag, h .

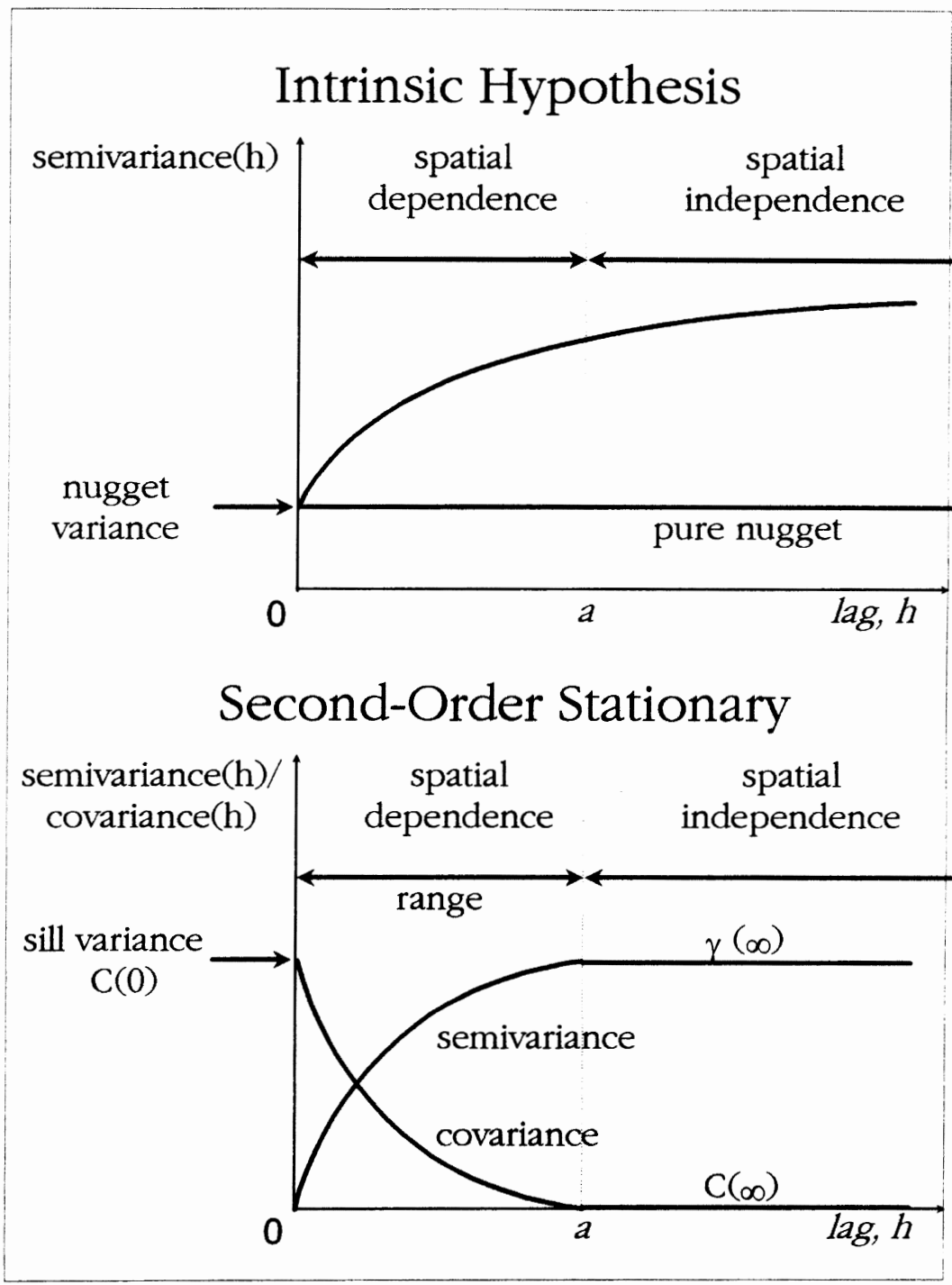


Figure 3. Relationship between Semivariance and Covariance (Journel & Huijbregts, 1978).

In order to minimize the error of estimation, a Lagrange multiplier, ψ , is introduced:

$$\sum_{i=1}^n \lambda_i \gamma(x_i - x_j) + \psi = \gamma(x_j - x_o) \text{ for all } j, \quad (7)$$

and the equation is solved for λ_i . Then, the weights are used to find the predicted value.

The estimation variance (kriging variance) is estimated using the following equation:

$$\sigma^2(x) = \sum_{i=1}^n \gamma(x_i - x_o) + \psi. \quad (8)$$

The estimation of weights and estimation variances depends on the semivariance at different lags, $\gamma(h)$ and the spatial configuration of the observations and points to be interpolated (McBratney & Webster, 1986; Oliver et al., 1989).

Semivariance and Variogram. Semivariance, $\gamma(h)$, is a function of lag h , and the graphical representation of them is a *semivariogram* or *variogram* (Webster & Oliver, 1990). Semivariances are estimated from the observations at discrete lags available in the observations. Then a mathematical function is used to model the true continuous variogram for the region. The accuracy of kriging depends on the fitted variogram.

The variogram describes the magnitude, spatial scale and general form of the variation (Oliver et al., 1989). Usually, the semivariance starts from zero. It increases as the lag, h , increases, and eventually levels off beyond a certain lag. This indicates the existence of a second-order stationary behavior. As shown in Figure 3, the distance at which the variogram levels off is called the *range*, a . Spatial dependence, or

autocorrelation, exists within this range. The semivariance is constant at the *sill variance* beyond the range. If the semivariance rises continuously, then only the intrinsic hypothesis holds. Sometimes, the variogram starts as a positive value, which is known as the *nugget effect*. This indicates that the existence of measurement error and/or the spatial dependence occurs on scales much shorter than the smallest observation interval. If the variogram is horizontal, the semivariance is *pure nugget*; no spatial dependence is detected at the scale of observations (Oliver et al., 1989).

McBratney and Webster (1986) list a very important criterion for fitting a model to a variogram—*conditional negative semi-definite*, CNSD. In other words, the variances cannot be negative (Oliver, et al., 1989). This constrains the possible simple models, referred to in geostatistics as *authorized models*. For second-order stationary situations, the models are called *bounded* or *transitive*. Some possible models include: linear, circular, spherical, exponential, and gaussian (see Figure 4). In addition, any combination of these models is also CNSD. Models without sill are called *unbounded models* and are estimated using power functions from 0 to 2 exclusive. As a bounded linear model is only CNSD in one dimension, it should not be used for two or three dimensional data.

While kriging provides a variance of estimation, there is "no simple way of determining confidence limits on variograms analytically" (Oliver et al., 1989, p. 264). Although the true variogram of an attribute in a region should remain the same, the sampling variogram changes depending upon which observations are sampled. It depends on the number of observations, shape and size of the study area, and the spatial configuration of the observations. Increased numbers of observations with less distance will improve the estimation. Oliver et al. (1989) recommend a minimum of one hundred

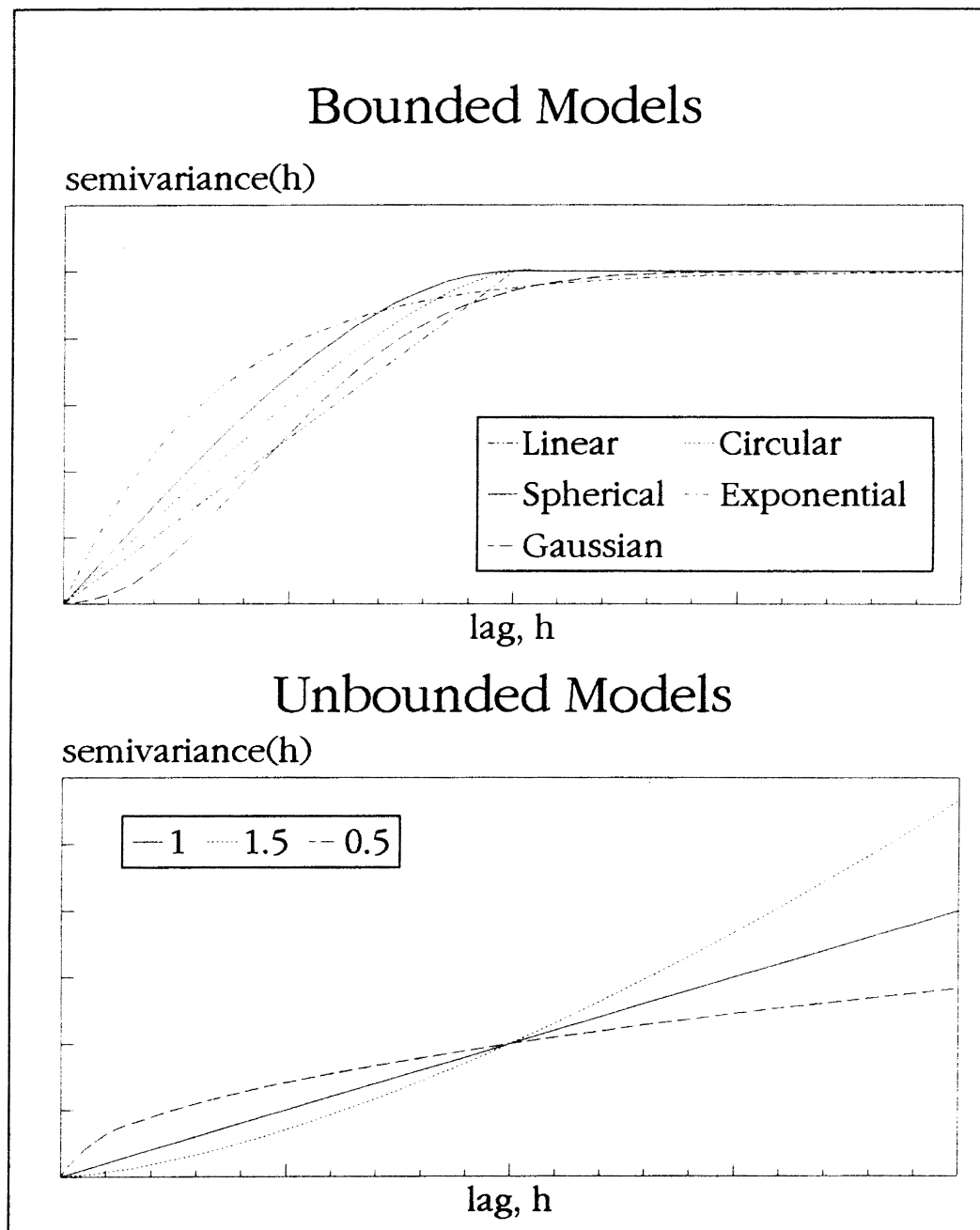


Figure 4. Bounded and Unbounded Models for Semivariograms (Webster & Oliver, 1990).

comparisons at the first lag, while Royle, Clausen and Frederiksen (1981) suggest a number of observations between 12 and 15. ARC/INFO 6.1.1 (1992) also suggests using 12 to 15 sample points. If the distribution of observed values is strongly skewed, the values should be normalized before estimating the semivariance.

Drift and Kriging. The intrinsic hypothesis assumes all variation is random. However, if the variogram is concave upward, it indicates that the deterministic component of the attribute has a trend, called *drift* in geostatistics. It may be necessary to remove the trend before estimating the semivariance. This kind of kriging is called *universal kriging*, *unbiased kriging of order k*, or *kriging with a trend model*; the normal kriging is often called *ordinary kriging*.

Royle et al. (1981) indicate that the drift is a matter of scale. If the drift is smaller than the observation interval, it remains undetected. If the drift is on a very large scale, it is practical to treat the attribute within a local neighborhood as stationary. The Royle et al. paper describes the procedure to estimate a linear drift or quadratic drift, and then use the residuals to estimate the semivariogram. Both the drift and semivariance of the residuals are used to predict values.

In 1989, Journel and Rossi indicated that it is not necessary to use universal kriging even if a drift exists. Usually, a local search window is used to estimate semivariance. If interpolation instead of extrapolation is the situation, "the global trend components and residual components as provided by [ordinary kriging] and [universal kriging] are, respectively, equal" (p. 736).

Advantages of Kriging. Lam (1983) called kriging perhaps the most distinctive interpolation method. Burrough (1986) used the term "optimal interpolation" instead of kriging. It is an appealing method because kriging provides the best linear unbiased estimator of the unknown characteristic studied (Journel & Huijbregts, 1978). The predicted values have minimum variances, which can also be estimated. Therefore, kriging can be used with known confidence, and is an exact method.

Disadvantages of Kriging. To solve equation (7), inversion of a matrix is required. If many points are used, the operation will take lots of time. The time required to invert a matrix is approximately proportional to the cube of its order (Webster and Oliver, 1990). Another problem is the accuracy of the variogram. McBratney and Webster (1986) recommended a method called weighted least-squares to find the fitted variogram instead of judging visually. However, they also admitted that there was "no agreement on a generally best (in terms of computational and statistical efficiency and reality of assumptions) way of model fitting" (p. 635).

Applications of Kriging. In that regionalized variable theory was developed at the French mining school, kriging has been widely applied in mining. Soil science has used the method in estimating nutrients and other soil constituents. Variograms have been used to improve the efficiency of sampling, i.e. locating observation sites. The study of Laslett et al. (1987) showed that kriging, as well as splines, performed best in interpolating soil acidity. That study also confirmed the existence of short range spatial dependence of soil acidity. In addition, groundwater modelling, rainfall monitoring and atmospheric pollutant estimation are some other applications of kriging (Oliver et al., 1989).

Tabios and Salas (1985) compared the performance of 12 methods in interpolating precipitation over an area of about 62,000 km² in Nebraska and Kansas. While most authors regard evaluation of both covariogram and variogram as means to obtain weights for kriging, and the latter as more generally applicable (as shown in the previous sections), Tabios and Salas treated them as two methods. Covariance was used to find the weights for optimal interpolation, and variogram was used in kriging. Nevertheless, the results show that both methods outperform the rest. Thus, kriging is an attractive methodology with which to interpolate Oklahoma Mesonet data (see section Meteorological Data of this chapter).

Evapotranspiration Estimation

Hydrologic Cycle and Evapotranspiration

The exchange of water over the earth's surface is known as the hydrologic cycle. There are many ways to represent this cycle, depending on the focus and scope of study. It is possible to represent the processes in either descriptive or quantitative ways.

Figure 5 is a qualitative representation of the hydrologic cycle on land. Although there is neither beginning nor end in the cycle, it is possible to express the relationship between the different processes in a hydrologic equation (Oliver, 1973):

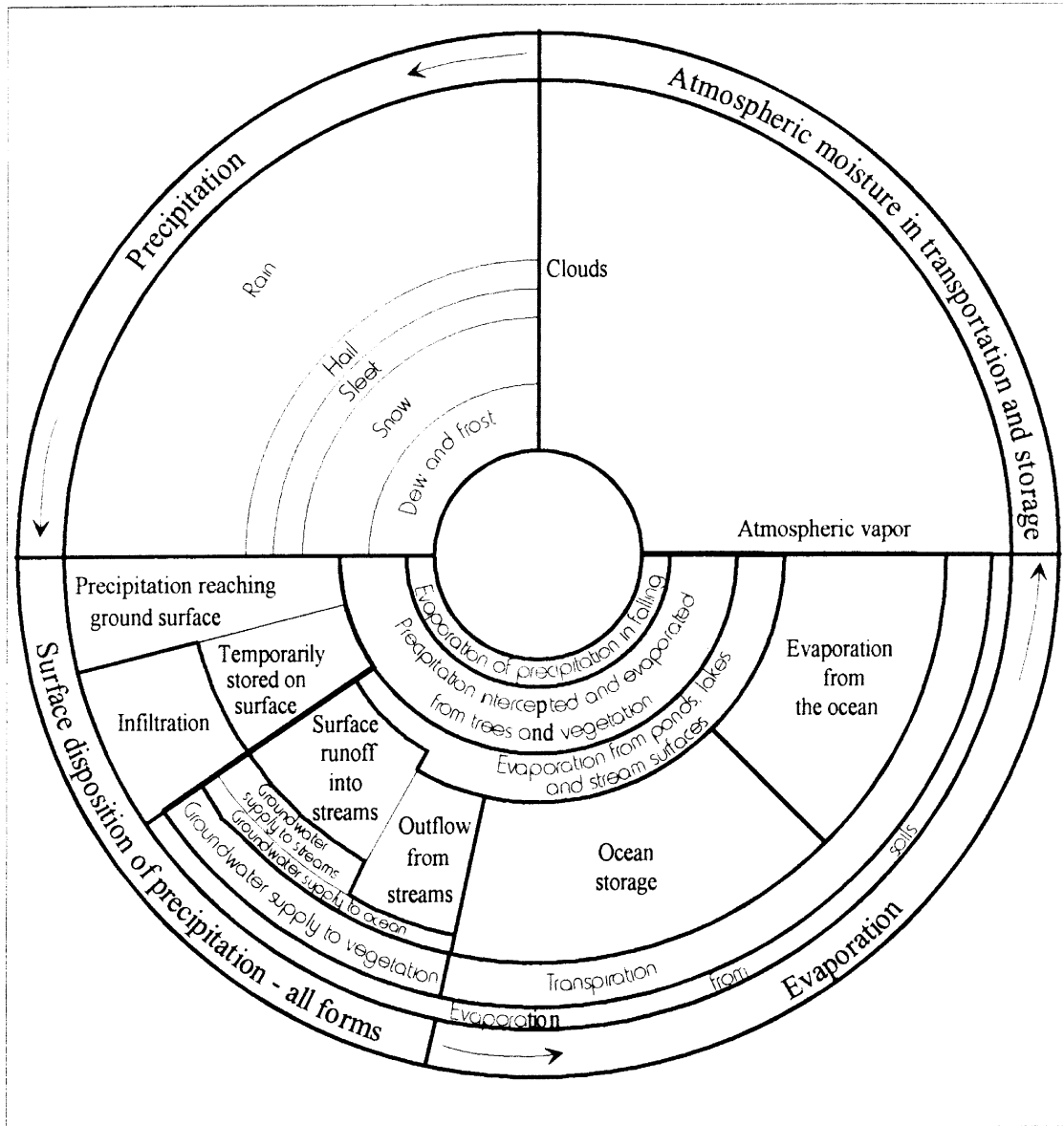


Figure 5. A Qualitative Representation of the Hydrologic Cycle (Chow, 1964).

$$P = E + T + I + SW + RO + GW + \Delta ST, \quad (9)$$

where P is precipitation, E is evapotranspiration, T is transpiration, I is interception, SW is change in soil water, RO is runoff, GW is change in ground water and ΔST is change in surface storage.

All these processes are integrated in the cycle. Precipitation brings the water to the land surface. Water infiltrates into soil, runs over land, or is intercepted by plants. Evaporation and transpiration return the water to the atmosphere. As a result of transpiration, green plants obtain water from soil moisture, and dissolved nutrients in the soil moisture.

The hydrologic equation expresses the hydrologic cycle on land as inflow on the left and outflow on the right. There have been many studies on the amount and proportion of the evaporation and runoff components. Sanderson (1990) summarized the findings of different authors (see Figure 6).

Figure 6 shows that the literature's estimation of the proportion of runoff has tended to increase slightly through time and that of evapotranspiration perhaps decrease. However, evapotranspiration is still the larger of the two. A study in 1974 showed that 60.6% of precipitation on land is returned to the atmosphere through evapotranspiration (Sanderson, 1990). In Oklahoma, the proportion of evapotranspiration is probably greater than this. Yet, there are no climatological measurements of evapotranspiration in Oklahoma and this leaves great uncertainty in Oklahoma's water budget.

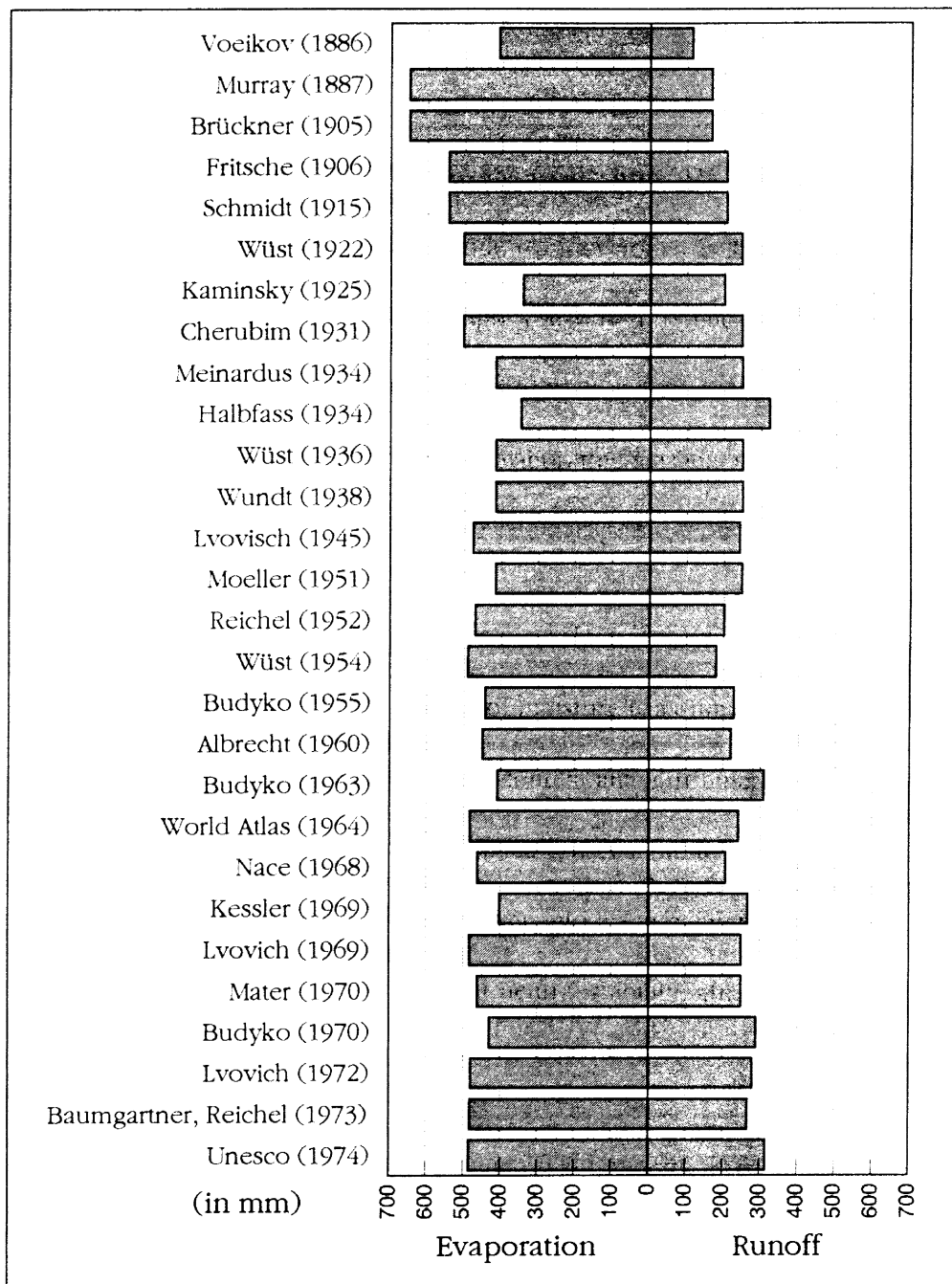


Figure 6. Water Balance on Land According to Different Authors (Sanderson, 1990).

Estimation of Evapotranspiration

Although evapotranspiration is a significant component of the hydrologic cycle, it is difficult to measure. Evaporation from free water surfaces can be measured by using evaporation pans and atmometers (Veihmeyer, 1964). However, the size of water body affects the evaporation rate. It is difficult to compare the results between different types of pans and the evaporation rate is usually lower over large water bodies. Empirical coefficients are developed to estimate evapotranspiration from the USA Class-A pan (Jensen et al., 1990). However, an evaporation pan is not a common instrument. For instance, in 1992, there were only 13 evaporation pans throughout Oklahoma.

One way to describe the hydrologic cycle is through modelling. A lysimeter can be viewed as a physical model of the hydrologic cycle. According to Curtis and Trudgill (1974), accuracies up to 0.02 mm may be achieved by some types of weighing lysimeters. However, "[the] direct measurement of evapo-transpiration on any sufficiently large scale requires very expensive equipment" (Curtis and Trudgill). Lysimeters have difficulty estimating the real field conditions (Jensen et al., 1990). Wang and Ray (1984) described a standard weighing lysimeter for researching purposes. It is "approximately" 20 feet (6 m) in diameter and 38 inch (96.5 cm) deep, with a capacity of 50 tons of soil and water. In fact, a lysimeter has no strict standard and is usually used by researchers only. There are no long-term lysimeter records for Oklahoma.

Since it is difficult to measure evapotranspiration directly, it is usually estimated using other methods. Mather (1978) classified the techniques into six categories: mass transport techniques, aerodynamic or profile techniques, eddy correlation techniques,

energy-budget techniques, empirical techniques, and combination techniques. Jensen et al. (1990) included water balance and soil water depletion.

Mass Transport Techniques. Penman (1948) stated two requirements for evaporation: a supply of energy and a removing mechanism. He described the removing mechanism as a sink for vapor. The technique was developed by Dalton. Evapotranspiration is proportional to the vapor pressure difference between the surface and the air above. A function of wind speed is used as a coefficient. One problem is the difficulty of measuring vapor pressure at the evaporating surface; standard instrumentation is usually somewhere above the surface.

Aerodynamic Techniques. Assumptions on the turbulent diffusion of heat and water vapor can be made. Vertical diffusion of moisture is assumed to be proportional to the product of the height gradient of moisture content and a turbulent-diffusion coefficient, which is dependent on the wind speed profile (Mather, 1978). The size and shape of the evaporating surface need to be taken into account (Penman, 1948). However, if temperature lapse rate is not near neutral stability, atmospheric buoyancy influences the diffusion coefficient (Mather).

Eddy Correlation Techniques. It is found that upward diffusion of water vapor can only happen if upward moving turbulent eddies are more moist than the downward moving eddies. The sensing of such eddies requires sensitive and fast-response instruments (Mather, 1978). Although the complex instruments are available, well-trained personnel are required to obtain accurate results (Jensen et al, 1990).

Energy-Budget Techniques. Energy is required to supply the latent heat of vaporization so that water can change from the solid or liquid state to the gaseous state. The main supply of energy is solar radiation. Net radiation, R_n , equals the sum of atmospheric heat flux, soil heat flux and latent heat of vaporization (Mather, 1978). About 51% of net radiation onto land surfaces is converted to latent heat of vaporization. If the whole world is considered, 83% of net radiation is used to evaporate water annually (Budyko, 1974).

The energy-budget technique provides reliable results as long as the measurements are accurate. Jensen et al. (1990) comment that "the instrumentation requirements and technical procedures involved generally limit the ... method to research studies over relatively short periods of time" (p. 83).

Empirical Techniques. Thornthwaite (1948) used mean monthly temperature to estimate potential evapotranspiration (E_p) empirically, and then used water balance model to calculate the actual evapotranspiration (E_a). This method "is less effective on a daily basis because daily variations in wind speed and humidity are not included in the expression for potential evapotranspiration" (Mather, 1978, p. 19). Thornthwaite's method is widely used because of its simplicity. The requirement for complex parameters usually restricts the practicality of the other methods to localized, short-term studies. Table I shows estimates for Oklahoma City.

Water Balance. If the water balance method, the precipitation and runoff of a large area, e.g. a basin, are monitored. Then evapotranspiration is calculated (Jensen et

TABLE I
MONTHLY POTENTIAL EVAPOTRANSPIRATION OF OKLAHOMA CITY
USING THE THORNTHWAITE METHOD^a

	Potential Evapotranspiration (in mm)	Precipitation (in mm)
Jan	2	33
Feb	7	35
Mar	22	50
Apr	56	79
May	98	132
Jun	143	114
Jul	167	60
Aug	167	64
Sep	108	77
Oct	61	64
Nov	18	40
Dec	5	36
Total	854	784

^a The estimates is provided by the Waterbud program.

al., 1990). This method can estimate the water balance for a large area, instead of a specific point. However, the coarse spatial and temporal resolutions often limit its application.

Soil Water Depletion. Soil water can be measured using a neutron probe or other methods. Then the change over time is used to estimate the evapotranspiration. Adequate precautions must be made for "reliable" (as apart from accurate) estimation. Some of the considerations are number and location of sampling sites, number of samples, depth to water tables, and timing of sampling (Jensen et al., 1990). Again, this is a method which is relatively costly and dependent upon trained personnel.

Combination Method

In 1948, Penman derived the first combination equation. The equation eliminates the requirement of knowing the evaporating surface temperature in the mass transport technique by combining it with the energy balance technique (Van Bavel, 1966). The evaporation from a free water surface, E_o , with an albedo of 0.05 is evaluated as follows (Jensen et al., 1990):

$$\lambda E_o = \frac{\Delta}{\Delta + \gamma}(R_n - G) + \frac{\gamma}{\Delta + \gamma} \lambda (e_z^o - e_z) f(u) \quad (10)$$

In 1963, Penmen modified his formula to find the evapotranspiration of well-watered short grass (referred to as grass reference evapotranspiration, E_{ro}):

$$\lambda E_{io} = \frac{\Delta}{\Delta + \gamma} (R_n - G) + \frac{\gamma}{\Delta + \gamma} 6.43 W_f (e_z^o - e_z) \quad (11)$$

$$W_f = a_w + b_w u_2 .$$

Potential Evapotranspiration. Actual evapotranspiration from a surface depends on many different factors: climate, soil type, soil moisture content, vegetation type and depth of rooting, and land management practices (Sanderson, 1990). However, in order to facilitate the study of evapotranspiration, a conceptual evapotranspiration rate, which is only controlled by atmospheric factors is used, i.e. *potential evapotranspiration, Etp* (Shuttleworth, 1991).

There are different opinions on who developed the concept. In 1948, Thornthwaite defined potential evapotranspiration as the water loss from an extensive, closed, homogeneous cover of vegetation that never suffers from a lack of water. Later in 1954, he further specified an albedo between 0.2 and 0.25 (Sanderson, 1990). On the other hand, Penman (1948) used the evaporation from a free water surface under the influence of weather elements as a reference to compare the evaporation from other surfaces, bare soil and vegetation, under the same weather conditions. In 1956, he defined "the amount of water transpired in unit time by a short green crop, completely shading the ground, of uniform height and never short of water" (Jensen et al., 1990, p. 44) as potential evapotranspiration. In 1966, Gangopadhyaya et al. defined potential evapotranspiration as "the maximum quantity of water capable of being lost, as water

vapor, in a given climate, by a continuous, extensive stretch of vegetation covering the whole ground, when the soil is kept saturated" (Shuttleworth, 1991, p. 108).

Instead of finding the actual evapotranspiration, the Penman combination method estimates the potential evapotranspiration. Then an empirical coefficient based on crop, cropping stage and soil moisture is used to find the actual evapotranspiration. It is necessary to estimate the potential evapotranspiration of a surface that fulfills the water and vegetation requirement. Usually short grass and alfalfa are used for this purpose.

Reference Crop Evapotranspiration. Early researchers thought that if the soil moisture is always adequate, different vegetation types will consume the same amount of water, i.e. potential evapotranspiration (Sanderson, 1990). Shuttleworth (1991) suggested that the finding was caused by using only short crops. Later studies discovered that the maximum possible evapotranspiration varies by vegetation type, especially in an arid environment. As a result, a new concept *reference crop evapotranspiration* was created. It is the potential evapotranspiration for a specific reference crop. One advantage of this concept is that the coefficient used to find the evapotranspiration of another crop is based on a specific reference crop (Jensen et al., 1990).

Based on Penman's work, there have been many variations of the combined method. In 1982, Wright presented an equation for alfalfa-reference evapotranspiration, E_{tr} , referred to as the 1982 Kimberly-Penman by Jensen et al. (1990). The method is quite similar to Penman's method developed in 1963, which is a grass-reference evapotranspiration, E_{to} . In addition, it uses a different wind function, W_f . Cuenca (1989) mentioned that it is essential to use the specific wind function and vapor pressure deficit

$(d_a, e_z^o - e_z)$ for a particular method. If a calibrated wind function for the study area is available, it is preferred (Michael Kizer, personal communication, February, 1994).

Penman used short grass to find the potential evapotranspiration—actually grass-reference evapotranspiration. The FAO method uses grass of 8 to 15 cm tall as a reference crop. However, alfalfa is preferred in an arid region, for it can use its extensive root system to maintain a high transpiration rate even under dry conditions. As a reference crop, alfalfa should be at least 30 cm tall and stand erect. Alfalfa reference evapotranspiration is usually larger than grass reference evapotranspiration, especially in dry, windy conditions (Jensen et al., 1990).

In *Evapotranspiration and Irrigation Water Requirements* (Jensen et al., 1990), 13 methods were used to estimate evapotranspiration and the results were compared to lysimeters. The results showed that the 1982 Kimberly-Penman gave a low standard error of monthly and daily estimates. However, the daily estimates were only calibrated in three locations: Kimberly, Idaho, Coshocton, Ohio, and Davis, California. For the monthly estimates, 1982 Kimberly-Penman works better in arid locations, but not as well as 1963 Penman at humid locations. "Penman-Monteith and 1982 Kimberly-Penman methods are recommended for daily or longer periods because they provide reliable E_t estimates over a wide range in climatic conditions. The 1963 Penman and FAO-PPP-17 methods provide reliable estimates for grass reference evapotranspiration under semihumid and humid climatic conditions" (Jensen et al., 1990, p. 263).

Crop Coefficient. A crop coefficient, K_c , is used to find the E_t of a specific crop from the reference crop E_r . Throughout the growing cycle of a crop, the water used by

the crop changes. The FAO method divides the growing season into initial period, crop development period, mid-season period and late season period and the crop coefficient of a crop changes according to the period.

In 1982, Wright proposed another method to find the crop coefficient. He divided the crop coefficient into two parts: a coefficient based on the crop, K_{cb} and a coefficient of evaporation from a wet soil surface, K_s . The *basal crop coefficient*, K_{cb} , is the coefficient of the crop when there is enough soil moisture for the crop but the soil surface is dry. If the available soil moisture decreases, the basal crop coefficient is modified by another coefficient, K_a . A generalized crop curve is shown in Figure 7. The relationship between evapotranspiration and different coefficients are as follows:

$$E_t = K_c E_{tr} \quad (12)$$

$$K_c = K_{cb} K_a + K_s \quad (13)$$

If it is not practical to estimate the effect of wet soil, K_{cb} and K_s are not distinguished.

Instead, a *mean crop coefficient*, K_{cm} is used. The relationship between K_{cm} and K_c is:

$$K_c = K_{cm} K_a \quad (14)$$

The soil coefficient, K_a depends on the available soil moisture (Jensen et al., 1990). Unless there is an actual soil moisture measurement, a water budget procedure as that suggested by Thornthwaite is required to find the value. In reality, soil moisture measurements are rare in space and time over Oklahoma.

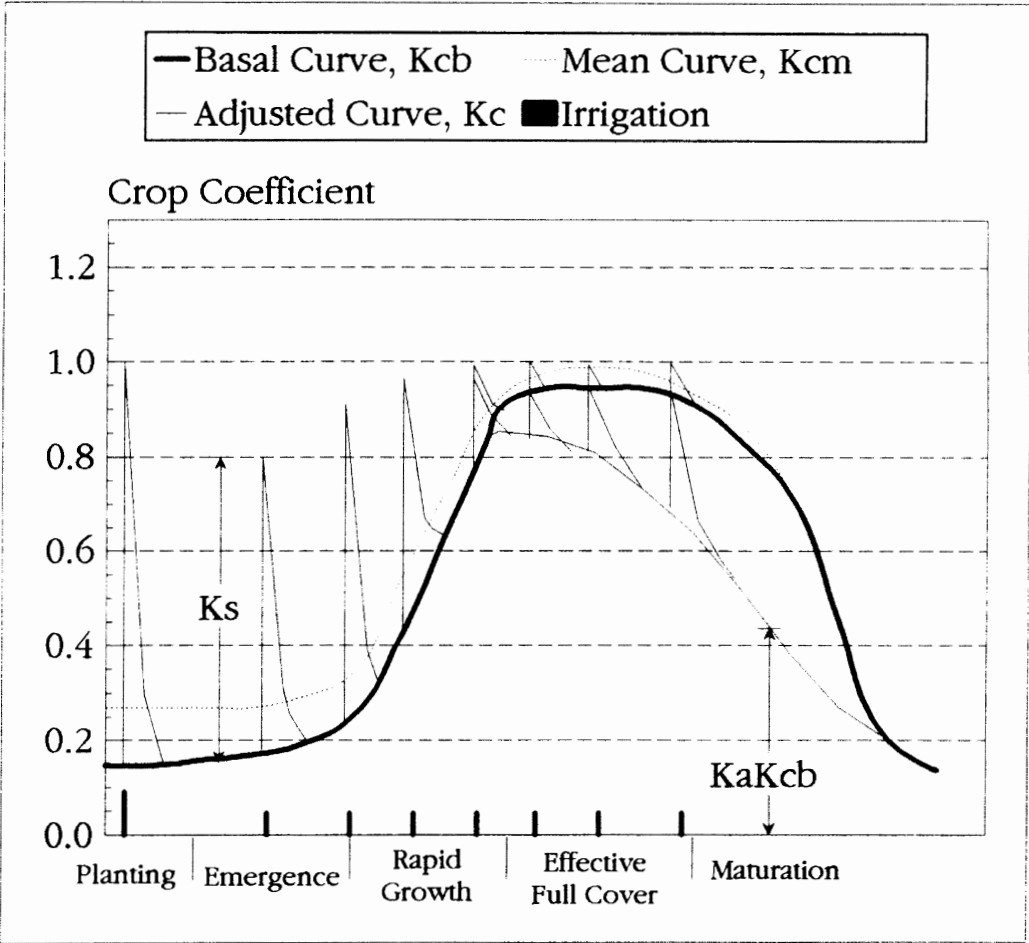


Figure 7. Generalized Crop Curves Showing the Effects of Growth Stages, Wet Soil Surface, and Limited Available Soil Water (Jensen et al., 1990; Wright, 1982).

Problems of the Combination Method

The Penman combination method is recommended for finding daily evapotranspiration (Jensen et al., 1990). In order to use the method, it is necessary to obtain the meteorological data with daily resolution. However, data are usually not available for the location of interest (Running, Nemani & Hungerford, 1987). In a study of forest evapotranspiration and photosynthesis, Running, Nemani and Hungerford employed a simulator called MT-CLIM to extrapolate daily meteorological data at a base weather station to the sites of interest, which were from 32 to 48 km away. However, the simulator is for a mountain microclimate and only adjusted for elevation and aspect. This is similar to using Thiessen polygons with value adjustment.

Even if data are available at the desired location, they are zero-dimensional point data. The result is point evapotranspiration. However, some applications, such as climate modelling, require characterization of regional evapotranspiration for very large areas, e.g. grid cells 500 km on a side (Running, 1991). For watershed, regional and global studies, data in continuous spatial scale are required (Running, Nemani & Hungerford, 1987). It is possible to use the water balance method for regional evapotranspiration estimation. However, it would tend to be unreliable at a daily resolution (Jensen et al., 1990).

Meteorological Data

The 1982 Kimberly-Penman method requires temperature, net radiation, wind speed, and vapor pressure measurements. Temperature is widely recorded, but only the

daily maximum and minimum are available in terms of regional studies. In 1992, there were 120 cooperative stations in Oklahoma that measured air temperature. Relative humidity, by contrast, is recorded at a few major airports. In the western United States, there is less than one primary station per 100,000 km² recording relative humidity and solar radiation (Running 1991; Running, Nemani & Hungerford, 1987). In Oklahoma this sparse spacing of stations seriously limited evapotranspiration studies until recently.

Oklahoma Mesonet

The Oklahoma Mesonet (Mesonet) consists of 111 automated observing stations (see Figure 8). At every station, rainfall, insolation, air temperature, relative humidity, air pressure, wind speed and direction, and soil temperature are measured (see Table II). The parameters are recorded every five minutes and then relayed back to a central processing site every 15 minutes. At about 50 stations, supplementary readings of air temperature, soil temperature and wind speed at different elevations, and leaf wetness are measured (Brock et al., 1994).

The average distance between stations is 35 kilometers (19 miles) (Crawford, 1993). With site standards set by a subcommittee, sites were selected to provide a fairly uniform coverage over the state. Moreover, the physical characteristics of a site are thought to represent the surroundings. The Mesonet sites are fairly level (with slope less than 5%), and have good ventilation. Uniform short grass is the preferred surrounding land cover. Irrigation areas, lakes, forests and urban areas are avoided. Recorded data are screened for basic errors (Brock et al., 1994). These data represent the most intense statewide system, in both space and time, in the country.

Oklahoma Mesonet

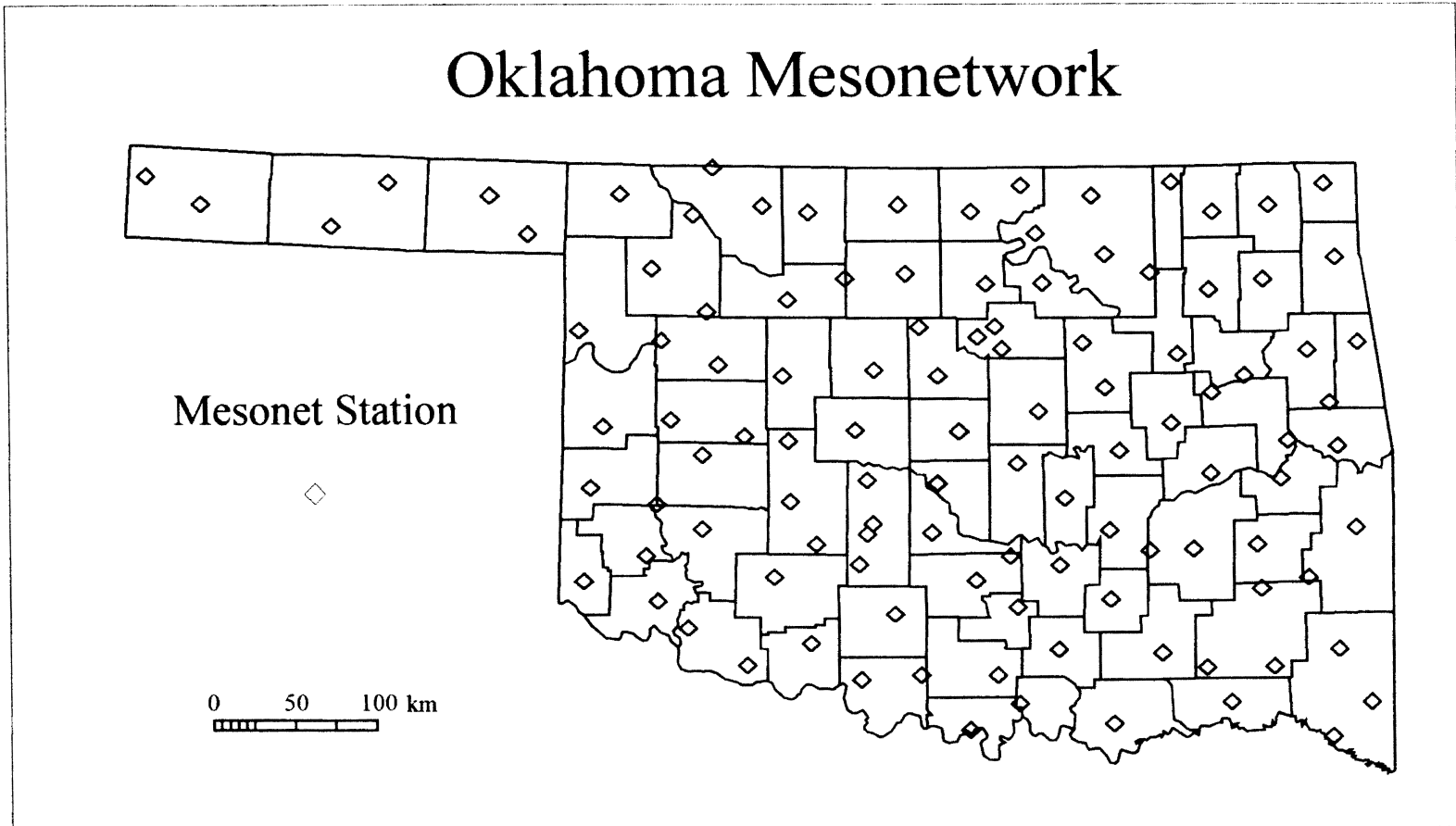


Figure 8. The Oklahoma Mesonet Stations.

TABLE II
VARIABLES MEASURED AT MESONET SITES

Variable	Height	Sensor	Resolution	Sample	Mean
Core					
Wind speed	10 m	Propeller-vane	0.03 m s ⁻¹	3 s	5 min
Wind direction	10 m	Propeller-vane	0.05 °	3 s	5 min
Air temperature	1.5 m	Thermistor	0.01 °C	3 s	5 min
Relative humidity	1.5 m	Capacitive sorption sensor	0.03 %	3 s	5 min
Barometric pressure	0.75 m	Barometer	0.10 hPa	12 s	5 min
Rainfall	0.6 m	Rain gauge	0.25 mm	N/A	5 min
Solar radiation	1.8 m	Pyranometer	0.23 W m ⁻²	3 s	5 min
Soil temperature	-10 cm	Thermistor	0.03 °C	30 s	15 min
Supplemental					
Wind speed	2 m	Cup anemometer	0.25 m s ⁻¹	3 s	5 min
Soil temperature	-5 cm	Thermistor	0.03 °C	30 s	15 min
Soil temperature	-30 cm	Thermistor	0.03 °C	30 s	15 min
Air temperature	9 m	Thermistor	0.03 °C	3 s	5 min
Leaf wetness	1 m			30 s	15 min

(Brock et al, 1994)

Conclusions

Water supply is important for agriculture and industries. In the arid regions, e.g. western United States, understanding of evapotranspiration is important for more effective water conservation. Moreover, evapotranspiration converts part of the insolation to latent heat of vaporization. This partition of energy influences meteorology from local to global scales (Running, 1991).

Although the mechanism of evapotranspiration is well known, measuring it directly is not an easy task. The lysimeter is regarded as the most accurate method, but it is not widely available. The concepts of potential evapotranspiration and reference crop evapotranspiration are important and methods have been developed to estimate potential evapotranspiration; among them, Penman's combination method is the most theoretically sound. Studies demonstrate that the method can provide accurate estimation for daily, or smaller, time step. There are many variations of combination methods; the 1982 Kimberly Penman method estimates the alfalfa reference evapotranspiration and performs well in the arid western United States.

One limitation of Penman's method has been the data requirement. Relative humidity and solar radiation are rarely measured. Even for places where required data are available, the point data can only provide point evapotranspiration estimation.

With the Oklahoma Mesonet, for the first time, all the required meteorological data for evapotranspiration estimates are available in both high spatial and temporal resolution over a considerable area. The meteorological data provide valuable point

evapotranspiration estimations, while the high density of observations makes it possible to study the relationship between point and regional evapotranspiration.

Spatial autocorrelation is a basic property of most spatial data (regionalized variables or spatial attributes). This provides a basis for interpolation; measuring data at all locations is impossible and unnecessary. Many interpolation methods have been used. Kriging has gained recent attention for it is a best linear unbiased estimator. It is an exact method and is the only one that provides estimation variance. Meteorology and mining contributed to the development of this method and it is quite natural to apply it to evapotranspiration and other meteorological elements.

Some studies show that kriging outperforms other interpolation methods. However, no single method is best for all situations. The biggest drawback of kriging is the demanding computational requirements. However, as computers become more powerful, this becomes less of a concern. It is valuable to see if kriging can improve regional evapotranspiration estimation.

Oliver and Webster (1990) strongly recommended geographical information systems (GIS) to incorporate kriging. Now, both ordinary and universal kriging are provided in ARC/INFO 6.1.1, which was available to the current researcher. In addition, the output surface can be used readily in further analyses.

CHAPTER III

METHOD

Design

Objectives

The purpose of this study is to investigate the effectiveness of using kriging on reference evapotranspiration (E_r) derived from Mesonet data. There are different ways to characterize effectiveness, for example, accuracy, information gained, time, etc. Moreover, the effectiveness usually depends on the situation; so there is no standard definition. In this study, effectiveness of kriging will be judged by the apparent accuracy of the results and the information gained.

The purpose, as given in Chapter I, has been operationalized into four specific objectives. The first one is to examine if there is any difference between using various spatial resolutions. If there is no difference between the spatial resolutions of the interpolating surface, it would be computationally more efficient to use a coarser resolution. However, if too big a cell size is used, even if the results are accurate, the information gained may not be enough to meet the requirements of certain applications.

The second objective is to find the best resolution. Finer spatial resolution provides more information, but not necessarily more accurate. It is important that the

result is accurate. If a certain resolution is more accurate, then the regional evapotranspiration of a larger area would be better obtained by aggregating the interpolated result of that resolution.

The third objective is to compare the results of kriging, inverse distance weighting (IDW) and Thiessen polygons because these are the three primary spatial interpolation techniques in use today. Thiessen polygons are used to find regional aggregates while inverse distance weighting gives point results. If there is no difference between the methods, there is no reason to use kriging, which is the most complicated method.

The fourth objective is to compare the results of interpolating derived E_r and deriving E_r from interpolated meteorological data. Evapotranspiration is influenced by more than one meteorological factor, and the contribution of each factor is not linear. Two locations can have the same evapotranspiration resulting from two different sets of meteorological factors. Instead of just interpolating the E_r from point data to an E_r surface, individual meteorological factors can be interpolated and then used to estimate the E_r . The question is whether the latter method will be significantly better than the former one. Through these four objectives, the study will try to shed light on the effectiveness of kriging in interpolating reference evapotranspiration.

Study Area

Oklahoma was chosen to be the *study area* because of its Mesonet network. All 111 automated weather stations record the required meteorological elements—air temperature, relative humidity, air pressure, solar radiation, and wind speed, every five minutes (Brock, 1994). Although the Mesonet network has stations in every county of Oklahoma, only the

"main body" of Oklahoma was included in the study (see Figure 9). As interpolation becomes suspect with non-rectangular study areas, the three counties of the Oklahoma Panhandle were not included. However, in order to include as many stations as possible, the boundary of the study area actually extended outside of Oklahoma.

The 180,000 km² study area was rectangular in shape, with a dimension of 513 km by 351 km with the longer side in the east-west direction. It was the extent used for actual interpolation. However, the extent of interpolation at 1 km and 3 km resolutions were smaller than the study area as described above. It was because two stations at the southeast corner of Oklahoma were not in service at that time. It is a property of the kriging command in ARC/INFO that the outermost data points and the resolution affect how far from the data points the edge of interpolation can be.

The study area was selected to capture as many stations for interpolation as possible. On the other hand, because interpolation becomes unreliable at the edge, a fringe of 27 km on all sides was excluded from the comparisons. Furthermore, the study area extended well out of Oklahoma at the southwest corner, where no Mesonet station is located. To minimize this effect, an area of 4,293 km² was also excluded from analysis. The remaining 132,030 km², where the results of various interpolations were compared, was the *test area*.

Map Projection

As the study area was 513 km wide, stretching across two UTM zones (14 and 15), the handling of map projection should be careful. In interpolation, distance is the most important parameter. However, there is no true equidistant projection. Instead, the

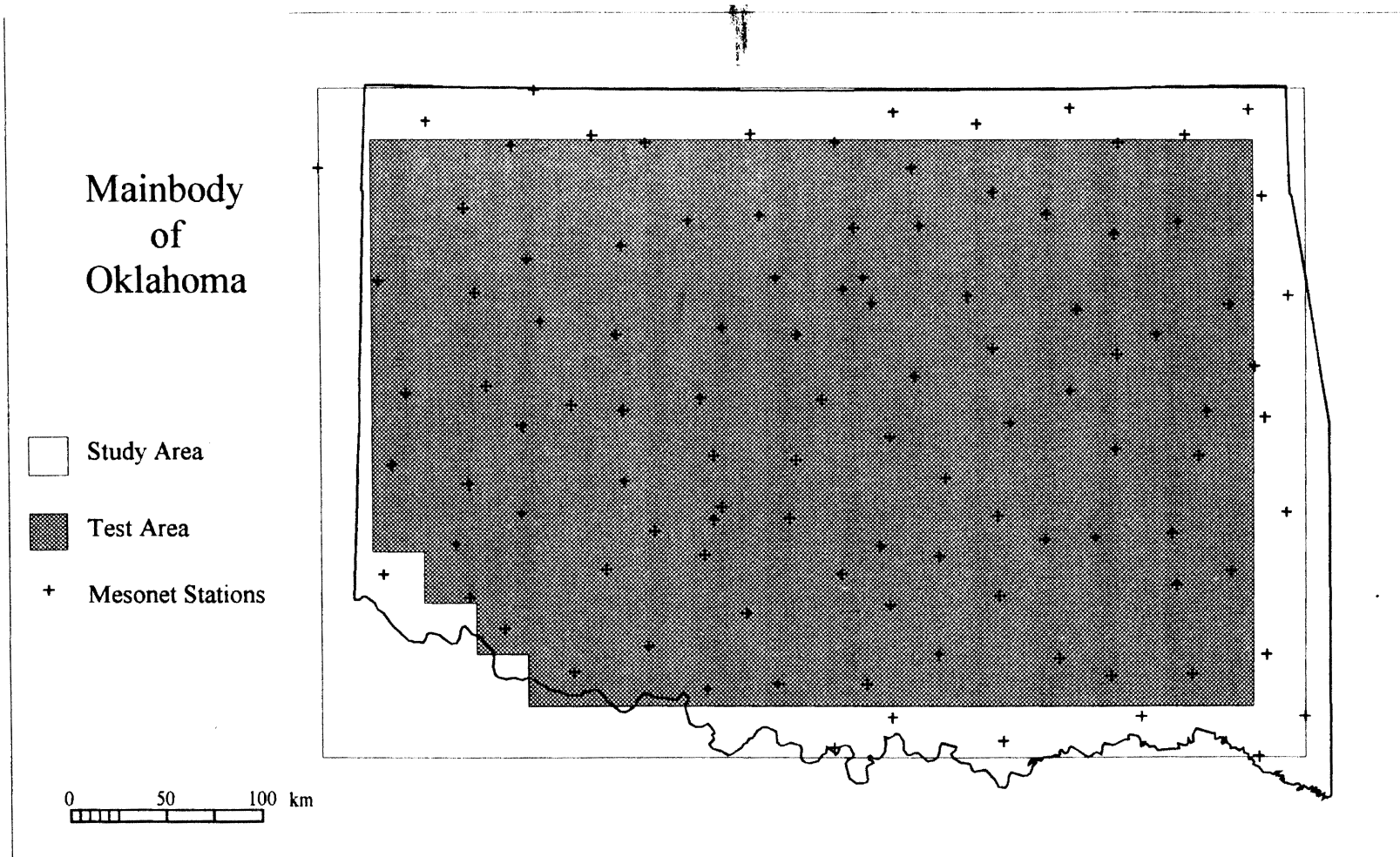


Figure 9. The Extent of the Study Area, Test Area and Main Body of Oklahoma.

Albers Conic Equal Area projection was used. The projection is suited for mid-latitude study areas with longer east-west dimensions (Synder, 1987). The parameters of the projection are shown in Appendix B. The first and second standard latitudes was chosen so that the error factor at the middle latitude was the reciprocal of the error factors at the north and south bounding latitudes (Synder). An offset is added to the center meridian to avoid negative coordinates. The coordinates of the southwest and northeast corners were designated as (326000, 426000) and (839000, 777000) in meters respectively.

Study Dates

The Oklahoma Mesonet has been in full operation since the start of 1994. As winter temperatures are low and most plants are dormant, the actual evapotranspiration is low during winter. Therefore, three warm season days in 1994 were chosen as study days. Moreover, the study days were to be non-rainy with no synoptic influence. The lack of significant frontal or upper air forcing was to make the interpolations made in this thesis usable in the context of the larger National Science Foundation Surface Water Hydrology study of which it was a part. As a result, March 3, May 6, and June 16 of 1994 were chosen as study days.

On March 1, it generally rained across Oklahoma. It continued to rain in eastern Oklahoma on the next day. Then the rain died down on March 3. That date was chosen to test the data and methods in the early phase of research and remained as one of the study days. The main study days are May 6 and June 16, when the vegetation was mostly green and the solar radiation was higher. These three days were chosen to insure that the

results are not likely date-dependent. Because of limited study days, this thesis made no attempt to characterize evapotranspiration by weather type.

Units of Measurement

Although Imperial units are used in the United States, SI units are the standards for scientific investigations. Therefore, SI units were used in this study. Moreover, the data collected from Mesonet stations are in SI units. To facilitate understanding, other units are given wherever it is appropriate. The measurement of evapotranspiration is in millimeters (mm) as in measuring precipitation. In order to assure the consistency of data, Central Standard Time was used rather than Daylight Saving Time. Though calendar day is used, all study days begin at Greenwich Mean Time 18:00 (Central Standard Time Midnight).

Spatial and Temporal Resolution

In order to investigate the effect of spatial resolution on interpolation, various spatial resolutions were used for analysis. The resolutions used were 1 km, 3 km, 9 km and 27 km. The 1 km resolution was used because it is close to the 1.1 km grid cell size of the AVHRR data used in so many regional studies. Besides, for studies of surface-atmospheric interaction, 1 km by 1 km is a known resolution that might be significant. This relates to the size orders of convective cloud development. The original data were interpolated into a surface with value points of regular spacing, which is called a *lattice*.

The other resolutions were chosen so that the resulting lattices of all resolutions had a common factor besides one. The dimensions of the study area are 513 km by 351

km, which are common multiples of the four resolutions. The aggregated value from a finer resolution is, therefore, directly comparable to a coarser one. Furthermore, the odd resolutions ensure that the lattices of all four resolutions fit within each other. For example, any value point of a 27 km lattice is also a value point of the other three lattices.

A summary of the spatial resolution is shown in Figure 10. The crosses represent the center of the 1 km cells, and the circles, pluses and triangles represent the centers of 3 km, 9 km and 27 km cells respectively. When the original lattices of two resolutions were compared, only those cells with spatially coincident centers were used. For comparisons of resampled lattices, all the inscribed cells of the finer resolution were used (see section Difference between Resolutions of this chapter).

Although the Mesonet data are measured every five minutes, the reference evapotranspiration was only estimated at the daily scale and required hourly data. In most applications, like irrigation, daily evapotranspiration estimates are the most common in the literature. Moreover, the main concern of this study is interpolation rather than the specification of E_{tr} on sub-daily time scales.

Equipment and Tools

Evapotranspiration Estimation. A variation of the 1982-Kimberly Penman method was used to estimate the daily alfalfa-reference evapotranspiration, E_{tr} . A research project in the mid-1980s in Fort Cobb, Oklahoma used this method and obtained a calibrated wind function (Michael Kizer, personal communication, February, 1994). This wind function was used in place of that derived from Kimberly, Idaho. The equation used in this thesis was:

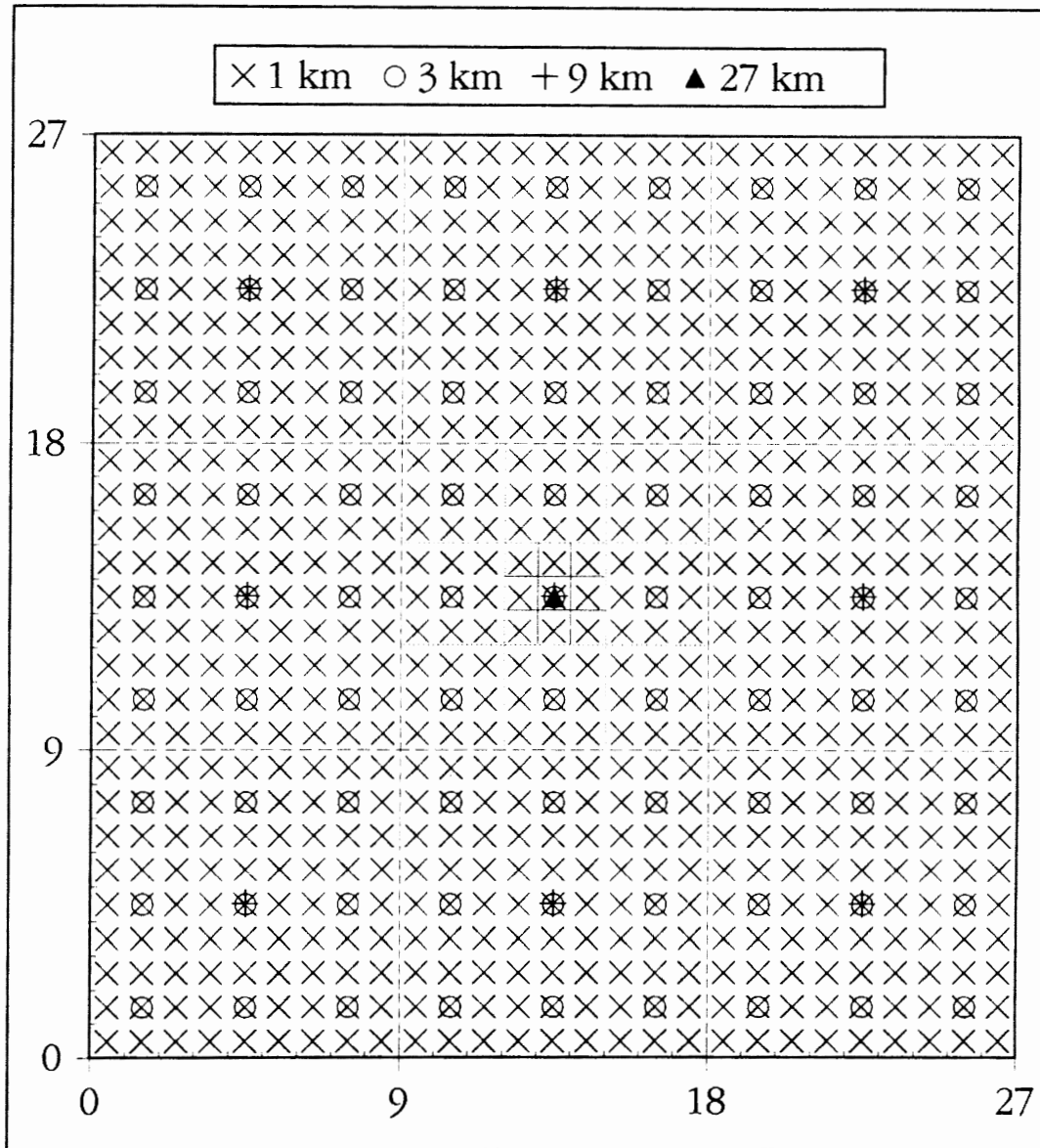


Figure 10. Relationship between Lattices of Various Resolutions.

$$\lambda E_{tr} = \frac{\Delta}{\Delta + \gamma} (R_n) + \frac{\gamma}{\Delta + \gamma} 6.43 W_f (e^o - e)$$

where

(15)

$$W_f = -0.3405 + 0.93312 u_2 .$$

The soil heat flux, G , found in the original equation was assumed to be negligible in daily resolution. As shown in the literature review chapter, the combination method was used because it provides good estimation at daily resolution. In addition, as the method is based on the meteorological control of evapotranspiration, the Mesonet provides the required data at a spatial scale previously unprecedented.

Alfalfa-reference evapotranspiration was chosen instead of actual evapotranspiration because the latter requires landscape-related data to supplement meteorological elements. E_{tr} is the evapotranspiration requirement based on meteorological conditions with alfalfa as a reference crop. Rather than interpolating actual evapotranspiration, it was more straightforward to apply the interpolated E_{tr} in finding actual evapotranspiration.

ARC/INFO. ARC/INFO 6.1.1 (1992) for Sun OS4 running on a Sun IPC workstation with 12 Mb of memory was used for the estimation of E_{tr} and interpolation. ARC/INFO is one of the most popular geographical information systems (GIS) and 6.1.1 was the latest version at the time of the study. It has both vector and raster ability. Although most of this study was done in the GRID module using raster operations, vector operations were required as in Thiessen polygons.

The map projection ability of ARC/INFO facilitated the setup and input of data. Also, these results can be applied to other studies without tedious conversion. ARC/INFO 6.1.1 contains all the interpolation methods required in this study. Performing all operations in one package is an attractive approach. While kriging is available in both TIN and GRID modules, the one in the GRID module was chosen. On one hand, TIN and GRID recognize coordinate of extent differently; on the other hand, most operations used in this study were in GRID. Therefore, it was more convenient and consistent to perform kriging in the GRID module.

S-PLUS. S-PLUS 3.2 for Sun workstation (Release 1) with ARC/INFO Link was used for the statistic analyses (1993). Preliminary analyses were done in Systat 5.03 for Windows, Version 5 (1992) and Quattro Pro for Windows, Version 5 (1993) on a personal computer. While the other packages work, the conversion of data was found to be more convenient in S-PLUS and it was not necessary to transfer data from one platform to another.

Procedures

Preparing Daily Meteorological Data

The Mesonet data were converted into files of INFO, which is the internal database of ARC/INFO. While there are Mesonet data every five minutes, only data *at the hour* were used. Daily meteorological data were calculated from the 24 hourly files. The hourly data used were air temperature (T), relative humidity (RH), wind speed at 10 m (u_{10}), air pressure (P), and solar radiation (R_s , $W m^{-2}$). Hourly saturation vapor pressure

(e^o), saturation vapor pressure at dew point (e_d), and vapor pressure deficit (d_a), were calculated by the following equations (Jensen, Burman & Allen, 1990):

$$e^o(i) = 3.38639 [(0.00738 T(i) + 0.8072)^8 - 0.000019 |1.8 T(i) + 48| + 0.001316] \quad (16)$$

$$e_d(i) = \frac{e^o(i) \times RH(i)}{100} \quad (17)$$

$$\begin{aligned} d_a(i) &= e^o(i) - e(i) \\ &= e^o(i) T(i) \left[\frac{100 - RH(i)}{100} \right] \end{aligned} \quad (18)$$

Besides the above elements, the fourth power of the absolute temperature required for the estimation of net outgoing long-wave radiation, R_{bo} , was also calculated on an hourly basis:

$$T^4(i) = [T(i) + 273.2]^4, \text{ K} \quad (19)$$

The next step was to calculate the daily value for T , RH , u_{10} , R_s , P , e_d , d_a , and T^4 . Except for R_s , the daily value of all other elements was the 24-hourly mean (mean of the 24 at the hour values). The 24-hourly mean was used because this would characterize the whole day better than just using the maximum and minimum values. For solar radiation, the Mesonet measures the power (W m^{-2}) instead of the energy. Although broken or scattered cloudiness might produce significant variations in the solar flux for time periods

much shorter than an hour, the hourly reading was treated as a sample for the whole hour. Therefore, the daily R_s , in MJ m^{-2} , was 3.6×10^{-3} times the 24-hourly sum, in W m^{-2} .

Bad Data. Sometimes, missing values or bad data may be found in the Mesonet files. When such a flag was found in the hourly T , RH , R_s , u_{10} , or P , the station was flagged as invalid; the station was excluded from subsequent interpolations. In addition, visual examination of the data was performed to detect other possible errors.

Wind Speed at 2 m. The Penman equation requires wind speed at 2 m. Although wind speed at 2 m, u_2 , is measured in Mesonet, only about half of the stations have this. In order to use as many sites as possible, the wind speed at 10 m was used and was adjusted to 2 m by the following equation (Jensen, Burman, & Allen, 1990):

$$u_2 = u_{10} \frac{\ln[(z_2 - d)/z_o]}{\ln[(z_{10} - d)/z_o]} \quad (20)$$

The zero plane displacement of wind profile, d , was $2/3$ of the height of crop canopy, h_c , which was assumed to be 50 cm; the roughness length of momentum, z_o , was 0.123 times h_c . z_2 was 200 cm and z_{10} was 1000 cm. To verify the conversion, the daily u_2 was also calculated wherever available. Then the correlation between measured u_2 and estimated u_2 was examined.

The extrapolated u_2 and measured u_2 were highly correlated, but the former was found to be consistently lower than the latter. The Pearson's correlation between extrapolated and measured u_2 was 0.98 ($p < .01$) on all study days. The mean differences

were 0.10 m s^{-1} , 0.43 m s^{-1} and 0.65 m s^{-1} for March 3, May 6 and June 16 respectively. This could be attributed to the vegetative cover at most sites being shorter than 50 cm.

Estimating Alfalfa-Reference Evapotranspiration

After all required daily meteorological data were ready, the daily E_{tr} for every valid station was estimated. All intermediate variables were saved as a separate item in the INFO file. Eventually, the E_{tr} , in mm d^{-1} , was stored as an item. The equations and program used are found in Appendix B.

In addition, E_{tr} was derived from interpolated meteorological data. The daily T , u_{10} , P , R_s , e_a , d_a , and T^d were interpolated by ordinary kriging, as described in the next section, to four lattices of different resolutions. Then these lattices were used to find the daily *estimated* E_{tr} using the GRID language (see Figure 11). All intermediate variables were saved as separate lattices.

Interpolating Zero-Dimensional Data to a Surface

The point daily E_{tr} data were interpolated to a two-dimensional surface. The physical surface is two-dimensional, but the interpolation methods treat the value of the spatial attribute, in this case E_{tr} , as the third dimension. Kriging, inverse distance weighting (IDW) and Thiessen polygons were used.

Kriging. The "kriging" function of the GRID module in ARC/INFO was used to interpolate the E_{tr} into surfaces. Before the interpolation, variograms were created to examine the spatial dependence of the attributes of interest. The default spherical model

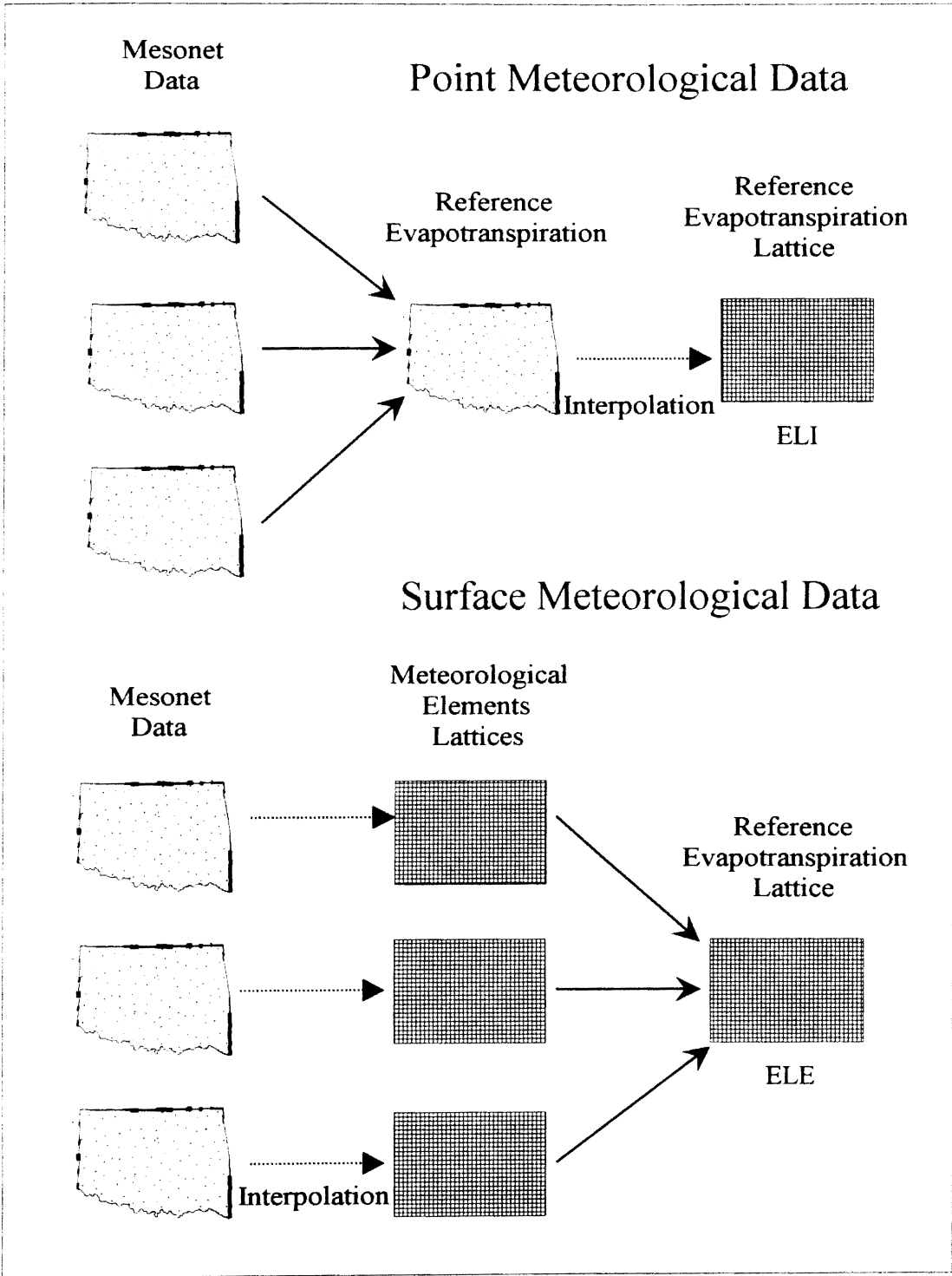


Figure 11. Procedures of Deriving Reference Evapotranspiration Lattices from Point and Surface Meteorological Data.

was chosen to fit the variogram and ordinary kriging. Other models were examined but none provided a better fit.

Then the spherical model was used to fit variograms created by using different numbers of sample points and searching radii. Instead of using all the observations, a moving window was used to construct the variogram. The sample point option uses the specified number of observations nearby, while the radius option searches for observations within the specified radius (ARC/INFO, 1992). The variogram was examined by eye to judge its fit. Fitted variograms with low nugget variance that resembled the actual variograms were preferred. The parameters, which were best fit in most cases, were selected for subsequent kriging. Although some methods, other than fitting by eye, were suggested by McBratney and Webster (1986) to find the best model, those procedures are too computationally intensive and were not included in this study.

May 6 was used to search for the best kriging parameters, which were then used for the other two study days. Sample points from 12 to 96, with increments of 12, were examined. Radii from 20 km to 140 km, with increments of 20 km, were also examined. The attributes examined included E_r , T , u_{10} , P , R_s , e_d , d_a , and T^d . After variograms of the above attributes for all four desired spatial resolutions were examined, a searching radius of 120 km was selected for kriging. Moreover, the variograms did not show significant drift. This eliminated the need to use universal kriging, which requires more intensive computation and in which no variogram is available for examination. Examples of the variograms produced are found in Appendix D.

Each of the eight attributes necessary to calculate E_r was interpolated to four lattices: 1 km, 3 km, 9 km and 27 km. Variance lattices (the estimation variance of

kriging) were also created. The names of the lattices for each attribute are shown in Table III. The four interpolated E_r lattices were designated ELI1, ELI3, ELI9 and ELI27. The four estimated E_r lattices from surface meteorological data were ELE1, ELE3, ELE9 and ELE27.

Inverse Distance Weighting. The "idw" function in GRID was used to interpolate the point E_r to a surface. A power of 2, the default, was used. A searching radius of 120 km was used so that the result was more comparable to that of kriging. The resulting E_r lattices were ELD1, ELD3, ELD9, and ELD27.

Thiessen Polygons. Thiessen polygons for the study area were created by the ARC/INFO command "thiessen". The E_r of each polygon was the estimated E_r at that station. Figure 12 is the Thiessen polygons of May 6, 1994. The Thiessen polygons were then converted into four lattices—ELT1, ELT3, ELT9 and ELT27, which had corresponding cell sizes of 1 km, 3 km, 9 km and 27 km.

Preparing Data for Statistical Test

As the lattices of all four resolutions fit with each other, they could be compared directly. However, while a value in the 27 km lattice represents 729 km², the value of the same location on the 1 km lattice represents 1 km² (the lattice is viewed as a discrete cells). Conversely, every value point of the 27 km lattice has 729, 81, and 9 equivalent value points on the corresponding 1 km, 3 km and 9 km lattices respectively. The relationship is shown in Table IV. The finer resolution was resampled to the coarser resolution for comparison using the nearest neighbor interpolation.

TABLE III
 INTERPOLATED LATTICES AND VARIANCE LATTICES OF DIFFERENT
 ATTRIBUTES CREATED BY KRIGING

Attributes	Symbol	Lattice ^a	Variance ^a
Daily Alfalfa Reference Evaporation	E_r	ELI x	ELV x
Air Temperature	T	TAIR gx	TAIR vx
Wind Speed at 2 m	u_2	WSP2 gx	WSP2 vx
Air Pressure	P	PRES gx	PRES vx
Solar Radiation	R_s	SRAD gx	SRAD vx
Saturation Vapor Pressure at Dew Point	e_d	EDEW gx	EDEW vx
Vapor Pressure Deficit	d_a	EDEF gx	EDEF vx
Air Temperature to the Power 4	T^4	TAIR4 gx	TAIR4 vx

^a The x is the size of resolution, e.g. ELI1, ELI3, ELI9, ELI27

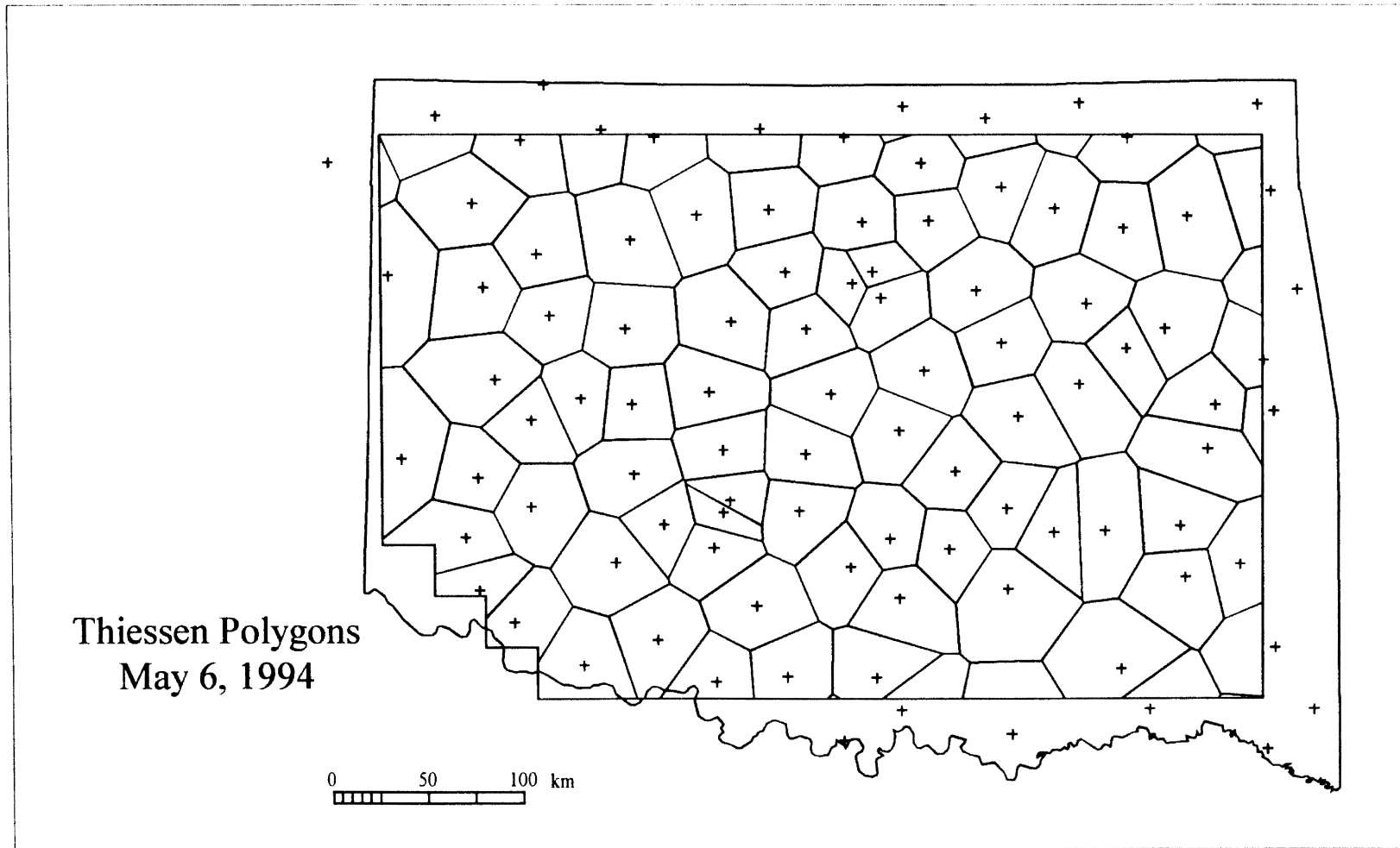


Figure 12. Thiessen Polygons Created from Mesonet Stations, May 6, 1994.

TABLE IV
CONFIGURATION OF DIFFERENT SPATIAL RESOLUTIONS

	Eastings ^a	Northings ^a	
Maximum (m)	839,000	777,000	
Minimum (m)	326,000	426,000	
Dimension (km)	513	351	
Resolution	Columns	Rows	Number of Points
Study Area			
1 km	513	351	180,063
3 km	171	117	20,007
9 km	57	39	2,223
27 km	19	13	247
Test Area			
1 km	461	299	132,030
3 km	153	99	14,661
9 km	51	33	1,629
27 km	17	11	181

^a Albers conic equal area projection, see Table X in Appendix.

Besides comparing the values of the coincident lattice points (original lattice), values of the coarser lattice were also compared with all the inscribed values in each finer lattice. To achieve this goal, the mean of the inscribed cells was calculated, and then the mean was resampled to coarser resolutions. Every value of the coarser resampled lattice was the mean of all inscribed values on the original lattice. Figure 13 is an illustration of the procedure.

In addition, all cells were further divided into five *subsets* by distance from Mesonet stations. The subsets were 0 km, 0.1 to 10 km, 10.1 to 20 km, 20.1 to 30 km and over 30 km. Depending on the number of valid stations, the actual locations and cell number of each subset varied from one study day to another (see Appendix A).

Method of Investigation

Difference between Resolutions

Descriptive Statistics. The descriptive statistics of ELI1, ELI3, ELI9 and ELI27 were compared. The maximum, minimum, mean, quantiles and other measurements were examined. This served as a qualitative comparison between different resolutions. In addition to this, the positive and negative differences between different lattices were examined. Means of positive and negative difference were calculated for the whole surface and subsets.

Correlation and Statistical Tests. Correlations and differences between the whole surface and different subsets were examined. Pearson's product-moment correlation between each pair of the four lattices was calculated. In addition, a paired-t test was used

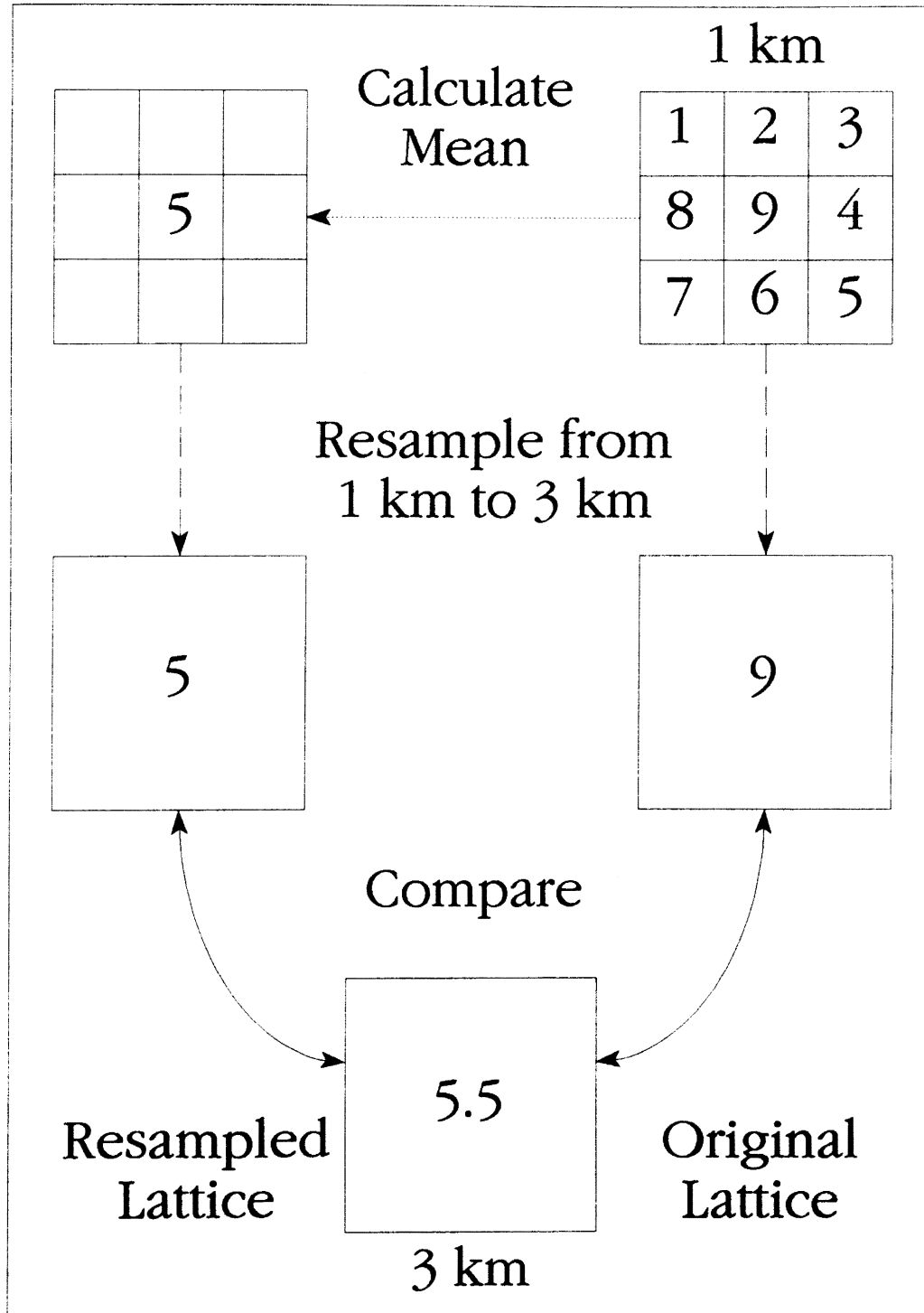


Figure 13. The Procedures of Comparing Original Lattice and Resampled Lattice.

to test if there was any difference between the four lattices. Altogether, thirty correlation and paired-t tests were performed for the original lattices. The same tests were repeated for the resampled lattices.

Best Resolution

Descriptive statistics of the variance lattices of different resolutions were examined and compared. Lattices of percentage interpolation-error was derived. Interpolation error of kriging were two times the square root of estimation variance (ARC/INFO, 1992). There was a 95.5% probability that the actual E_r was within interpolated E_r plus and minus the interpolation error.

A Jack-knife procedure similar to the one described by Phillips, Dolph and Marks (1992) was carried out for May 6 and June 16. One Mesonet station was removed and then kriging was performed. The interpolated E_r at the removed station was compared to the original value. The same procedure was repeated for all stations using the four resolutions.

"Kriging-error" (Kerror), different from the interpolation error of kriging, was the difference between interpolated E_r and E_r . The sum and mean kriging-error were examined. The sum and mean of absolute kriging-error were calculated too. Paired t-tests were performed and Pearson's product-moment correlation was calculated.

Difference between Interpolation Methods

Inverse Distance Weighting (IDW). The lattices from kriging were compared to those from IDW, e.g. ELI1 and ELD1. The mean positive and negative differences

between kriging and IDW were calculated for all resolutions. The spatial distribution of the positive and negative differences was examined.

Pearson's product-moment correlation and paired t-test results were then examined. For all four resolutions, the interpolated surface from kriging and that from IDW were compared. The five subsets were also compared. A total of six paired t-tests were performed for every resolution.

In addition, the jack-knife procedure was performed for May 6 and June 16 using IDW. The "IDW-error" (Derror) was also compared with the kriging-error (Kerror). Paired t-test were used to test the difference between IDW and kriging.

Thiessen Polygons. Thiessen polygons were created and converted to lattices of different resolutions. Then the lattices were compared with E_r , generated by kriging of the same resolution (for instance, ELI1 versus ELT1). The mean positive and negative differences were calculated. The spatial distribution of differences between surfaces was reviewed. The same statistics were calculated for the whole surface and all five subsets. Correlation and paired t-test results were also used.

The jack-knife procedure was performed for Thiessen polygons. The "proximal-error" (Nerror) of any station was the difference between the E_r of the nearest Mesonet station and the estimated E_r of that station. The proximal-error was compared with the kriging-error. The E_r of the nearest station was compared with kriging.

Point and Surface Meteorological Data

Finally, the lattices from point and surface meteorological data were compared, e.g. ELI1 was compared with ELE1. Correlation analysis and paired-t test were used. The mean positive and negative difference were calculated for the whole surface and subsets. The spatial distribution of difference was examined.

Conclusions

Paired t-tests and Pearson's product-moment correlation were used in all comparisons. Besides considering the whole surface, the test area was divided into five subsets by distance from Mesonet stations. Positive and negative differences were examined separately so that they would not offset each other. Spatial view of the positive and negative difference was used to find any pattern.

The jack-knife procedures were performed using kriging, IDW and nearest neighbor (proximal station). They were compared with the estimated E_{ir} . Then the IDW-error and proximal-error were compared with kriging-error.

CHAPTER IV

RESULTS

Alfalfa-Reference Evapotranspiration

Summary of Weather

To gain an idea of the impact of various meteorological conditions on evapotranspiration, three days were chosen for study. The three study days were March 3, May 6, and June 16, 1994. Table V is a summary of the weather elements measured at Oklahoma Mesonet (Mesonet) sites. The spatial variation of individual weather element are found in Appendix C. March 3 was a mild day with a mean air temperature (T) of 12 °C. The air temperature was highest in the west and lowest in the northeast. The relative humidity (RH) was above 60% in most of the area except for the northwest corner, where RH was below 50%. The mean vapor pressure deficit (d_a) was 0.78 kPa while that of the northwest corner was close to 1.4 kPa. The mean solar radiation (R_s) was 17.9 MJ m⁻². The mean wind speed at 10 m (u_{10}) was 3.35 m s⁻¹.

May 6 was a warm day with a mean T of 22.6 °C. The air temperature was highest in the southwest and lowest in the northeast. The RH was about 80% throughout the interpolation area except for the northwest, where RH was around 70%. The mean d_a , 0.61 kPa, is the lowest of the three study days. The highest d_a was found in the

TABLE V
SUMMARY OF STUDY DAYS

	March 3	May 6	June 16
Number of Stations	96	97	103
Air Temperature /°C			
Maximum	16.70	25.45	30.10
Minimum	8.60	20.19	25.17
Mean	12.00	22.55	27.62
Standard Deviation	1.68	1.12	0.88
Relative Humidity /%			
Maximum	77.6	89.5	92.6
Minimum	35.7	68.8	60.5
Mean	63.0	80.8	74.6
Standard Deviation	8.30	4.2	6.1
Vapor Pressure Deficit /kPa			
Maximum	1.45	0.98	1.86
Minimum	0.42	0.28	0.30
Mean	0.78	0.61	1.04
Standard Deviation	0.21	0.15	0.29
Air Pressure /kPa			
Maximum	100.27	100.37	100.70
Minimum	92.83	92.25	92.23
Mean	97.85	97.23	97.55
Standard Deviation	1.63	1.64	1.77

TABLE V (Continued)

	March 3	May 6	June 16
Solar Radiation /MJ m ⁻²			
Maximum	22.30	26.31	29.78
Minimum	12.31	10.56	13.13
Mean	17.94	19.58	22.04
Standard Deviation	1.16	3.53	3.01
Wind Speed at 10 m /m s ⁻¹			
Maximum	6.92	7.36	11.25
Minimum	1.24	1.13	0.90
Mean	3.35	5.12	6.48
Standard Deviation	1.11	1.30	2.22
Extrapolated Wind Speed at 2 m /m s ⁻¹			
Maximum	4.51	4.80	7.34
Minimum	0.81	0.74	0.58
Mean	2.19	3.34	4.23
Standard Deviation	0.72	0.85	1.45
Alfalfa-Reference Evapotranspiration /mm			
Maximum	6.70	6.93	11.81
Minimum	2.33	2.16	3.34
Mean	3.72	4.69	6.66
Standard Deviation	0.82	1.08	1.43

southwest. The mean R_s was 19.6 MJ m^{-2} . However, values close to 10 MJ m^{-2} were found in the northeast and southeast. The mean u_{10} was 5.12 m s^{-1} .

June 16 was a hot day with a mean T of $27.6 \text{ }^\circ\text{C}$. The mean RH was 74.6% . It was lowest in the northwest, 60% , and increased to over 90% in the southeast. The mean d_a , 1.04 kPa , was highest among the three study days. The mean R_s was 22 MJ m^{-2} . Low values were found in the north central area. Except for the southeast corner, the study area was very windy. the mean u_{10} was 6.48 m s^{-1} .

Reference Evapotranspiration

March 3, 1994. The number of reporting stations with 24 hours of data in the study area on March 3, 1994 was 96 (see Figure 14). The E_{tr} ranged from 2.33 mm to 6.70 mm , with a mean of 3.72 mm and a standard deviation of 0.82 mm . Clayton had the lowest E_{tr} while Cheyenne had the highest. The general trend of E_{tr} was lowest in the southeast and highest in the northwest. The estimated E_{tr} of March 3, 1994 is shown in Figure 15. The large "+" mark indicates that the E_{tr} was above mean plus one standard deviation; the small "+" mark indicates that the E_{tr} was below mean minus one standard deviation.

May 6, 1994. The number of reporting stations in the study area on May 6, 1994 was 97. The E_{tr} ranged from 2.16 mm to 6.93 mm , with a mean of 4.69 mm and a standard deviation of 1.08 mm . Lane had the lowest E_{tr} while Seiling had the highest one (see Figure 16). The general trend of E_{tr} was lowest in the east and highest in the west.

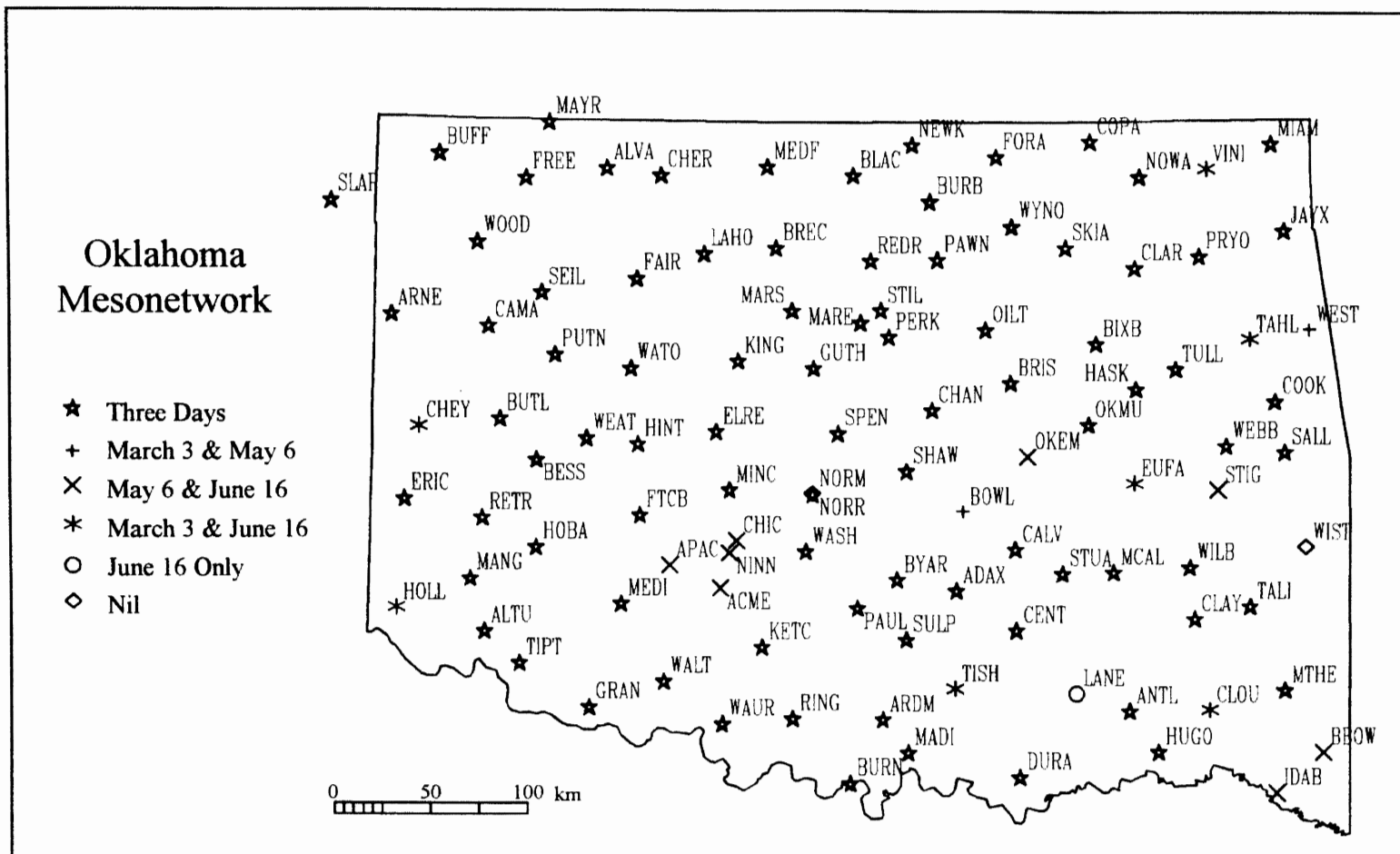


Figure 14. Oklahoma Mesonet Stations Used to Calculate Daily Reference Evapotranspiration of the Three Study Days.

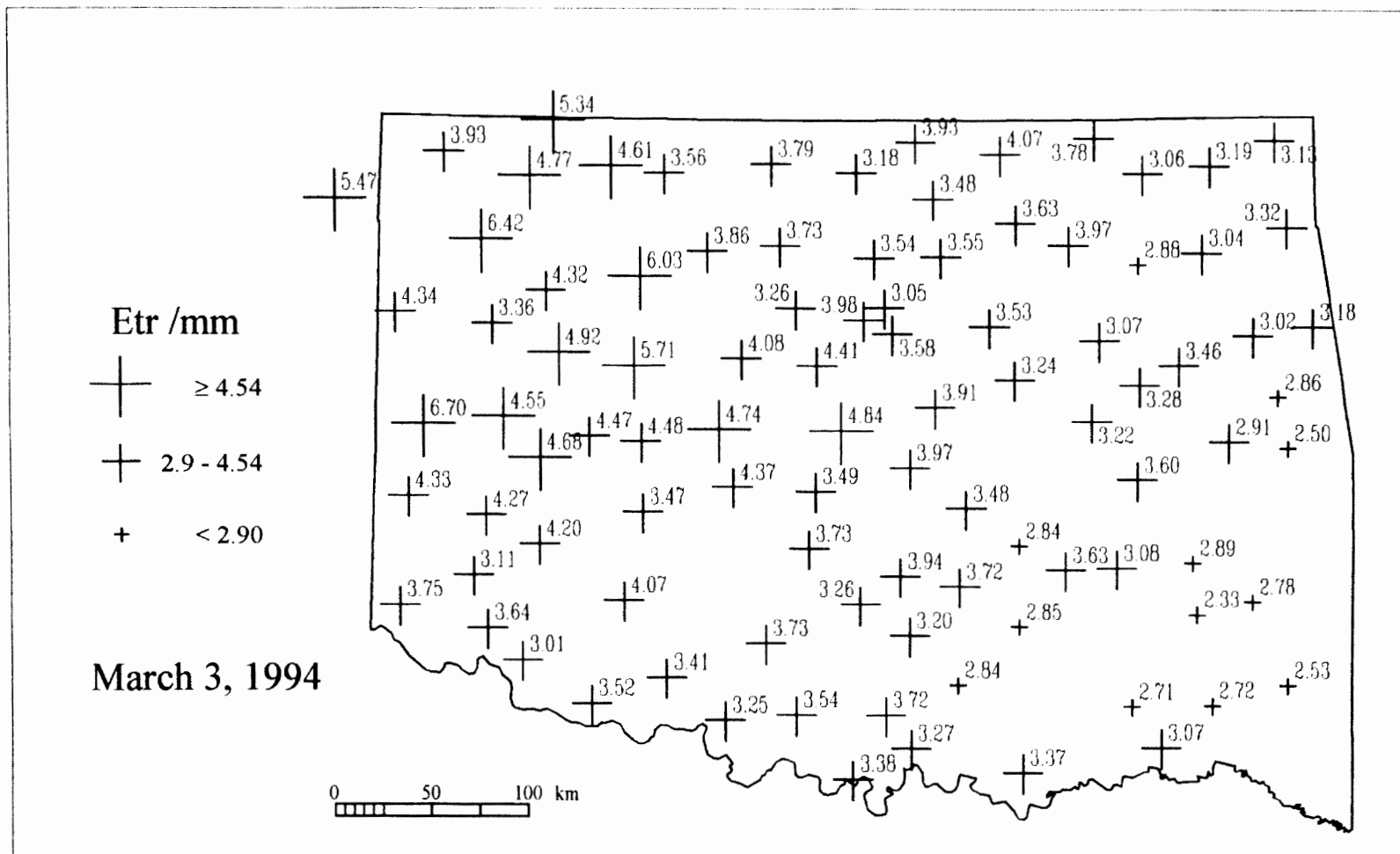


Figure 15. Daily Reference Evapotranspiration at Mesonet Sites, March 3, 1994.

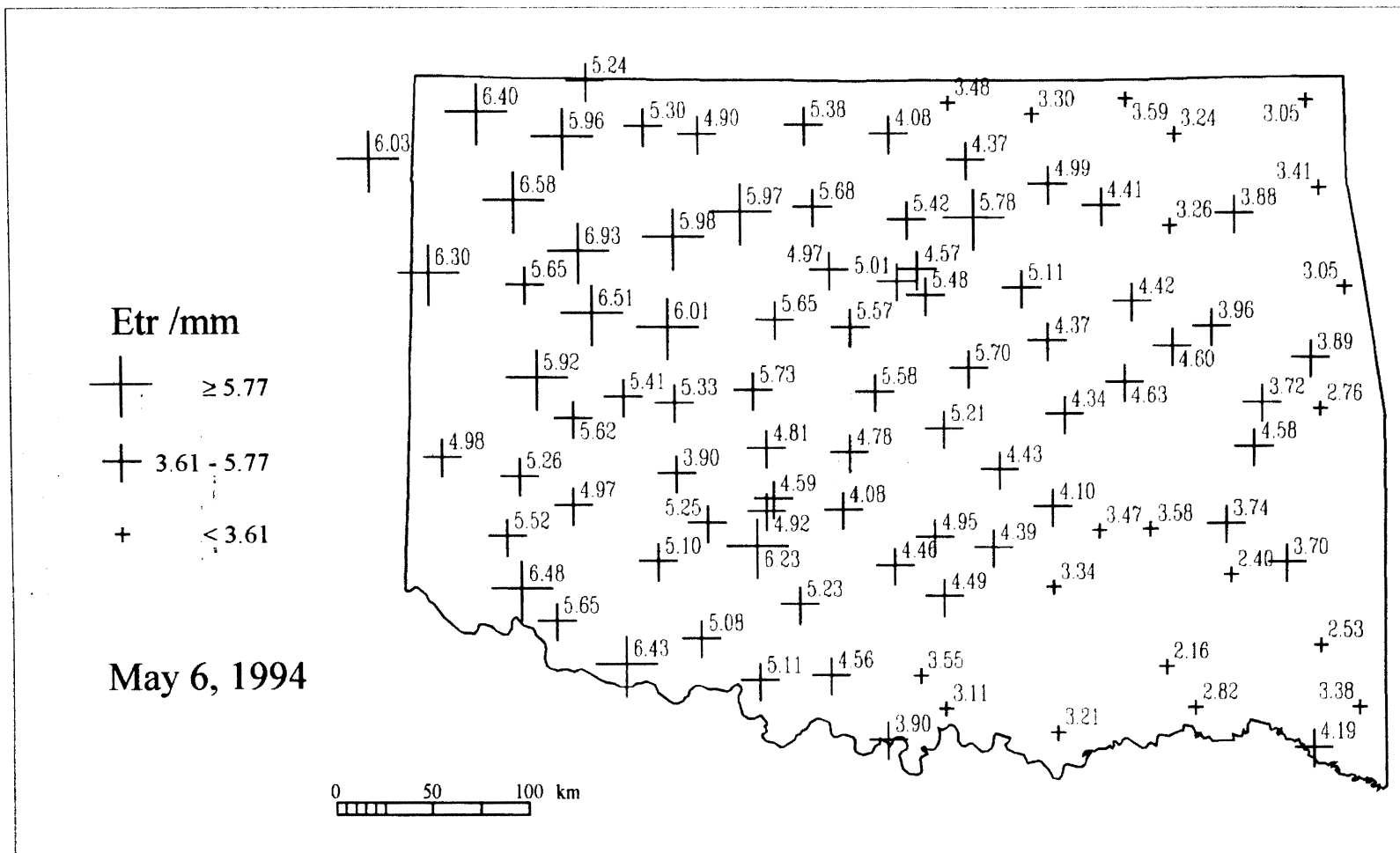


Figure 16. Daily Reference Evapotranspiration at Mesonet Stations, May 6, 1994.

June 16, 1994. The number of reporting stations in the study area on June 16, 1994 was 103. The E_r ranged from 3.34 mm to 11.81 mm, with a mean of 6.66 mm and a standard deviation of 1.43 mm. Cloudy had the lowest E_r , while Slapout had the highest (see Figure 17). The general trend of E_r was lowest in southeast and highest in northwest. However, there was more local variation than for the other study days.

Difference between Resolutions

Four lattices were created for each study day using ordinary kriging. The spatial resolutions of the four lattices were 1 km, 3 km, 9 km and 27 km. Then the spatially coincident cells of the four lattices were compared (see Original Lattice of Chapter 3). In addition, the inscribed cells of the lattices with finer resolution were compared to the cell of the coarser one (See Resampled Lattice of Chapter 3). The comparisons were within days.

Original Lattice

For all study days, there were very high correlations between interpolated surfaces of various resolutions ($r > 0.993$, $p < .01$). March 3 had lower correlations than the other two days. Furthermore, the correlations between 27 km and other resolutions were lower. Despite these variations, analysis showed that interpolated surfaces between all resolutions were highly correlated.

Paired t-tests were performed between different resolutions for each day. The results are shown in Appendix F. Differences between 1 km and 3 km were found significant for March 3, 1994 ($t[14660] = -5.13$, $p = 0$) and May 6, 1994 ($t[14660] =$

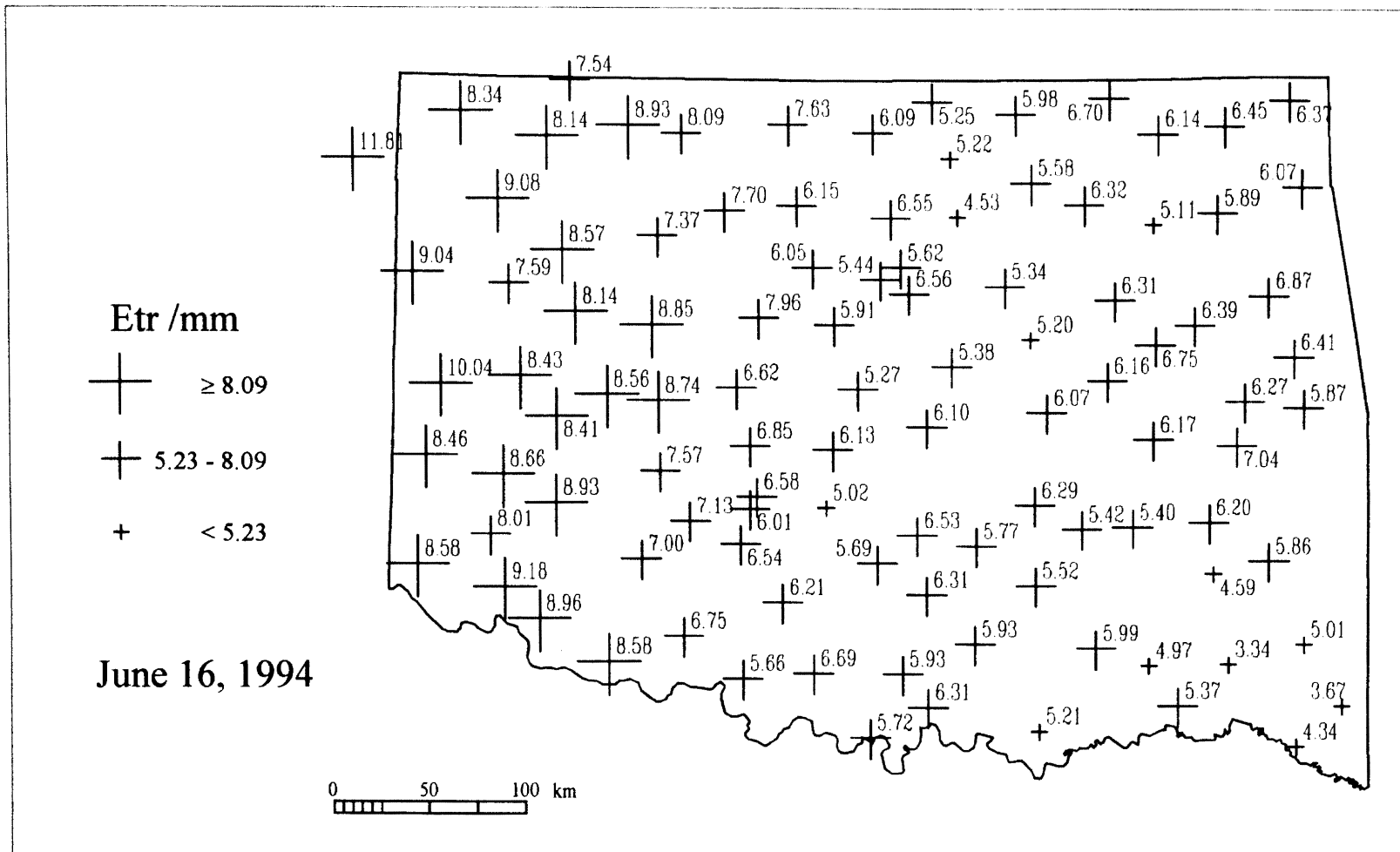


Figure 17. Daily Reference Evapotranspiration at Mesonet Stations, June 16, 1994.

-23.07, $p = 0$). However, the mean difference between all resolutions was less than 0.01 mm. Therefore, any difference, despite being statistically significant, is not practically significant for these study days.

The absolute differences (the magnitude of the differences between two lattices) between various resolutions were examined. Although paired t-test found no significant differences between all resolutions for June 16, the mean absolute difference between 1 km and 3 km ($1.2E-2$ mm) was much higher than that of May 6 ($1.0E-5$ mm). This shows that while the paired t-test can test the mean difference between two surfaces, it cannot account for the difference between two surfaces at various locations.

When the test area was subdivided by distance from Mesonet site, the correlations between different resolutions was found to increase with distance (see Appendix E). However, there were high correlations between the results of various resolutions for all distances ($r > -0.98$, $p < .01$). Paired t-tests showed that there were significant differences between the results of 1 km and 3 km with distances over 10 km from Mesonet stations on all days (see Appendix F).

Despite the results of the paired t-test, both positive and negative differences between resolutions were found at all distances. Figure 18 shows the positive and negative differences between interpolation results of various resolutions by distance. The numbers of top of the graphs indicate the resolutions (e.g. "1 - 3" means 1 km minus 3 km). The top of the I-bar is the maximum positive difference, while the bottom is the maximum negative difference. The "x" shows the mean of positive difference and the "+" shows the mean negative difference.

In general, both mean positive difference and mean negative difference decreased with distance from Mesonet stations. The maximum positive difference and maximum negative difference also decreased with distance. The greatest difference between E_r value at different resolutions were found at the Mesonet sites (original data points). March 3 had the largest maximum absolute difference, while May 6 had the smallest.

The magnitude of difference between various resolutions differed from one day to another. On March 3, 1 km minus 27 km had the smallest difference while 3 km minus 9 km had the largest one. On May 6, 1 km minus 3 km had the smallest difference while 9 km minus 27 km had the largest one. On June 16, 1 km minus 9 km had the smallest difference while 9 km minus 27 km had the largest one.

There was no consistent structure in the spatial patterns of difference between various resolutions in the three study days. However, there were consistent spatial patterns for the difference between the four resolutions on the same study day (see Appendix G). In other words, if the interpolated E_r was viewed as the third dimension, the four surfaces (of different resolutions) intersected each other at more or less the same locations on the same day. Yet, the meeting locations varied from one day to another (see section Spatial Pattern of Interpolation of Chapter V).

Resampled Lattice

For all study days, there were very high correlations between resampled interpolated surfaces of various resolutions ($r > 0.993$, $p < .01$). March 3, as for the original lattice, had lower correlations than the other two study days.

Paired t-tests showed that there were differences between resampled 1 km and 3 km on March 3 ($t[14660] = -5.1064$, $p = 0$) and May 6 ($t[14660] = -2.7266$, $p = 0.0064$). However, all mean difference between the lattices of various resolutions was less than 0.01 mm.

When the test area was subdivided by distance from Mesonet site, the correlations between various resolutions were found to increase with distance (see Appendix E). All correlations were high ($r > 0.08$, $p < .01$). Paired t-tests only found significant difference on May 6 in areas over 20 km from Mesonet sites (see Appendix F).

Again, both the positive and negative differences between various resolutions were found at all distances from the Mesonet sites (see Figure 19). The mean positive difference and mean negative difference decreased with distance from Mesonet stations. The maximum positive differences and maximum negative difference were largest at the Mesonet sites. March 3 had the largest maximum absolute difference, while May 6 had the smallest. The magnitudes of difference between various resolutions differed from one day to another and were consistent with the results of the original lattice.

The spatial patterns of difference between resolutions were similar to those of the original lattice. The direction (positive or negative) of difference between most resolutions was generally the same as the corresponding resolutions of the original lattice. The two exceptions were 1 km minus 3 km on May 6 and 1 km minus 9 km on June 6.

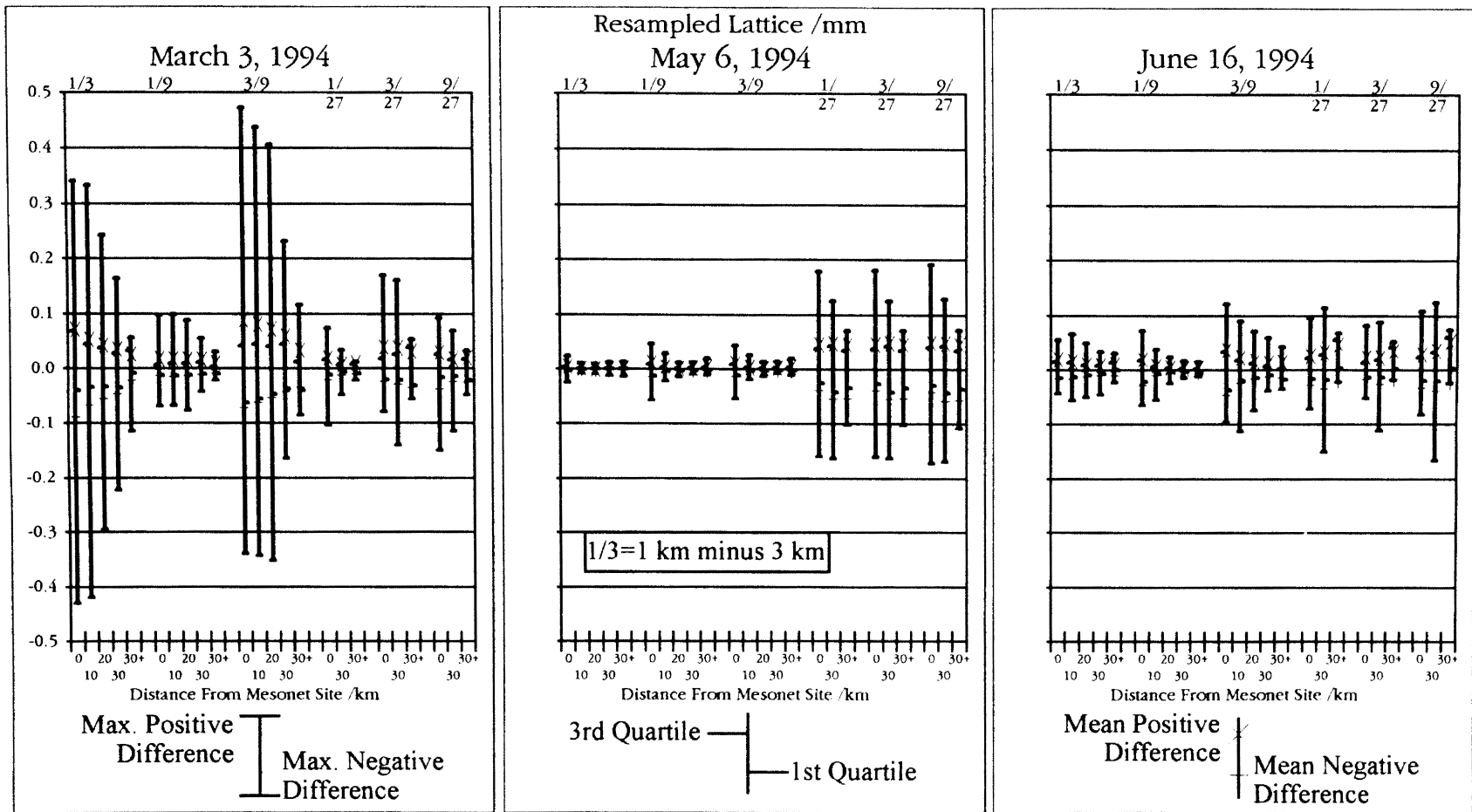


Figure 19. Positive and Negative Differences between Interpolation Results of Reference Evapotranspiration Using Various Resolutions in Kriging (Resampled Lattice).

Best Resolution

Estimation Variance of Kriging

Kriging provided a variance of estimation, σ^2 . The variances of various resolutions are shown in Figure 20. The I-bars show the range of the estimation variance with the mean signified by a "-" mark. June 16 had the highest mean estimation variance of 0.145. May 6 had a mean estimation variance of 0.131. March 3 had the minimum mean estimation variance of 0.114. On both May 6 and June 16, the 1 km resolution yielded the lowest estimation variance ($\sigma^2[\text{May 6, 1 km}] = 0.084$; $\sigma^2[\text{June 16, 1 km}] = 0.093$). On March 3, 3 km resolution had the lowest estimation variance ($\sigma^2[\text{March 3, 3 km}] = 0.072$) while 1 km yielded the second lowest.

Percent error of interpolation ($2\sigma \div \text{predicted } E_r \times 100\%$) was obtained from the estimation variance. The relative percent error between various resolutions on any study day was similar to the relative estimation variance of the corresponding resolutions. On May 6 and June 16, 1 km yielded the lowest percent error (May 6 = 12.6%; June 16 = 8%). On March 3, 3 km yielded the lowest percent error (15.4%).

On the other hand, the comparative percent error of kriging among the three study days was exactly opposite to that of estimation variance (see Figure 20). June 16 had the lowest percent error while March 3 had the greatest one. The mean percent error of June 16 was 11.4% and that of March 3 was 18.4%. May 6 had a percent error of 15.6%.

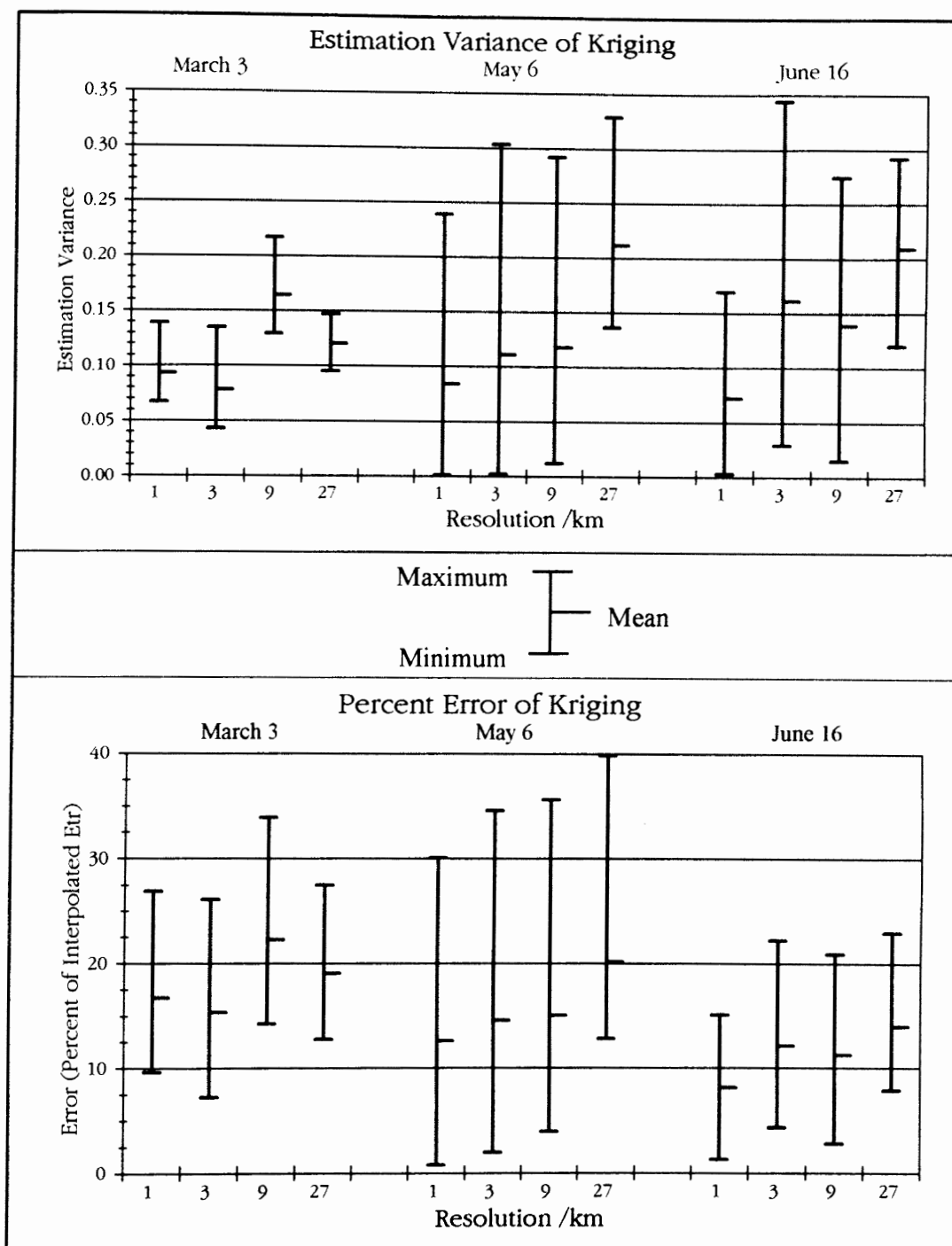


Figure 20. Estimation Variance of Kriging and Percent Error of Kriging.

Jack-Knife Procedure

A jack-knife procedure, as described in Chapter III, was performed for May 6 and June 16. The results are found in Table VI. While kriging over-estimated at some Mesonet sites, it underestimated at others. If all stations were considered as a whole, the total Kerror (sum of the Kerror at every station) was close to zero. On May 6, the total Kerror was 1.03 mm at 1 km and increased to 9.31 mm at 27 km. On June 16, the total Kerror was 0.73 mm at 1 km and increased to 7.02 mm at 27 km.

The absolute Kerror does not allow the under-estimation errors to cancel out the over-estimation errors. The results also showed that the total absolute Kerror (sum of the absolute Kerror at every station) increased as the resolution became coarser. However, the relative difference between the total absolute Kerror of various resolutions was smaller than that between the total Kerror. On May 6, the total absolute Kerror was 37.91 mm at 1 km and increased to 40.91 mm at 27 km. On June 16, the total absolute Kerror was 59.09 mm at 1 km and increased to 62.70 mm at 27 km. In practicality, these are small differences. However, paired t-test indicated that the difference between E_r and the interpolated E_r was significant on May 6 ($t[96] = -10.43, p < .01$).

Difference between Interpolation Methods

Inverse Distance Weighting

For all study days, the correlations were high between the results of using kriging (ELI) and inverse distance weighting (ELD) ($r > 0.97, p < .01$). June 16 had the highest

TABLE VI
KRIGING ERROR OF JACK-KNIFE PROCEDURE

Resolution	Kriging Error /mm				Kriging Error Percentage			
	1 km	3 km	9 km	27 km	1 km	3 km	9 km	27 km
May 6								
Sum	1.03	1.60	3.52	9.31				
Mean ^a	0.01	0.02	0.04	0.10	1.59%	1.72%	2.20%	3.81%
Absolute Sum	37.91	38.14	39.48	40.91				
Absolute Mean	0.34	0.34	0.36	0.37	7.99%	8.04%	8.33%	8.67%
Maximum	1.17	1.17	1.18	1.26	41.67%	41.67%	42.75%	44.20%
Minimum	-1.14	-1.14	-1.09	-1.11	-24.86%	-25.14%	-26.76%	-23.51%
June 16								
Sum	-0.73	-0.03	2.21	7.02				
Mean ^b	-0.01	-0.00	0.02	0.07	1.00%	1.10%	1.41%	2.14%
Absolute Sum	59.09	59.21	59.63	62.70				
Absolute Mean	0.53	0.53	0.54	0.56	8.28%	8.31%	8.38%	8.83%
Maximum	1.60	1.56	1.61	1.62	47.90%	46.71%	48.20%	48.50%
Minimum	-3.02	-3.04	-3.03	-3.08	-25.57%	-25.74%	-25.66%	-26.08%

^a N = 96; ^b N = 102

correlation while March 3 had the lowest. There was very little difference among the four resolutions.

Paired t-tests showed that the ELI and ELD were different at 1 km and 3 km on all three days (see Appendix F). On June 16, the ELI and ELD were also different at 9 km. However, the mean differences between ELI and ELD in all cases were less than 0.1 mm. Concerning the direction of difference, kriging produced larger E_r values than inverse distance weighting (IDW) on all the three days, if the test area is considered as a whole.

All absolute differences (the magnitude of ELI minus ELD) were below 1 mm. March 3 had the largest maximum absolute difference (1.0 mm) while June 16 had the smallest one (0.47 mm). The mean absolute difference between ELI and ELD was below 0.2 mm on all the study days.

There were high correlations between ELI and ELD at all distances from Mesonet stations. On May 6 and June 16, the correlation was close to 1.0 at the Mesonet stations and decreased with distance. On March 3, the correlation increased with distance.

The maximum positive difference and maximum negative difference showed similar trends. On March 3, the mean positive and mean negative differences decreased with distance. However, on May 6 and June 16, the mean positive and mean negative differences increased with distance (see Figure 21).

The spatial patterns of difference between ELI and ELD showed similarity between various resolutions. However, no consistent pattern was found in the three days. Many Mesonet sites could be recognized as local peaks and sinks (see Appendix G). This is consistent with the shape of the surface created by IDW.

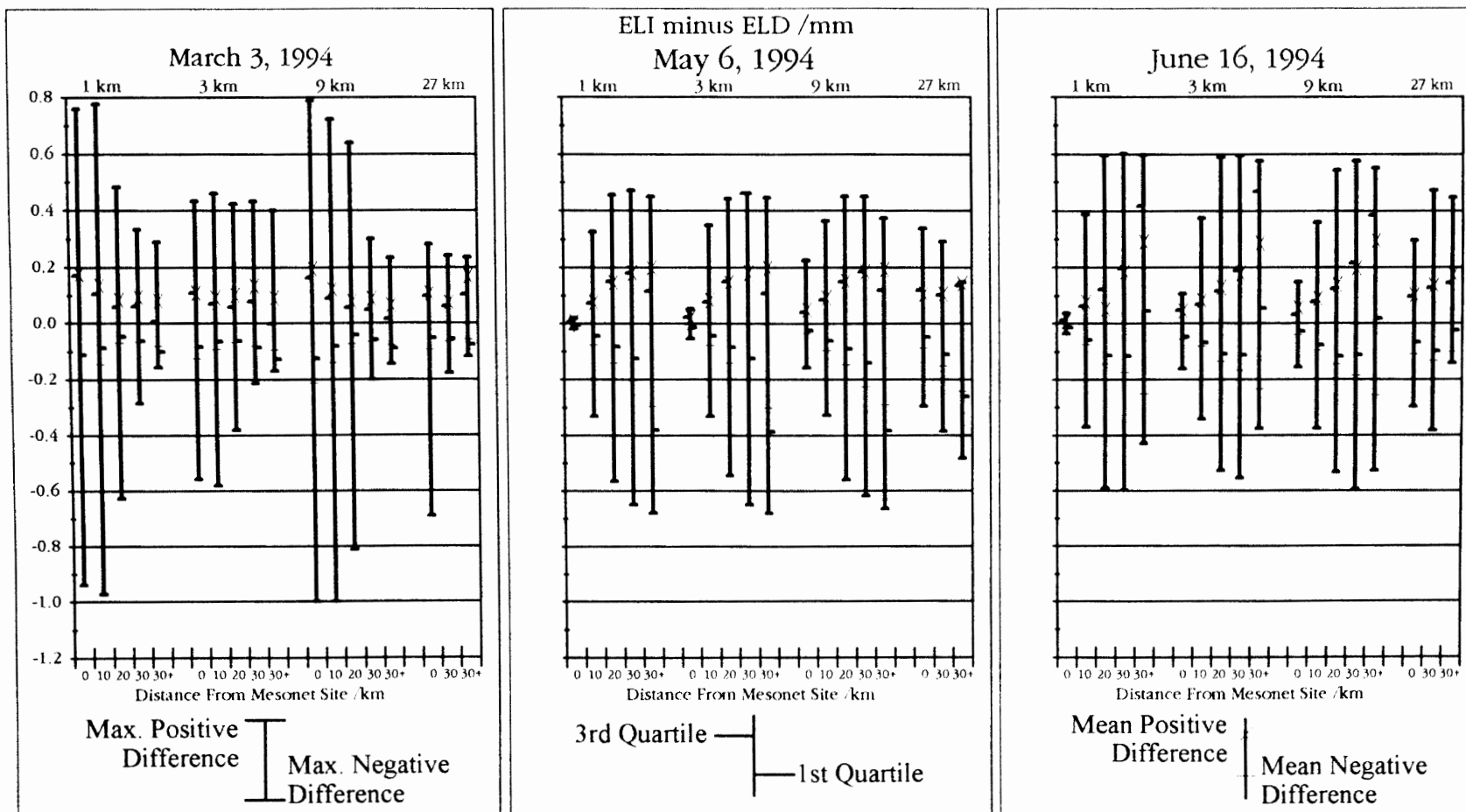


Figure 21. Positive and Negative Differences between Interpolation Results of Reference Evapotranspiration Using Kriging and Inverse Distance Weighting.

Jack-Knife Procedure. The same jack-knife procedures were performed for both kriging and inverse distance weighting (IDW) methods on May 6 and June 16 (see Table VII). The total IDW-error (Derror) were greater than that of kriging (Kerror) on both days. On May 6, the total Derror was 2.95 mm while the total Kerror 1.03 mm. On June 16, the total Derror was -4.04 mm while the total Kerror was -0.73 mm.

However, the total absolute Derror was less than the total absolute Kerror on June 16. At 1 km, the total absolute Derror was 53.34 mm while the total absolute Kerror was 59.09 mm. On May 6, the total absolute Derror was 41.45 mm while the total absolute Kerror was 37.91 mm at 1 km resolution. The maximum absolute Derror was larger than the maximum absolute Kerror on both study days.

Thiessen Polygons

For all study days, there were fairly high correlations between the results of using kriging (ELI) and Thiessen polygons (ELT). On May 6 and June 16, the correlation was between 0.95 and 0.96 ($p < .01$). On March 3, the correlation was about 0.88 ($p < .01$). There was no significant difference between resolutions within each study date.

Paired t-tests showed that ELI and ELT were different at 1 km on March 3 and June 16 (see Appendix F). In both cases, the mean absolute difference of ELI minus ELT were less than 0.01 mm. On the other hand, the maximum absolute difference of ELI minus ELT were high on both days. The maximum absolute difference was 1.8 mm on March 3 while that of June 6 was 2.1 mm, which was the largest one. May 6 had the smallest maximum absolute difference (1.25 mm).

TABLE VII

INTERPOLATION ERRORS OF KRIGING, INVERSE DISTANCE WEIGHTING AND
THIessen POLYGONS USING JACK-KNIFE PROCEDURE^a

	1 km			3 km		9 km		27 km	
	Nerror	Kerror	Derror	Kerror	Derror	Kerror	Derror	Kerror	Derror
May 6									
Sum	(0.28)**	1.03*	2.95	1.60*	3.82	3.52*	6.23	9.31*	12.05
Mean	(0.00)	0.01*	0.03	0.02*	0.04	0.04*	0.06	0.10*	0.13
Absolute Sum	60.18**	37.91*	41.45	38.14*	41.38	39.48*	42.33	40.91*	43.21
Absolute Mean	0.54**	0.34*	0.37	0.34*	0.37	0.36*	0.38	0.37*	0.39
Maximum	1.69**	1.17*	1.42	1.17*	1.42	1.18*	1.43	1.26*	1.48
Minimum	(1.41)**	(1.14)*	(1.31)	(1.14)*	(1.31)	(1.09)*	(1.27)	(1.11)*	(1.15)
June 16									
Sum	(14.38)**	(0.73)*	(4.04)	(0.03)*	(3.34)	2.21	(1.22)*	7.02	5.20*
Mean	(0.14)**	(0.01)*	(0.04)	(0.00)*	(0.03)	0.02	(0.01)*	0.07	0.05*
Absolute Sum	68.06**	59.09	53.34*	59.21	53.58*	59.63	53.98*	62.70	59.68*
Absolute Mean	0.61**	0.53	0.48*	0.53	0.48*	0.54	0.49*	0.56	0.54*
Maximum	2.03**	1.60*	1.79	1.56*	1.81	1.61*	1.84	1.62*	1.84
Minimum	(3.47)**	(3.02)*	(3.32)	(3.04)*	(3.32)	(3.03)*	(3.32)	(3.08)*	(3.33)

* Smaller error between kriging and inverse distance weighting

** Largest error among the three methods

^a Daily E /mm

tr

The correlation between ELI and ELT decreased with distance from Mesonet stations. On May 6 and June 16, the correlation dropped from close to 1.0 at Mesonet sites to below 0.95 at places beyond 20 km. March 3 had a similar trend with lower correlations (see Appendix E).

The mean positive difference and mean negative difference increased with distance on all study days. The largest mean absolute difference was below 0.3 mm. Although the maximum positive and negative differences demonstrated similar pattern, there were greater variations between study days and the magnitudes of differences were larger (see Figure 22).

The spatial patterns of difference between ELI and ELT resembled the boundaries of Thiessen polygons. Alternative corridors of positive and negative differences were shown. However, there was no specific similarity among the three days (see Appendix G).

Jack-Knife Procedure. The difference between the E_r and the E_r of the nearest station (Nerror) was compared to the kriging-error (Kerror) of the jack-knife procedure. The total Nerror were -0.28 mm on May 6 and -14.38 mm on June 16. The corresponding total Kerror at 1 km were 1.03 mm and -0.73 mm (see Table VII).

The total absolute Nerror were 60.18 mm on May 6 and 68.06 mm on June 16. The corresponding total absolute Kerror at 1 km were 37.91 mm and 59.09 mm. The maximum absolute Nerror on both days were larger than the corresponding maximum absolute Kerror.

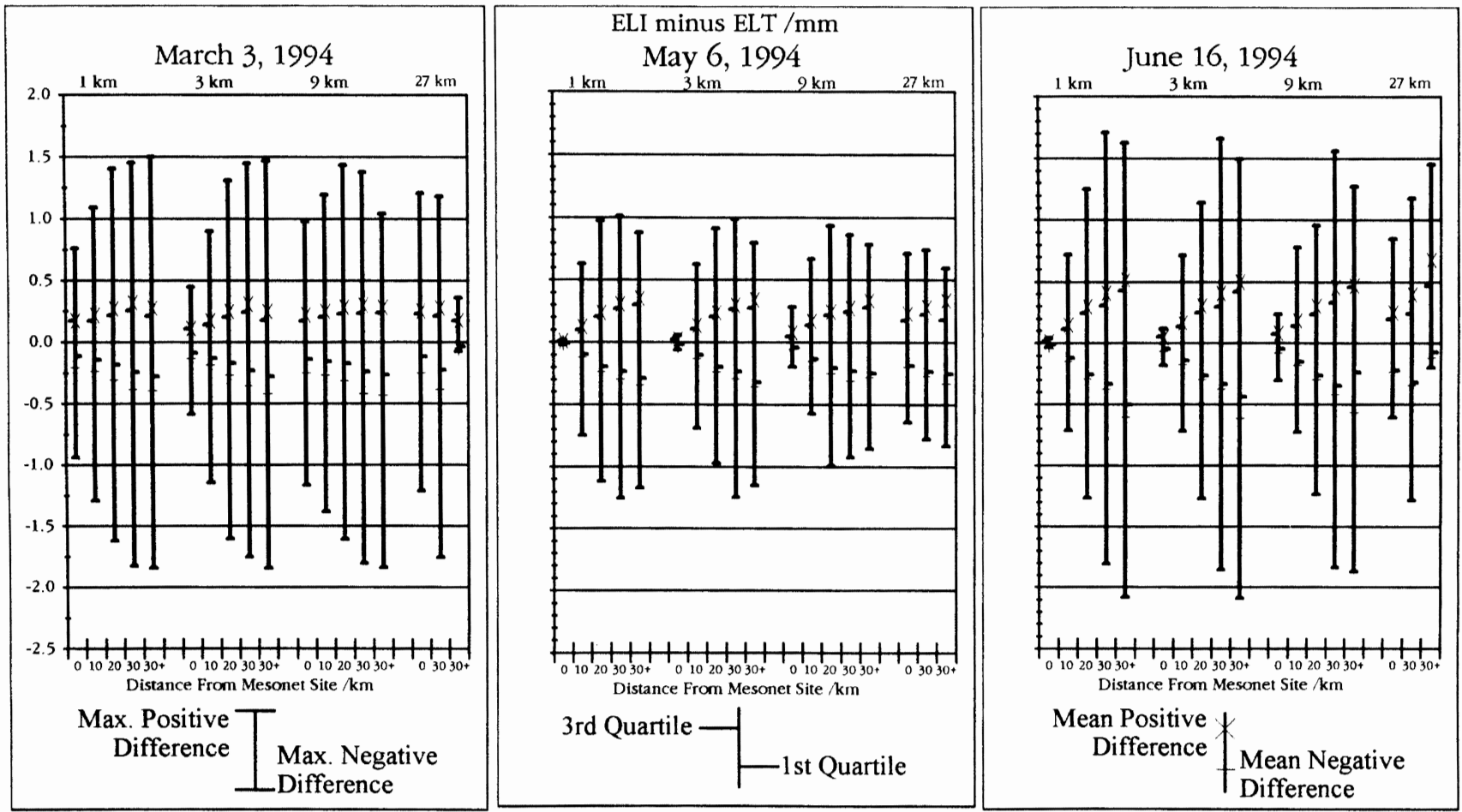


Figure 22. Positive and Negative Differences between Interpolation Results of Reference Evapotranspiration Using Kriging and Thiessen Polygons.

Point and Surface Meteorological Data

For all study days, there were very high correlations between lattices created from point meteorological data (ELI) and surface meteorological data (ELE) ($r > 0.99$, $p < .01$). June 16 had the highest correlation while March 3 had the lowest. Paired t-tests showed that ELI and ELE were different at 1 km and 3 km on all three study days. On March 3 and May 6, ELI and ELE were different at 9 km too. Nevertheless, all mean differences between ELI and ELE were less than 0.01 mm. Again, there was a similar number of positive and negative differences in terms of the study area. The maximum absolute difference between ELI and ELE was below 0.5 mm while the mean absolute difference was below 0.08 mm.

The correlation between ELI and ELE increased with distance from Mesonet stations (see Appendix E). Paired t-tests showed that ELI and ELE were different at 1 km on May 6 and June 16 except at the Mesonet sites. However, all mean differences were less than 0.1 mm.

Both the mean positive and mean negative differences of ELI minus ELE decreased with distance from Mesonet stations (see Figure 23). At 1 km, 3 km and 27 km, June 16 had the smallest difference, while May 5 had the largest. At 9 km, March 3 had the smallest difference. However, all mean absolute differences were smaller than 0.1 mm. In general, the difference increased as the resolution became coarser. The maximum positive and negative differences also decreased with distance from the Mesonet site. However, all differences were below 0.6 mm. The spatial distribution of the positive and

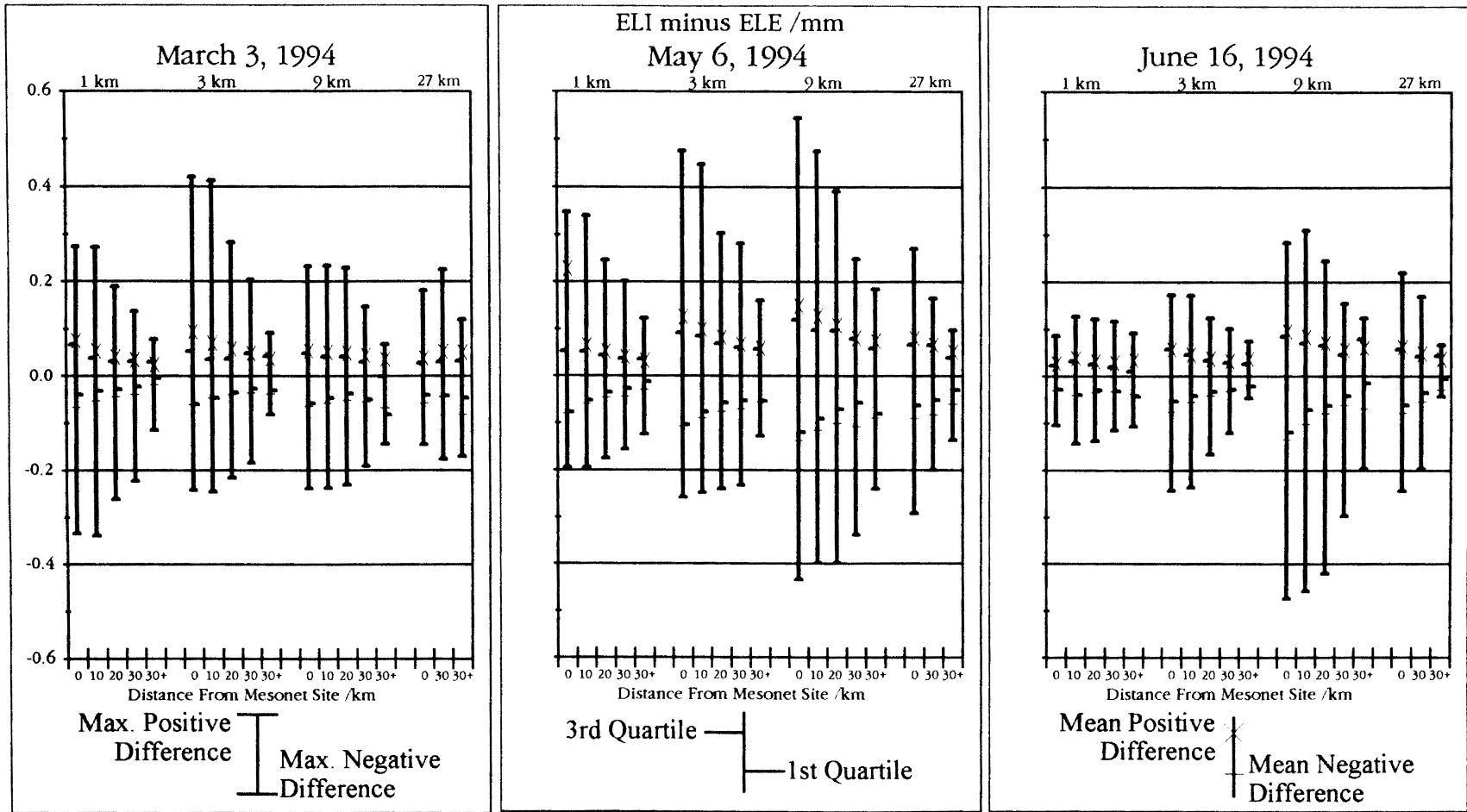


Figure 23. Positive and Negative Differences between Reference Evapotranspiration Surfaces Resulting from Point and Surface Meteorological Data.

negative differences is shown in Appendix G. No consistent spatial pattern of difference was found for the three study days.

CHAPTER V

CONCLUSIONS AND DISCUSSION

Conclusions

Difference between Resolutions

Although varying resolutions of interpolation yielded different surfaces, the magnitude of difference was very small. On March 3, the maximum absolute difference (sign of difference not considered) was 0.5 mm between 3 km and 9 km. On May 6, it was 0.28 mm between 1 km and 27 km. On June 16, it was 0.21 mm between 9 km and 27 km. For all study days, the mean absolute difference of the whole test area was below 0.1 mm.

The results using the original lattice show that if a location of interest lies in the middle of a cell, the choice of resolution makes little difference. However, at the edge of a large cell the difference could be large. Although only spatial coincident points were used in the tests, the difference at other locations could be inferred using Thiessen polygons. On May 6, the mean distance between stations with valid data was 31.28 km and the mean reference evapotranspiration (E_r) difference between the neighboring stations was 0.53 mm.

In addition to comparing the spatially coincident points of various resolutions, each point on the coarser resolution lattice was compared to the mean of all inscribed points on the finer resolution lattice. The resampled lattice produced results similar to that of the original lattice. Both the spatial distribution and magnitude of the differences showed only little dissimilarity. In most cases, the difference between resolutions for the resampled lattices was less than that for the original lattices. This suggests that if the regional E_r is the focus of a study, coarser resolutions can be used. While the error of a finer resolution may be less than that of a coarser resolution (as show in the next section), the amount of that difference is little. However, the use of a coarser resolution could result in a substantial reduction in computation time (see section Kriging of this Chapter).

The spatial pattern of the difference between different resolutions were quite similar. This showed that the interpolated surfaces of different resolutions meet each other at more or less the same places.

Best Resolution

Although the finest resolution might not have the smallest estimation variance on a particular study day, it was always among the lowest. In other words, if accuracy is of paramount importance, it would be better to use a finer resolution. For the four resolutions chosen, the difference in mean percent error was within 8%. For an E_r of 10 mm, this translates into a 0.8 mm difference. If 8% less in error is desired, using a finer resolution could be justified. Yet, a finer resolution may not always deliver a lower estimation variance (see section on variogram). While, in theory, there is a 95.5% probability that the actual E_r lies within two times the square root of the estimation

variance (2σ) from the estimated E_r (ARC/INFO, 1992), the results of the current study showed less optimistic results (see section Kriging of this chapter).

The jack-knife procedure (Mesonet stations were removed one at a time, and then the E_r was interpolated from the remaining stations) also showed that a finer resolution performs better than a coarser resolution. However, the difference was very little. On May 6, the mean absolute kriging-error (Kerror) between 1 km and 27 km was only 0.02 mm. On June 16, it was 0.03 mm. Moreover, one possible cause of the larger error with coarser resolutions is the increasing distance of the Mesonet station from the cell center. Again, the choice of resolution depends on the variation of E_r . If the range of E_r between neighboring stations is large, it would be better to use a finer resolution in order to gain more information.

Difference between Interpolation Methods

Inverse Distance Weighting. As both kriging and inverse distance weighting (IDW) are exact methods, the difference between interpolated surfaces would be expected to be smaller at the Mesonet sites. May 6 and June 16 conformed to this model. However, the greatest difference was found at the Mesonet site on March 3. This could be a result of the high nugget variances on March 3 (see section Kriging of this chapter). Nevertheless, all differences between ELI (lattice created by kriging) and ELD (lattice created by IDW) were less than 1 mm. No mean absolute difference was above 0.2 mm. Although the differences were smaller at the Mesonet sites, many stations showed up as peaks and sinks in the E_r surface.

Thiessen Polygons. As expected, the difference between ELI (lattice created by kriging) and ELT (lattice created by Thiessen polygons) increased with distance. The difference was bigger than that between ELI and ELD. The maximum absolute difference was over 1 mm on all study days and the largest one was 2.09 mm (spatial resolution of 3 km) on June 16. All mean absolute differences were below 0.35 mm, which was about double that between ELI and ELD.

Point and Surface Meteorological Data

The difference between ELI (lattice resulted from point meteorological data) and ELE (lattice resulted from surface meteorological data) decreased with increasing distance from Mesonet stations. However, the magnitudes of differences were much smaller than that between different interpolation methods. For instance, the maximum absolute difference was 0.54 mm (spatial resolution of 9 km) on May 5. The mean absolute difference was below 0.1 mm.

Problems and Discussion

Designs

Paired t-test. The original design was to use a paired t-test to test if any difference between two surfaces was significant. Although the tests showed some differences were statistically significant, the amount of difference (in mm) was too little to be practical.

One problem of the paired t-test method is that it is not a spatial measure. In addition, the t-test tested the mean difference between two surfaces. It tested if one

surface was significantly greater (or smaller) than the other. As all interpolation methods used in this study were exact methods, all resulting surfaces undulate around the observed data points (Mesonet stations). In most instances, there was just not enough evidence to show any differences in the outcomes of the various interpolation methods. If any significant difference was detected, it might well have been the result of the high degree of freedom. At spatial resolution of 9 km, there were 1,629 degrees of freedom (df). At spatial resolution of 3 km, there were over 10,000 degrees of freedom.

Limitation of ARC/INFO

ARC/INFO (1992) was chosen for this study because of its availability, its wide use by many disciplines, and the wide range of geographic information system functions available. It contains all three interpolation methods used in this study. In addition, it contains both vector and raster models. Although most operations of this study were performed in GRID—a raster module, vector operations were also used.

However, ARC/INFO was not free of problems. Both TIN (a vector module) and GRID modules have a kriging command. At first, the kriging command of the TIN model was used. Although the result of both commands is a lattice, the two modules recognize the coordinates differently. TIN reads the coordinates as the center of a cell while GRID reads them as a corner.

ARC/INFO documentation (1992) is unclear regarding how kriging is performed. Although it is likely that the command uses punctual kriging, the command reference does not specify. While the variogram is the heart of kriging, ARC/INFO does not allow manipulation of the variogram. Therefore, the cross validation as described by McBratney

and Webster (1986) could not be performed. During the testing of kriging parameters, some strange variograms were created. For instance, on June 16, the spherical model with a searching radius of 60 km yielded a variogram with only two data points.

Another problem was the limitation of INFO, the database used in the ARC/INFO GIS. For any workspace, only 999 INFO files were allowed. While it is more than enough for many applications, the exploration of variograms related to the several parameters used to create E_r soon produced enough files to challenge this limit.

Kriging

Variograms. Variograms are the heart of kriging. However, it is very difficult to objectively justify which one to use. In order to limit the variations for this study, the same parameters were used to estimate all variograms. However, the author recognizes that it was impossible for the consistent parameters to create good variograms for all the interpolated variables on all study days. This is one inherent limitation of the present study. An alternative is to use the best fit variogram in every case, but its great time and computational demands and the uncertainty related to its additional utility preclude it from this study.

A variogram includes information on semivariance at different lags. Nugget variance, sill variance and range of the three study days are shown in Table VIII. March 3 had the highest nugget variance. Although the spatial resolution of 27 km usually had the largest nugget variance, the nugget variance was not related to resolution in any simple fashion.

TABLE VIII
 NUGGET VARIANCE, SILL VARIANCE AND RANGE
 OF REFERENCE EVAPOTRANSPIRATION

Resolution	Nugget Variance	c	Sill Variance	Range /km
March 3				
1 km	0.047	0.388	0.435	359
3 km	0.024	0.554	0.578	360
9 km	0.091	0.577	0.668	360
27 km	0.060	0.507	0.566	351
May 6				
1 km	0.000	1.006	1.006	359
3 km	0.000	1.336	1.336	360
9 km	0.000	1.206	1.206	306
27 km	0.074	1.294	1.368	351
June 16				
1 km	0.001	0.890	0.892	359
3 km	0.014	1.807	1.820	360
9 km	0.000	1.781	1.781	360
27 km	0.061	1.576	1.637	351

Nevertheless, many results of kriging seem to relate to the nugget variance. For instance, the estimation variance and error of kriging showed relation with nugget variance. March 3 was the only day that the difference between ELI and ELD was larger at Mesonet sites. On June 16, difference between resolutions of 1 km and 9 km was the smallest while both resolutions had similar nugget variances.

Size of Study Area. The size of study area is always a concern for kriging. Geostatistics assume that the spatial relationship described by a variogram holds for the whole study area (Burrough, 1986). This is problematical for a large region in which the spatial relationship may vary.

In this study, the study area (and test area as defined in Chapter III) were held constant so that interpolated lattices of different resolutions coincided with each other. On the other hand, the arrangement of data points at the edge of the study area determined the largest possible study area. ARC/INFO refused to run kriging if a different extent was used. As a result, the spatial extent of the 1 km and 3 km resolutions on March 3 were different from the 9 km and 27 km resolutions. This casted doubts on the results of comparing the two surfaces with the others.

Resolution of Kriging. The first concern of resolution is accuracy of kriging. Both the estimation variance and the jack-knife procedure showed that finer resolutions created smaller errors. However, the differences between resolutions were small and of little practical significance in the estimation of reference evapotranspiration.

The choice of resolution for kriging is not only a matter of accuracy. Kriging is computationally intensive. The CPU time of kriging is summarized in Figure 24. The

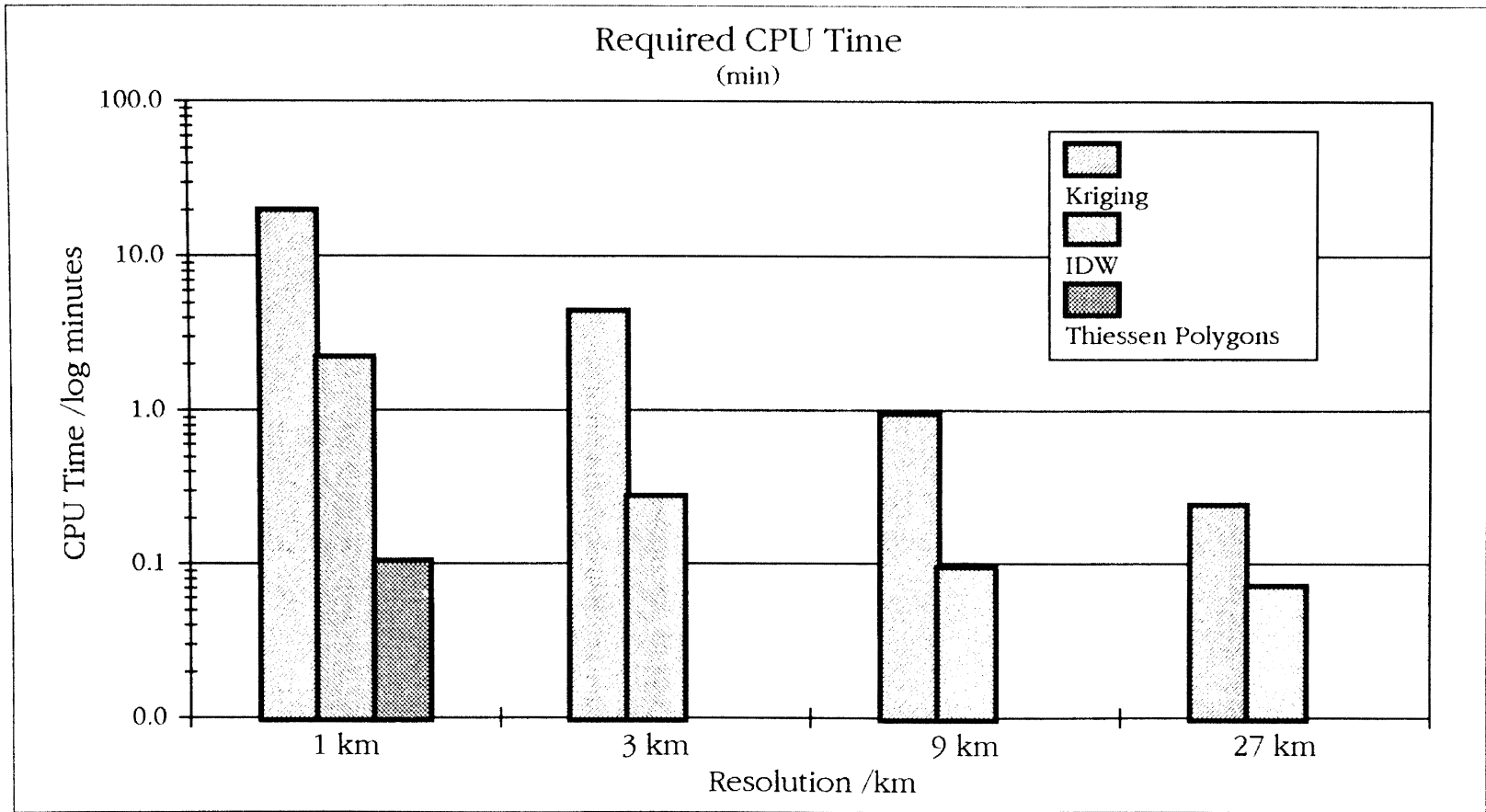


Figure 24. Comparison of Average CPU Time Used by Different Interpolation Methods.

average CPU time for interpolating from 100 data points in an area of 180,000 km² to a lattice of 1 km resolution was 20 min while the time required by the 3 km resolution was only 4.5 min. The CPU time for using 1 km resolution in kriging was 10 times that for using a resolution of 9 km. The time required to create Thiessen polygons for 100 stations was less than one-hundredth of that required by kriging with 1 km resolution (resolution is not applicable for Thiessen polygons). Inverse distance weighting required one-tenth of the time required by kriging. Therefore, it is necessary to balance the accuracy gained and the computational resources required. If a finer resolution is desired, interpolation other than kriging might be considered.

Estimation Variance. One advantage of kriging is the availability of estimation variance. Theoretically, there is a 95.5% probability that the actual E_r lies within two times the square root of estimation variance from the estimated E_r . However, the jack-knife procedure only produced a percentage of about 85. In addition, the 1 km resolution had the lowest percentage. This casted doubt on any blanket claim that the finer resolution is always more accurate.

Accuracy of Interpolation

Data quality. Results are accurate only if data are correct. However, it is a difficult to insure the quality of such a large amount of data. The Oklahoma Mesonet network had some quality control and missing data would be flagged as values below -90. Any station with such a value would be dropped for the study day. However, not all incorrect values were flagged. For example, Tishomingo recorded no solar radiation on May 6.

The current study also used a visual examination to detect any strange values. On March 3 the solar radiation of Tishomingo was 5 MJ m^{-2} less than the surrounding stations. It was quite possibly caused by sensor malfunctioning. This study made no attempt to assess sensor accuracy and it was only an assumption that the other data had errors at an acceptable level.

Another aspect of accuracy was the calculation of daily mean. Only measurements at the hour were used. Although this is better than maximum and minimum daily data usually used in E_{tr} studies, it allowed possible errors. While weather elements like relative humidity and air temperatures may change slowly, wind speed and solar radiation could change abruptly. It was only an assumption that the measurements at the hour were good samples. Furthermore, the wind speed was extrapolated by formula from 10 m to 2 m. Evidence showed that the extrapolated value was a bit lower than the actual measured values at the Mesonet sites where wind speed sensor at 2 m was available.

Instrumentation. In addition, the surrounding evapotranspirative environment (vegetation, soils, etc.) of different stations varies. As a result, the measurement would always be slightly different, which translated into different E_{tr} estimations. These external factors would vary the spatial dependence of a variable, thus creating the nugget variance. One possible example is Stillwater, Perkins and Marena in Payne county. Despite the close proximity of the three stations, measurements of meteorological elements varied considerably.

Error in Penman Equation. Although the Penman equation of E_{tr} estimation is one of the most theoretically sound methods, it is not an exact measurement. It could be

described as an educated guess. Therefore, estimation from the equation has inherit error. This type of error could well be in the range of 0.5 mm, which is even bigger than the mean absolute difference between kriging and Thiessen polygons (< 0.35 mm) on any study day.

The wind function used for the whole study area was calibrated at Fort Cobb (Dr. Michael Kizer, personal communication, February, 1994). In addition, the equation was quite sensitive to wind speed. On a windy day, for instance June 16, high wind speeds made the estimated E_r in western Oklahoma much higher than that in eastern Oklahoma.

Difference Between Resolutions. There was little difference between spatial interpolations of E_r at different resolutions. However, it should be understood that comparisons were made at spatially coincident cell centers. If the value in a coarse resolution is viewed as a representation of the whole cell, differences would be bigger towards the cell edge. The value of a coarse resolution was quite close to the mean of the inscribed cells of a finer resolution. In the other words, if regional E_r is of interest, coarse resolution can be employed.

Kriging versus IDW. Although finding which interpolation method is the most accurate was not the main objective of this study, some related results were generated. The jack-knife procedure was performed on IDW as well as kriging. The result is listed in Table VII (see Chapter IV). While kriging had less total absolute Kerror on May 6, IDW had smaller total absolute Derror on June 16. Of course, the total Kerror on both days was smaller than the total Derror. It is possible to interpret the result as the variograms captured the variation better than a power of 2 in IDW. Nevertheless, given the amount

of variation from one day to another and because only three study days were used, caution dictates that no definite conclusions should be drawn from the data used in this thesis.

Head-to-head comparison of the two methods in the test area showed that the absolute difference between kriging and IDW was within 1 mm on the three study days. The mean absolute difference was below 0.2 mm. Possibly, it does not really matter which interpolation method is more accurate. Visual comparison of surfaces created by the two methods showed that kriging produced a smoother surface. Mesonet sites could be recognized on the IDW surface as peaks and sinks.

Kriging versus Thiessen Polygons. The jack-knife procedure was performed on Thiessen polygons. Actually, it was the difference in E_r between a station and its nearest neighbor. On both May 6 and June 16, it had the largest error among the three methods used.

The statistical distribution of the absolute difference between kriging and Thiessen polygons had a strong positive skew. The mean absolute difference was below 0.35 mm, while some absolute differences were up to 2 mm. If the distance from a location of interest to the nearest Mesonet site is short, and the range of E_r of the few surrounding stations is small, Thiessen polygon could be the simplest and best method. This study did not attempt to provide a decision criterion.

Point and Surface Meteorological Data. Different weather elements, which are used to estimate E_r values in the Penman formula, have different spatial variations. Therefore, it is reasonable to think that interpolating individual weather elements separately and then estimating the E_r from interpolated values is better than just

interpolating E_{ir} estimated at the Mesonet sites. Although the study did not answer the question directly, results showed that the difference was so little that it did not really matter which method was used. However, the increase in computational time necessary to generate so many intermediate interpolated surfaces suggests that it is impractical to derive E_{ir} from interpolated meteorological data.

Practicality of Interpolating E_{ir} with Kriging

Acceptable error of E_{ir} . The choice of interpolation method is a function of the acceptable error, which is related to the application. If the acceptable error of E_{ir} is 1 mm, it seems that it does not really matter which interpolation method to use, with data of Mesonet quality and density. As E_{ir} is, in most cases, the maximum moisture flux between landscape and atmosphere, a 1 mm error in E_{ir} means a smaller error in the actual evapotranspiration. Nevertheless, if the application is something such as irrigation, the actual evapotranspiration could exceed the E_{ir} and a 1 mm might be magnified.

In most cases, E_{ir} over a period is required in water budget application. Would the positive and negative error of interpolated E_{ir} offset each other in the long run? What if it accumulates? At any rate, an a priori acceptable error level should be specified for any application instead of going the extra mile to get the "most accurate" result in a particular application. It is possible that no sophisticated interpolation is required. On the other hand, perhaps no interpolation method can satisfy the requirement and extra data should be collected.

Effect of nearby stations. The study showed that both kriging and IDW were strongly influenced by the neighboring stations. The correlations between Kerror and Nerror (E_r , difference of neighboring stations) were 0.75 on May 6 and 0.80 on June 16 (see Table IX). The corresponding correlations between Derror and Nerror were 0.73 and 0.81. This indicated that if the estimated E_r value of the nearby stations were quite close, the choice of interpolation method was not important. This would be a function of the distance between data collecting locations. If the distance is short, the E_r estimations should be within a small range.

Data availability. The mean distance between Mesonet stations is 35 km. Such a high density of data is not widely available in the United States. It is obvious that with decreasing density of data, the error of Thiessen polygons rose. It is uncertain how kriging and IDW would behave at decreasing data densities. Thus this study did not attempt to answer which interpolation method is best for E_r estimation using low density data.

Scale of Study. The scale of study shows a dilemma in using kriging to interpolate E_r . Kriging requires sufficient data to estimate the variogram. One way to collect more data for E_r is by increasing the area to include more weather stations, but this also threatens the spatial dependent assumption which is the underlying theory of kriging.

System requirements. Although the UNIX-based workstation and geographic information system software used in this study are quite common, they are not so common as a personal computer using simple database management software. Yet, the study

TABLE IX
CORRELATIONS BETWEEN RESULTS OF INTERPOLATION
METHODS USING JACK-KNIFE PROCEDURE

	Etr	NEtr	KEtr	DEtr	Nerror	Kerror	Derror
May 6							
Etr	1	0.76**	0.89**	0.86**	(0.39)**	(0.45)**	(0.62)**
NEtr		1	0.89**	0.87**	0.30**	0.75	0.73
KEtr			1	0.97**	(0.04)	0.01	(0.24)*
DEtr				1	(0.03)	0.01	(0.13)
Nerror					1	0.75**	0.73**
Kerror						1	0.90**
Derror							1
June 16							
Etr	1	0.81**	0.86**	0.88**	0.81**	(0.46)**	(0.62)**
NEtr		1	0.92**	0.93**	0.16	0.02	(0.15)
KEtr			1	0.99**	(0.04)	0.07	(0.15)
DEtr				1	(0.07)	0.01	(0.16)
Nerror					1	0.80**	0.81**
Kerror						1	0.94**
Derror							1

* $p < .05$

** $p < .01$

suggests that it is feasible to estimate daily E_{tr} , and interpolate the results, within a reasonable time-frame on personal computers.

Spatial Pattern of Interpolation

Difference between Resolutions. The difference between all four resolutions showed similar spatial patterns (see Appendix G). In other words, the four surfaces meet at similar locations. In addition, the mean absolute difference decreased with distance from Mesonet stations while correlation increased. It is possible to derive a schematic cross-section as shown in Figure 25. The difference between various resolutions is greatest at the Mesonet stations. The surfaces get closer together and meet somewhere between stations and then the direction of difference reverses. This enriched the results of difference between resolutions but was hard to explain. However, this proved that kriging created consistent results with the four resolutions selected

Difference between Interpolation Methods. The difference between the resulting surfaces of kriging and IDW increased with distance. This indicated that the two surfaces met close to the original data points. It is consistent with the fact that both interpolation methods are exact methods.

Difference between the resulting surfaces of kriging and Thiessen polygon showed the same phenomenon (see Appendix G). The two surfaces usually met at Mesonet stations. This can be used as an analogy for coarse resolution in kriging. The study tested only the spatially coincident lattice points and found little difference between resolutions. However, the difference was much larger at the edge of a large cell. If a coarse resolution

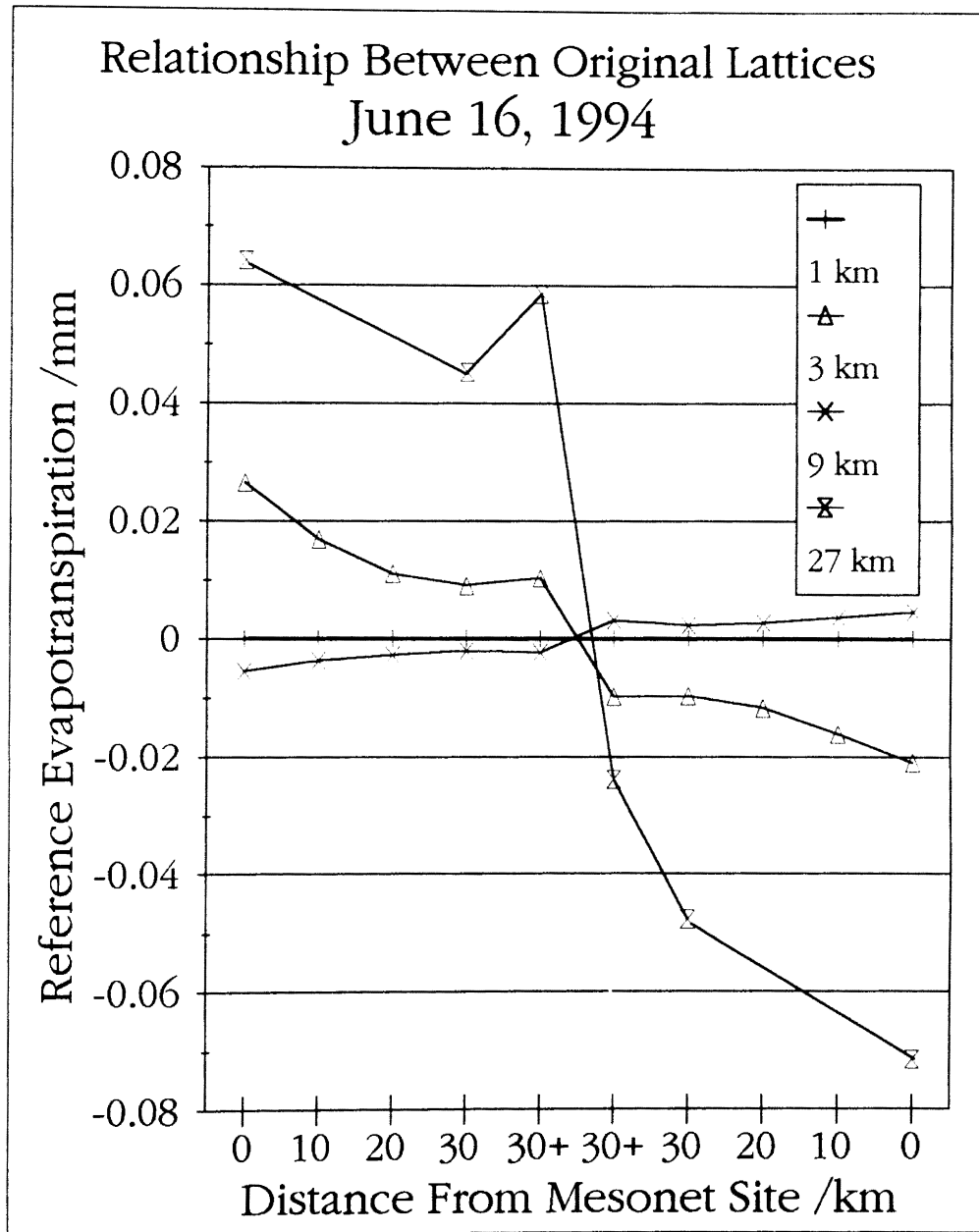


Figure 25. A Schematic Relationship between Reference Evapotranspiration Lattices of Various Resolutions (Original Lattice), June 16, 1994.

is used in interpolation, the distance of the location of interest from the center of the cell should be considered.

Point and Surface Meteorological Data. ELI (Etr surface interpolated from point Etr) and ELE (Etr surface derived from interpolated meteorological data) usually met away from Mesonet stations (see Appendix G). Although kriging is an exact method, if nugget variance exists, then the predicted value will be different from the original value. As a result, differences between ELI and ELE were found at the Mesonet stations.

Further Studies

Daily Variations

This research studied the effects of different interpolation methods, but did not consider the daily variation. As daily E_r is usually accumulated over multiple days, time series study is necessary. One question is whether the differences between interpolation methods and interpolation errors are offset in the long run.

Regional Variations

This study used a large study area, and test area, containing the large majority of the Oklahoma landscape. It would be interesting to subset the whole area into smaller regions and compare them. In this way, it may be possible to detect spatial patterns important to agriculture and other applications. Would a smaller area produce a better variogram?

Density of Data Collection

The selection and accuracy of interpolation methods are a function of the density of data observation. With the dense Mesonet stations, it is possible to test the accuracy of interpolation with less dense data, such as the hourly reporting stations of the National Weather Service. What is the optimum density for IDW, kriging and Thiessen polygons? Besides selection of interpolation method, this can also help in the design of data collection. This would allow design of an optimal density of data collection network.

Kriging Parameters and Other Interpolation Methods

If the variogram used for interpolation could be controlled, cross validation of the variogram could be performed. This could test how well the variogram fits so that a better, "individualized" variogram could be chosen for each case. Besides, some other common interpolation methods, for instance triangulation, can be investigated.

Evapotranspiration Estimation

The present study contrasting interpolation techniques is by no means exhaustive. The Penman estimation should be calibrated with lysimeter measurements. A better wind function may be created. Instead of exclusively using a Penman type equation, it would be worthwhile to test Thornthwaite's empirical method.

Summary

Four resolutions—1 km, 3 km, 9 km and 27 km—were used to interpolate alfalfa-reference evapotranspiration from over 96 Oklahoma Mesonet stations to an area of 180 km². The study showed that there was little difference between different resolutions of kriging at the center of cells. The results of using a coarse resolution were close to the mean of the results using a finer resolution. Although smaller estimation variance indicated that the results of a finer resolution might be more accurate, the estimation variance of finer resolutions was found to be less reliable than that of the coarser ones.

Given the density of the Oklahoma Mesonet (mean distance of 35 km between sites), the interpolation results of kriging, inverse distance weighting and Thiessen polygons were quite similar, especially near the Mesonet stations. For the three study days chosen—March 3, May 6, and June 16 of 1994, the mean absolute differences between the results of the three methods were well below 0.5 mm.

In addition to interpolating reference evapotranspiration with kriging, the meteorological factors were interpolated to individual surfaces, from which reference evapotranspiration was estimated. The difference between using point and surface meteorological data to estimate daily reference evapotranspiration was small. The mean absolute difference of the two methods was less than 0.5 mm.

If all results were compared with each other, kriging and Thiessen polygons had the largest difference, followed by kriging and inverse distance weighting. The difference between point and surface meteorological data was smaller and the difference between using various resolutions was the smallest.

A jack-knife procedure of cross validation was performed for May 6 and June 16. The error of kriging (K_{error}) and inverse distance weighting (D_{error}) was correlated with the difference of reference evapotranspiration between neighboring stations (N_{error}). The mean absolute difference of reference evapotranspiration between the neighboring Mesonet stations in the main body of Oklahoma was about 0.6 mm. This translated into a mean error of about 0.3 mm, half of 0.6 mm, in using Thiessen polygons. If an error of 0.5 mm is acceptable, then it does not matter which of the three methods of interpolation is used.

With data density as high as the Oklahoma Mesonet, given the results of this study, kriging does not have a performance markedly better than inverse distance weighting and Thiessen polygons. Of course, as the density of traditionally available data is usually much lower, using Thiessen polygons with these data will produce larger error and kriging would be expected to be superior under these circumstances. Results of the jack-knife procedures did show that kriging and inverse distance weighting outperformed Thiessen polygons. Although kriging seems to produce less error than inverse distance weighting, the amount of difference did not show apparent advantage in using kriging at these scales, data density and study days.

While the same kriging parameter values were used in all interpolations for control, the researcher is aware that the spatial dependence of various variables are not the same and that this thesis is not a repudiation of the advantages of kriging in all instances. Moreover, given the same meteorological element, its spatial dependence may vary from one day to another. An area of over 180,000 km² was used in this study. The results may not be applicable for a smaller area. Since only three study days were chosen in the present

study, searching for the best interpolation method for reference evapotranspiration should be an ongoing process.

REFERENCES

- ARC/INFO 6.1.1* [Computer Software]. (1992). Redlands: ESRI.
- Brock, F., Crawford, K., Elliott, R., Cuperus, G., Stadler, S., Johnson, H., & Eilts, M. (1994). The Oklahoma mesonet: A technical overview. *Journal of Atmospheric and Oceanic Technology* (in press).
- Burrough, P. A. (1986). *Principles of geographical information systems*. New York: Oxford University Press.
- Budyko, M. I. (1974). *Climate and life*. New York: Academic Press.
- Chow, V. T. (1964). Hydrology and its development. In V. T. Chow (Ed.), *Handbook of applied hydrology: A compendium of water-resources technology* (Section 1). New York: McGraw-Hill.
- Crawford, K. (Ed.). (1993). *The Oklahoma Mesonet*. Oklahoma Climatological Survey.
- Cuenca, R. (1989). *Irrigation system design*. Englewood cliffs: Prentice Hall.
- Curtis, L., & Trudgill, S. (1974). *The measurement of soil moisture* (British Geomorphological Research Group Technical Bulletin No. 13). Norwich: Geo Abstracts.
- Griffith, D. A. (1987). *Spatial autocorrelation* (Resource Publication in Geography). Washington: Association of American Geographers.
- Jensen, M. E., Burman, R. D., & Allen, R. G. (Eds.). (1990). *Evapotranspiration and irrigation water requirements: A manual* (ASCE Manuals and Reports on Engineering Practice No. 70). New York: American Society of Civil Engineers.
- Journel, A. G., & Huijbregts, CH. J. (1978). *Mining geostatistics*. London: Academic Press.
- Journel, A. G., & Rossi, M. E.. (1989). When do we need a trend model in kriging? *Mathematical Geology*, 21(7), 715-739.

- Lam, N. SN. (1983). Spatial interpolation methods: A review. *The American Cartographer*, 10(2), 129-149.
- Laslett, G. M., McBratney, A. B., Pahl, P. J., & Hutchinson, M. F. (1987). Comparison of several spatial prediction methods for soil pH. *Journal of Soil Science*, 38, 25-341.
- Mather, J. R. (1978). *The climatic water budget in environmental analysis*. Lexington: Heath.
- McBratney, A. B., & Webster, R. (1986). Choosing functions for semi-variograms of soil properties and fitting them to sampling estimates. *Journal of Soil Science*, 37, 617-639.
- Oliver, J. E. (1973). *Climate and man's environment*. John Wiley & Sons.
- Oliver, M., Webster, R., & Gerrard, J. (1989). Geostatistics in physical geography. Part I: theory. *Trans. Inst. Br. Geogr. (N.S.)*, 14, 259-269.
- Oliver, M. A., & Webster, R. (1990). Kriging: a method of interpolation for geographical information systems. *Int. J. Geographical Information Systems*, 4(3), 313-332.
- Penman, H. L. (1948). Natural evaporation from open water, bare soil and grass. *Proc. Roy. Soc.*, A193, 120-145.
- Royle, A. G., Clausen, F. L., & Frederiksen, P. (1981). Practical universal kriging and automatic contouring. *Geo-Processing*, 1, 377-394.
- Running, S. W. (1991). Computer simulation of regional evapotranspiration by integrating landscape biophysical attributes with satellite data. In T. J. Schmugge, & J.C. André (Eds.), *Land surface evaporation measurement and parameterization* (pp. 359-381). New York: Springer-Verlag.
- Running, S. W., Nemani, R. R., & Hungerford, R. D. (1987). Extrapolation of synoptic meteorological data in mountainous terrain and its use for simulating forest evapotranspiration and photosynthesis. *Canadian Journal of Forest Resources*, 17, 472-483.
- Sanderson, M. (Ed.). (1990). *Unesco sourcebook in climatology for hydrologists and water resource engineers*. Paris: Unesco.

- Shuttleworth, W. J. (1991). Evaporation models in hydrology. In T. J. Schmugge, & J.C. André (Eds.), *Land surface evaporation measurement and parameterization* (pp. 93-120). New York: Springer-Verlag.
- Snyder, J.P. (1987). *Map Projections: A Working Manual*. (U.S. Geological Survey Professional Paper 1395). Washington, DC: U.S. Government Print Office.
- S-PLUS Version 3.2* [Computer Software]. (1993). Seattle: MathSoft.
- Systat for Windows Version 5.03* [Computer Software]. (1992). Evanston: Systat.
- Tabios, G. Q., & Salas, J. D. (1985). A comparative analysis of techniques for spatial interpolation of precipitation. *Water Resources Bulletin*, 21(3), 365-380.
- Thornthwaite, C.W. (1948). An approach toward a rational classification of climate. *Geography Review*, 38, 55.
- Van Bavel, C. H. M. (1966). Potential evaporation: The combination concept and its experimental verification. *Water Resources Research*, 2, 455-467.
- Veihmeyer, F. J. (1964). Evapotranspiration. In V. T. Chow (Ed.), *Handbook of applied hydrology: A compendium of water-resources technology* (Section 11). New York: McGraw-Hill.
- Webster, R., & Oliver, M. A. (1990). *Statistical methods in soil and land resource survey*. New York: Oxford University Press.
- Wang, J.Y., & Ray, R. K. (1984). *Agriculture and Its Environment: Prediction and Control*. Dubuque, Iowa: Kendall/Hunt.
- Wright, J. L. (1982). New evapotranspiration crop coefficients. *Journal of the Irrigation and Drainage Division, ASCE*, 108(IR1), 57-74.

APPENDIXES

APPENDIX A—ADDITIONAL DATA ON OKLAHOMA MESONETWORK

TABLE X
LIST OF MESONET STATIONS

Station ID	Longitude (degree)	Latitude (degree)	Easting (m)	Northing (m)	Elevation (m)	Name
ADAX	-96.6692	34.7989	648,568	531,622	296	ADA
ALTU	-99.3378	34.5872	403,914	510,119	417	ALTUS
ALVA	-98.6717	36.7797	468,614	752,275	450	ALVA
ANTL	-95.7006	34.2242	738,149	468,774	181	ANTLERS
ARDM	-97.0850	34.1922	610,600	464,193	268	ARDMORE
ARNE	-99.9014	36.0728	356,714	676,165	719	ARNETT
BBOW	-94.6131	34.0144	838,933	447,581	110	BROKEN BOW
BEAV	-100.5303	36.8022	302,810	758,784	754	BEAVER
BESS	-99.0589	35.4017	431,184	599,960	511	BESSIE
BIXB	-95.8661	35.9625	720,305	661,425	184	BIXBY
BLAC	-97.2539	36.7544	595,187	748,498	303	BLACKWELL
BOIS	-102.4972	36.6925	126,769	754,253	1,267	BOISE CITY
BOWL	-96.6314	35.1717	651,788	573,005	286	BOWLEGS
BREC	-97.6942	36.4119	555,678	710,602	352	BRECKENRIDGE
BRIS	-96.3539	35.7808	676,485	640,782	241	BRISTOW
BUFF	-99.6408	36.8314	382,244	759,712	559	BUFFALO
BURB	-96.8111	36.6342	634,783	735,219	301	BURBANK
BURN	-97.2692	33.8939	593,602	431,098	228	BURNEYVILLE
BUTL	-99.2706	35.5914	412,403	621,390	513	BUTLER
BYAR	-97.0033	34.8497	617,983	537,151	347	BYARS
CALV	-96.3342	34.9925	679,031	553,320	237	CALVIN
CAMA	-99.3464	36.0283	406,581	670,013	587	CAMARGO
CENT	-96.3331	34.6086	679,504	510,728	209	CENTRAHOMA
CHAN	-96.8042	35.6528	635,839	626,317	291	CHANDLER
CHER	-98.3628	36.7481	496,148	748,396	361	CHEROKEE
CHEY	-99.7275	35.5458	370,882	617,295	692	CHEYENNE
CHIC	-97.9144	35.0319	534,819	557,587	329	CHICKASHA
CLAR	-95.6417	36.3172	739,929	701,079	213	CLAREMORE
CLAY	-95.3261	34.6556	771,741	517,210	195	CLAYTON
CLOU	-95.2494	34.2231	779,710	469,373	221	CLOUDY
COOK	-94.8486	35.6794	812,806	631,725	303	COOKSON
COPA	-95.8853	36.9097	717,185	766,502	252	COPAN
DURA	-96.3200	33.9206	681,378	434,414	200	DURANT
ELRE	-98.0358	35.5481	524,226	614,943	421	EL RENO
ERIC	-99.8033	35.2047	363,016	579,632	604	ERICK
EUFA	-95.6583	35.3000	740,185	588,186	203	EUFAULA
FAIR	-98.4978	36.2636	483,388	694,794	407	FAIRVIEW
FORA	-96.4278	36.8403	668,891	758,288	330	FORAKER
FREE	-99.1422	36.7256	426,491	746,989	530	FREEDOM
FTCB	-98.4667	35.1492	484,606	571,096	420	FORT COBB

TABLE X (Continued)

Station ID	Longitude (degree)	Latitude (degree)	Easting (m)	Northing (m)	Elevation (m)	Name
GOOD	-101.6014	36.6017	206,294	740,274	996	GOODWELL
GRAN	-98.7397	34.2392	458,166	470,494	342	GRANDFIELD
GUTH	-97.4800	35.8489	574,710	648,044	328	GUTHRIE
HASK	-95.6400	35.7475	741,072	637,866	183	HASKELL
HINT	-98.4822	35.4844	483,669	608,317	489	HINTON
HOBA	-99.0525	34.9897	430,911	554,245	474	HOBART
HOLL	-99.8339	34.6861	358,709	522,181	498	HOLLIS
HOOK	-101.2253	36.8553	241,059	766,963	912	HOOKER
HUGO	-95.5400	34.0308	753,299	447,567	175	HUGO
IDAB	-94.8806	33.8303	814,709	426,549	110	IDABEL
JAYX	-94.7831	36.4817	816,570	720,865	308	JAY
KENT	-102.8781	36.8297	93,653	771,335	1,322	KENTON
KETC	-97.7647	34.5289	548,161	501,683	341	KETCHUM RANCH
KING	-97.9111	35.8806	535,797	651,753	319	KINGFISHER
LAHO	-98.1114	36.3844	518,229	707,815	395	LAHOMA
LANE	-95.9975	34.3086	710,679	477,768	182	LANE
MADI	-96.9431	34.0361	623,728	446,901	232	MADILI
MANG	-99.4239	34.8361	396,635	537,901	461	MANGUM
MARE	-97.2128	36.0644	598,849	671,930	331	MARENA
MARS	-97.6014	36.1186	563,867	678,014	315	MARSHALL
MAYR	-99.0111	36.9869	438,731	775,765	552	MAY RANCH
MCAL	-95.7808	34.8819	729,710	541,635	230	MCALESTER
MEDF	-97.7456	36.7922	551,300	752,822	330	MEDFORD
MEDI	-98.5667	34.7292	474,854	524,618	482	MEDICINE PARK
MIAM	-94.8447	36.8886	809,974	765,874	248	MIAMI
MINC	-97.9556	35.2722	531,271	584,276	431	MINCO
MTHE	-94.8228	34.3108	818,780	479,964	286	MT HERMAN
NEWK	-96.9106	36.8981	625,803	764,469	369	NEWKIRK
NORM	-97.4836	35.2556	574,196	582,202	361	NORMAN
NOWA	-95.6078	36.7436	742,213	748,435	206	NOWATA
OILT	-96.4972	36.0314	663,332	668,485	257	OILTON
OKEM	-96.2628	35.4317	685,087	602,110	263	OKEMAH
OKMU	-95.9150	35.5811	716,444	619,046	205	OKMULGEE
PAUL	-97.2294	34.7156	597,303	522,247	292	PAULS VALLEY
PAWN	-96.7697	36.3611	638,617	704,935	283	PAWNEE
PERK	-97.0481	35.9983	613,698	664,603	292	PERKINS
PRYO	-95.2717	36.3689	773,037	707,395	196	PRYOR
PUTN	-98.9603	35.8992	441,117	654,997	589	PUTNAM
REDR	-97.1531	36.3556	604,213	704,235	293	RED ROCK
RETR	-99.3597	35.1231	403,195	569,603	538	RETROP
RING	-97.5883	34.1939	564,207	464,442	280	RINGLING

TABLE X (Continued)

Station ID	Longitude (degree)	Latitude (degree)	Easting (m)	Northing (m)	Elevation (m)	Name
SALL	-94.7978	35.4381	818,053	605,056	156	SALLISAW
SEIL	-99.0406	36.1903	434,471	687,428	540	SEILING
SHAW	-96.9483	35.3650	622,867	594,339	329	SHAWNEE
SKIA	-96.0372	36.4147	704,286	711,411	285	SKIATOOK
SLAP	-100.2619	36.5969	326,046	735,246	771	SLAPOUT
SPEN	-97.3411	35.5422	587,206	613,986	373	SPENCER
STIG	-95.1814	35.2653	783,628	585,111	175	STIGLER
STIL	-97.0950	36.1211	609,452	678,223	272	STILLWATER
STUA	-96.0700	34.8764	703,289	540,680	254	STUART
SULP	-96.9506	34.5661	622,888	505,694	320	SULPHUR
TAHL	-94.9869	35.9728	799,563	663,982	290	TAHLEQUAH
TALI	-95.0117	34.7106	800,421	523,901	204	TALIHINA
TIPT	-99.1375	34.4394	421,962	493,350	388	TIPTON
TISH	-96.6794	34.3328	647,899	479,905	268	TISHOMINGO
TULL	-95.4133	35.8397	761,383	648,444	189	TULLAHASSEE
VINI	-95.2211	36.7753	776,674	752,569	236	VINITA
WALT	-98.3206	34.3647	496,933	483,905	308	WALTERS
WASH	-97.5208	34.9817	570,711	551,821	340	WASHINGTON
WATO	-98.5261	35.8422	480,218	648,069	516	WATONGA
WAUR	-97.9878	34.1678	527,367	461,763	285	WAURIKA
WEAT	-98.7753	35.5081	457,125	611,319	538	WEATHERFORD
WEBB	-95.1322	35.4728	787,620	608,225	146	WEBBERS FALLS
WEST	-94.6450	36.0111	830,282	668,975	348	WESTVILLE
WILB	-95.3478	34.9008	769,248	544,383	201	WILBURTON
WIST	-94.6881	34.9847	829,284	555,014	143	WISTER
WOOD	-99.4169	36.4233	401,203	713,976	625	WOODWARD
WYNO	-96.3422	36.5172	676,834	722,506	269	WYNONA
NINN	-97.9528	34.9744	531,273	551,233	329	NINNEKAH
ACME	-98.0056	34.8056	526,303	532,531	407	ACME
APAC	-98.2917	34.9139	500,260	544,801	440	APACHE
NORR	-97.4842	35.2553	574,145	582,172	360	NORMAN REF.

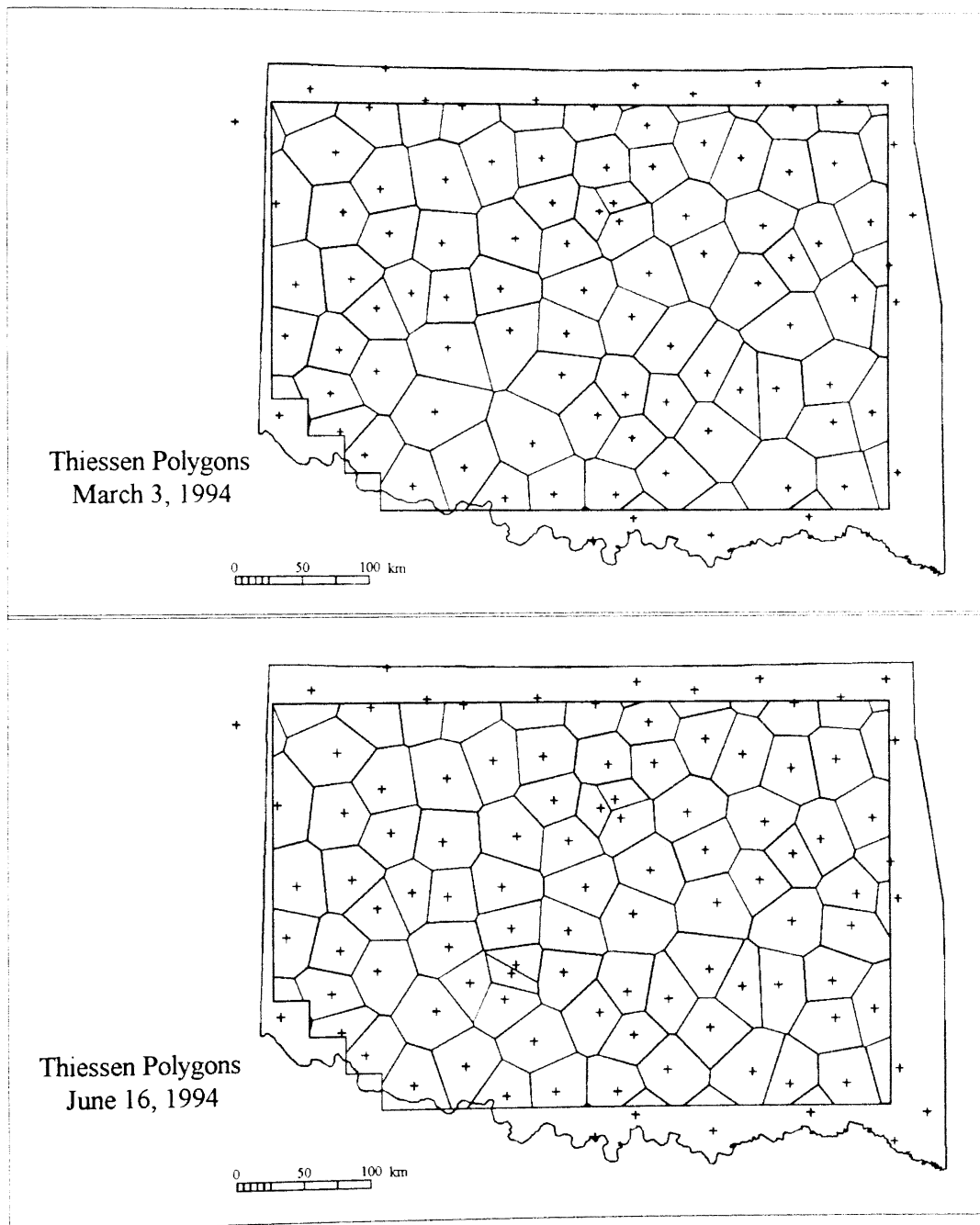


Figure 26. Thiessen Polygons Created from Mesonet Stations, March 3 and June 16, 1994.

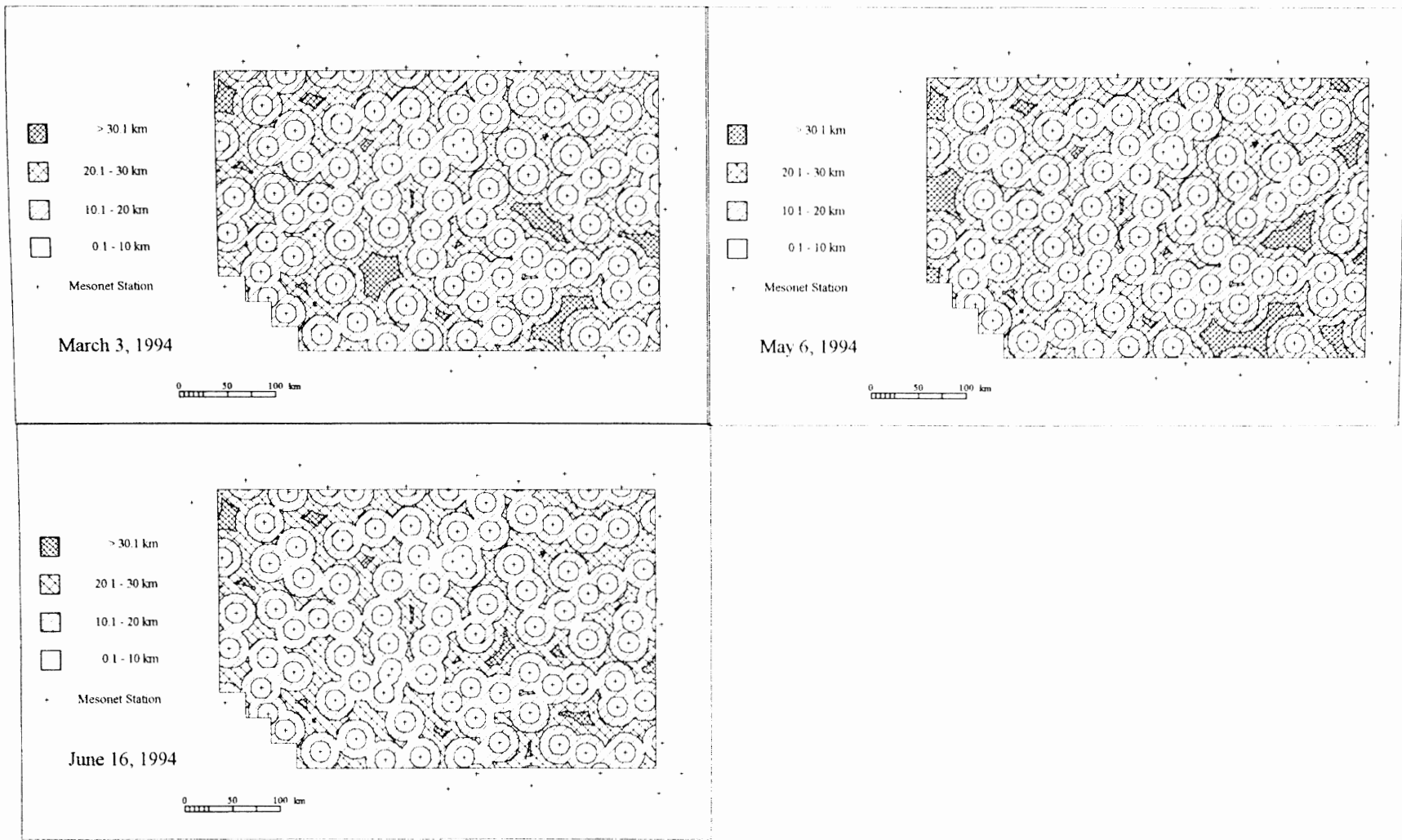


Figure 27. The Subsets of the Test Area by Distance from Mesonet Stations.

APPENDIX B—MAP PROJECTION AND PROGRAMS

TABLES XI

ALBERS CONIC EQUAL AREA PROJECTION USED IN THE STUDY

1st Standard Parallel	34° 1'
2nd Standard Parallel	36° 30'
Central Meridian	-97° 12'
Latitude of Projection Origin	30°
False Easting	6,000,000
Spheroid	Clarke 1866
Units	Meters

```

/* caletr.aml
/* calculate referenced evapotranspiration
/* March 11, 1994

tables
relate restore relate

select daily
reselect valid = 1

/* initialize constant items
&call initial
&call getcd
&call getnrad
&call getwfac
&call gettrml
&call gettrm2
&call getetr

q stop

&type REFERENCE EVAPOTRANSPIRATION CALCULATED
&return

/*****
/* initialize items
&routine initial

/* initialize constant items
calc albo = 0.23
calc hcrp = 50
calc disp = 2 * hcrp / 3
calc zom = 0.123 * hcrp
calc arb = 1.1
calc brb = -0.1

&return /* initial end

/*****
/* calculate Cd and Cg
&routine getcd

calc eslp = 0.2 * ( 0.00738 * tair + 0.8072 ) ** 7 - 0.000116
calc heat = 2.501 - 2.361e-3 * tair
calc psyk = 0.001013 * pres / ( 0.622 * heat )

calc cd = eslp / ( eslp + psyk )
calc cg = 1 - cd

&return /* getcd end

/*****
/* calculate Net radiation, MJ m^-2 d^-1
&routine getnrad

&call getnbakt
&call getnbak
calc nrad = ( 1 - albo ) * srad - nbak

&return /* getnrad end

/*****
/* calculate Net outgoing long-wave radiation, MJ m^-2 d^-1
&routine getnbak

&call getsradt
calc nbak = ( arb * srad / sradt + brb ) * nbakt

&return /* getsradt end

```

```

/*****
/* calculate Solar radiation on a cloudless day, MJ m-2 d-1
&routine getsradt

/* calculate A' and B'
&call getprm
/* calculate cos(angl)
&call getangl
calc sradt = aprm + bprm * angl

&return /* getsradt end

/*****
/* calculate cos(theta) for Solar radiation on a cloudless day
&routine getangl

&setvar cprm := 172
/* calculate Julian day
&setvar month := [substr [show &workspace] [calc [length [show &workspace]] - 3] 2]
&setvar day := [substr [show &workspace] [calc [length [show &workspace]] - 1] 2]

&select %month%
  &when 01
    &setvar jday := %day%
  &when 02
    &setvar jday := %day% + 31
  &when 03
    &setvar jday := %day% + 59
  &when 04
    &setvar jday := %day% + 90
  &when 05
    &setvar jday := %day% + 120
  &when 06
    &setvar jday := %day% + 151
  &when 07
    &setvar jday := %day% + 180
  &when 08
    &setvar jday := %day% + 212
  &when 09
    &setvar jday := %day% + 243
  &when 10
    &setvar jday := %day% + 273
  &when 11
    &setvar jday := %day% + 304
  &when 12
    &setvar jday := %day% + 334
&end

/* calculate cos(theta)
&setvar theta = 4 * 3.1416 ** 2 * %jday% / ( 365 - %cprm% ) / 360
calc angl = [cos %theta%]

&return /* getangl end

/*****
/* calculate A' and B' for Solar radiation on a cloudless day
&routine getprm

calc aprm = 31.55 - 0.273 * mgeog//lat + 0.0008 * mgeog//elev
calc bprm = -0.299 + 0.268 * mgeog//lat + 0.0004 * mgeog//elev

&return /* getprm end

/*****
/* calculate Net outgoing long-wave radiation on a cloudless day, MJ m-2 d-1
&routine getnbakt

/* Stefan-Boltzmann constant, MJ m-2 d-1 K-4
&setvar sb = 4.903e-9
/* calculate net emissivity
&call getemit
calc nbakt = emit * %sb% * tair4

&return /* getnbakt end

```

```

/*****
/* calculate Net emissivity
&routine getemit

/* calculate net emissivity
&setvar ka = 0.39
&setvar kb = -0.158
calc emit = %ka% + %kb% * edew ** 0.5

&return /* getemit end

/*****
/* calculate Wind factor
&routine getwfac

&call getwsp2
calc wfac = -0.3405 + 0.93312 * wsp2

&return /* getwfac end

/*****
/* calculate reference evapotranspiration, mm d^-1
&routine getetr

calc etr = ( trm1 + trm2 ) / heat

&return /* getetr end

/*****
/* calculate radiation term, MJ m^-2 d^-1
&routine gettrm1

calc trm1 = cd * nrad

&return /* gettrm1

/*****
/* calculate aerodynamic term, MJ m^-2 d^-1
&routine gettrm2

calc trm2 = cg * 6.43 * wfac * edef

&return /* gettrm2 end

/*****
/* calculate wind speed at 200 cm from wind speed at 1000 cm, m s^-1
&routine getwsp2

calc wsp2 = wspd * ( ln ( ( 200 - disp ) / zom ) ) / ( ln ( ( 1000 - disp ) / zom ) )

&return /* getwsp2 end

/*****

```



```

/* caletrg.aml
/* calculate referenced evapotranspiration from interpolated data
/* May 11, 1994

gird
relate restore relate
select daily
reselect valid = 1

/* initialize constant items
&call initial
&call getcd
&call getnrad
&call getwfac
&call gettrml
&call gettrm2
&call getetr

quit

&return &inform REFERENCE EVAPOTRANSPIRATION CALCULATED

/*****
/* initialize items
&routine initial

/* initialize constant items
albo = scalar (0.23)
hcrp = scalar (50)
disp = scalar (2 * hcrp / 3)
zom = scalar (0.123 * hcrp)
arb = scalar (1.1)
brb = scalar (-0.1)

&return /* initial end

/*****
/* calculate Cd and Cg
&routine getcd

eslpq1 = 0.2 * ( 0.00738 * tairg1 + 0.8072 ) ** 7 - 0.000116
heatq1 = 2.501 - 2.361e-3 * tairg1
psyq1 = 0.001013 * presg1 / ( 0.622 * heatq1 )
cdq1 = eslpq1 / ( eslpq1 + psyq1 )
cgq1 = 1 - cdq1

&return /* getcd end

/*****
/* calculate Net radiation, MJ m^-2 d^-1
&routine getnrad

&call getnbakt
&call getnbak
nradq1 = ( 1 - albo ) * srdaq1 - nbakq1

&return /* getnrad end

/*****
/* calculate Net outgoing long-wave radiation, MJ m^-2 d^-1
&routine getnbak

&call getsradt
nbakq1 = ( arb * srdaq1 / sradtq1 + brb ) * nbaktq1

&return /* getsradt end

```

```

/*****
/* calculate Solar radiation on a cloudless day, MJ m-2 d-1
&routine getsradt

/* calculate A' and B'
&call getprm
/* calculate cos(angl)
&call getangl
sradtgi = aprmgi + bprmgi * angl

&return /* getsradt end

/*****
/* calculate cos(theta) for Solar radiation on a cloudless day
&routine getangl

&setvar cprm := 172
/* calculate Julian day
&setvar month := [substr [show &workspace] [calc [length [show &workspace]] - 3] 2]
&setvar day := [substr [show &workspace] [calc [length [show &workspace]] - 1] 2]

&select %month%
  &when 01
    &setvar jday := %day%
  &when 02
    &setvar jday := %day% + 31
  &when 03
    &setvar jday := %day% + 59
  &when 04
    &setvar jday := %day% + 90
  &when 05
    &setvar jday := %day% + 120
  &when 06
    &setvar jday := %day% + 151
  &when 07
    &setvar jday := %day% + 180
  &when 08
    &setvar jday := %day% + 212
  &when 09
    &setvar jday := %day% + 243
  &when 10
    &setvar jday := %day% + 273
  &when 11
    &setvar jday := %day% + 304
  &when 12
    &setvar jday := %day% + 334
&end

/* calculate cos(theta)
&setvar theta = 4 * 3.1416 ** 2 * %jday% / ( 365 - %cprm% ) / 360
angl = scalar ( [cos %theta%] )

&return /* getangl end

/*****
/* calculate A' and B' for Solar radiation on a cloudless day
&routine getprm

calc aprm = 31.55 - 0.273 * mgeog//lat + 0.0008 * mgeog//elev
calc bprm = -0.299 + 0.268 * mgeog//lat + 0.0004 * mgeog//elev

&return /* getprm end

/*****
/* calculate Net outgoing long-wave radiation on a cloudless day, MJ m-2 d-1
&routine getnbakt

/* Stefan-Boltzmann constant, MJ m-2 d-1 K-4
&setvar sb = 4.903e-9
/* calculate net emissivity
&call getemit
nbaktgi = emitgi * %sb% * tair4gi

&return /* getnbakt end

```

```

/*****
/* calculate Net emissivity
&routine getemit

/* calculate net emissivity
&setvar ka = 0.39
&setvar kb = -0.158
emitg1 = %ka% + %kb% * edewg1 ** 0.5

&return /* getemit end

/*****
/* calculate Wind factor
&routine getwfac

&call getwsp2
wfacg1 = -0.3405 + 0.93312 * wsp2g1

&return /* getwfac end

/*****
/* calculate reference evapotranspiration, mm d^-1
&routine getetr

ele1 = ( trm1g1 + trm2g1 ) / heatg1

&return /* getetr end

/*****
/* calculate radiation term, MJ m^-2 d^-1
&routine gettrm1

trm1g1 = cdg1 * nradg1

&return /* gettrm1

/*****
/* calculate aerodynamic term, MJ m^-2 d^-1
&routine gettrm2

trm2g1 = cgg1 * 6.43 * wfacg1 * edefg1

&return /* gettrm2

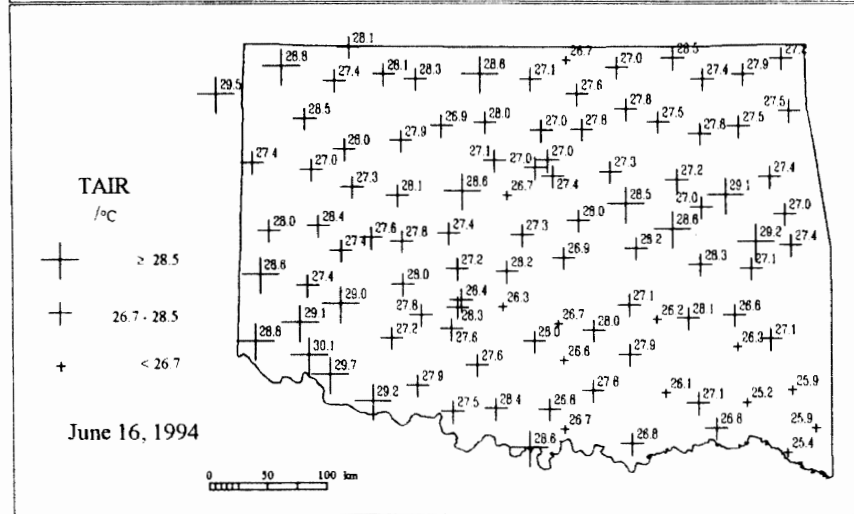
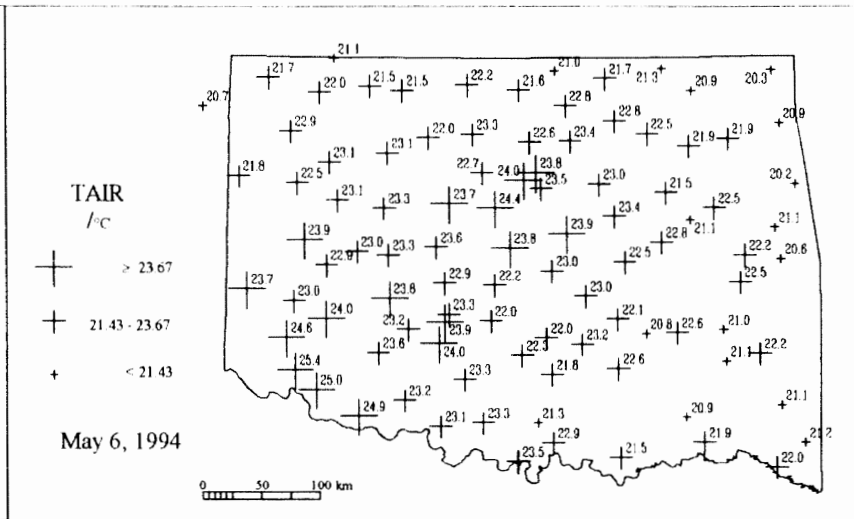
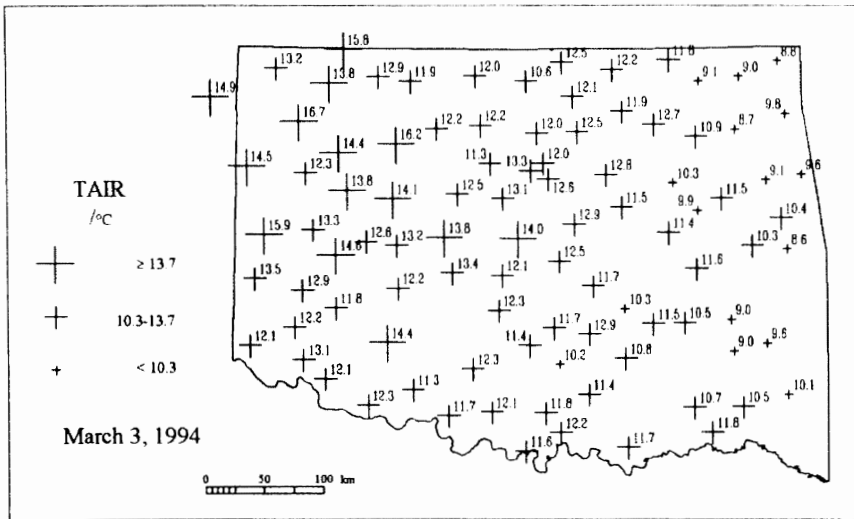
/*****
/* calculate wind speed at 200 cm from wind speed at 1000 cm, m s^-1
&routine getwsp2

wsp2g1 = wspdg1 * ( ln ( ( 200 - disp ) / zom ) ) / ( ln ( ( 1000 - disp ) / zom ) )

&return
/*****

```

APPENDIX C—METEOROLOGICAL ELEMENTS ON STUDY DAYS



Air Temperature

- + $\geq \text{Mean} + \sigma$
- + Mean - σ to Mean + σ
- + $< \text{Mean} - \sigma$

Figure 28. Daily Air Temperature at Mesonet Stations.

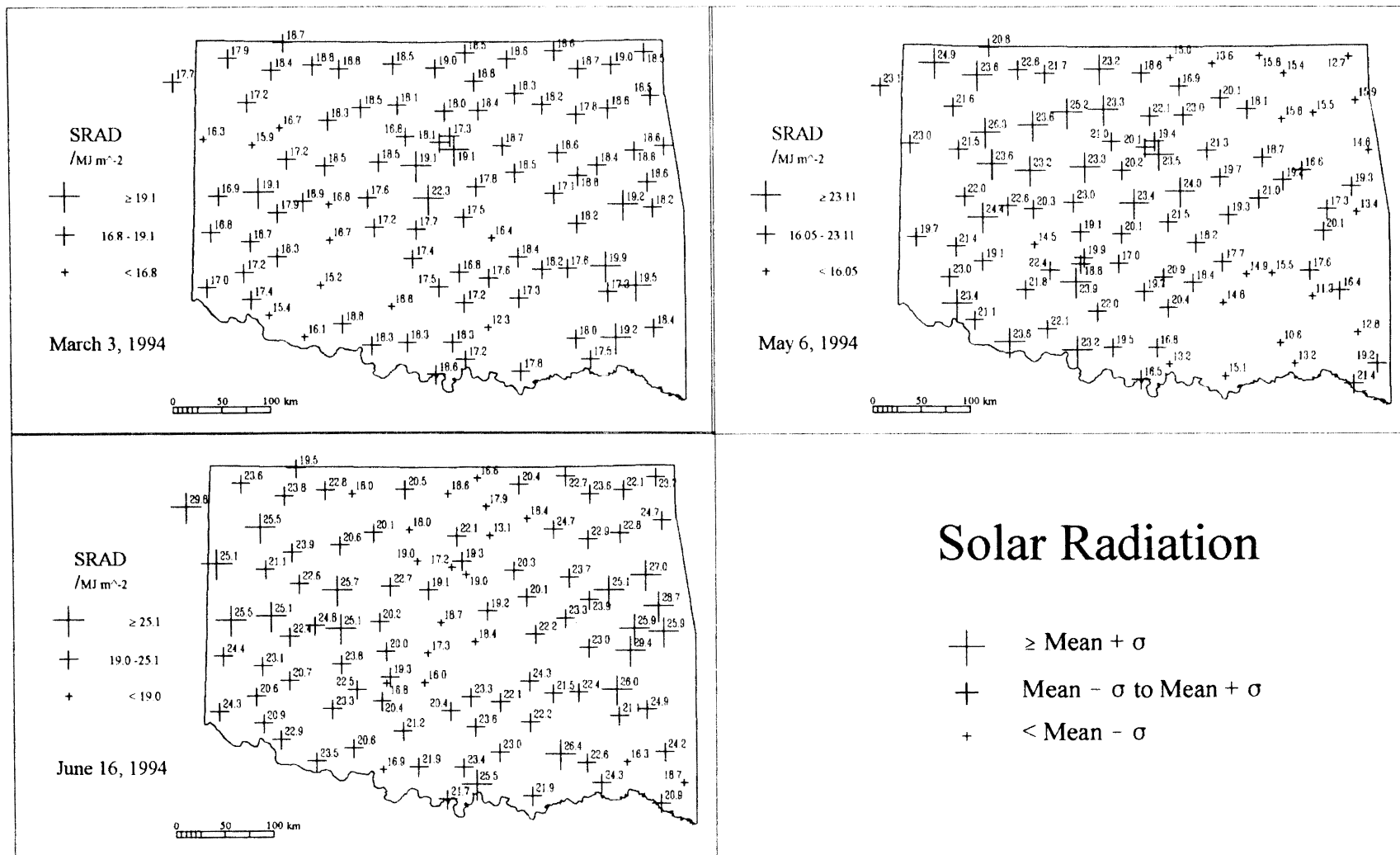
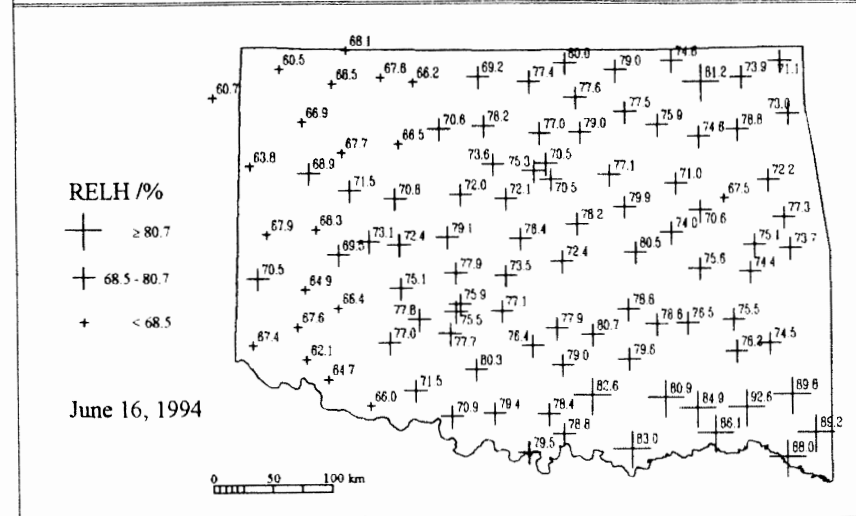
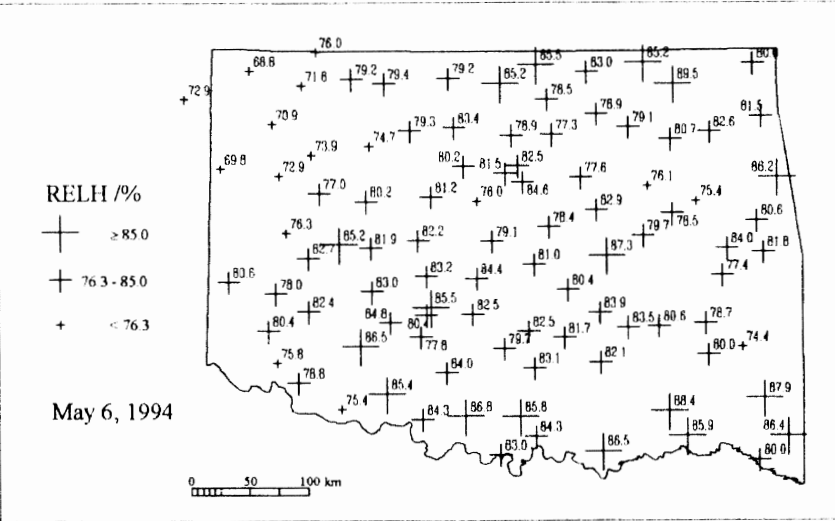
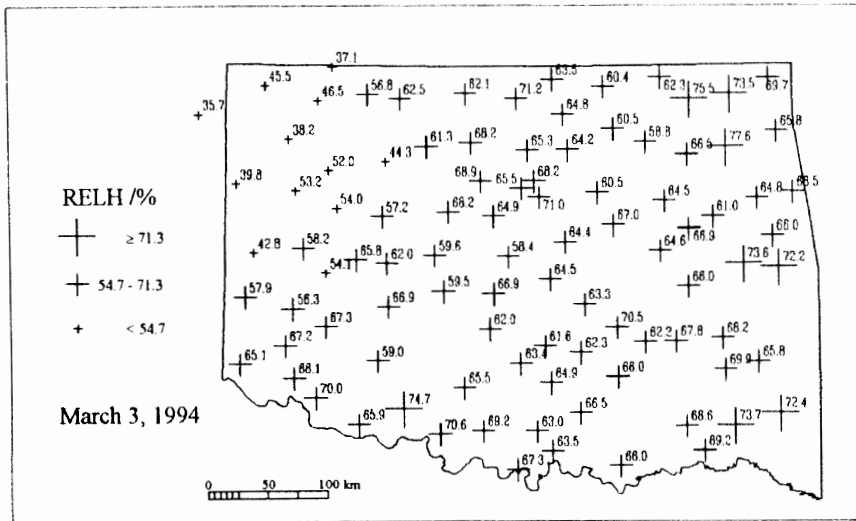


Figure 29. Daily Solar Radiation at Mesonet Stations.



Relative Humidity

- ⊕ ≥ Mean + σ
- ⊕ Mean - σ to Mean + σ
- + < Mean - σ

Figure 30. Daily Relative Humidity at Mesonet Stations.

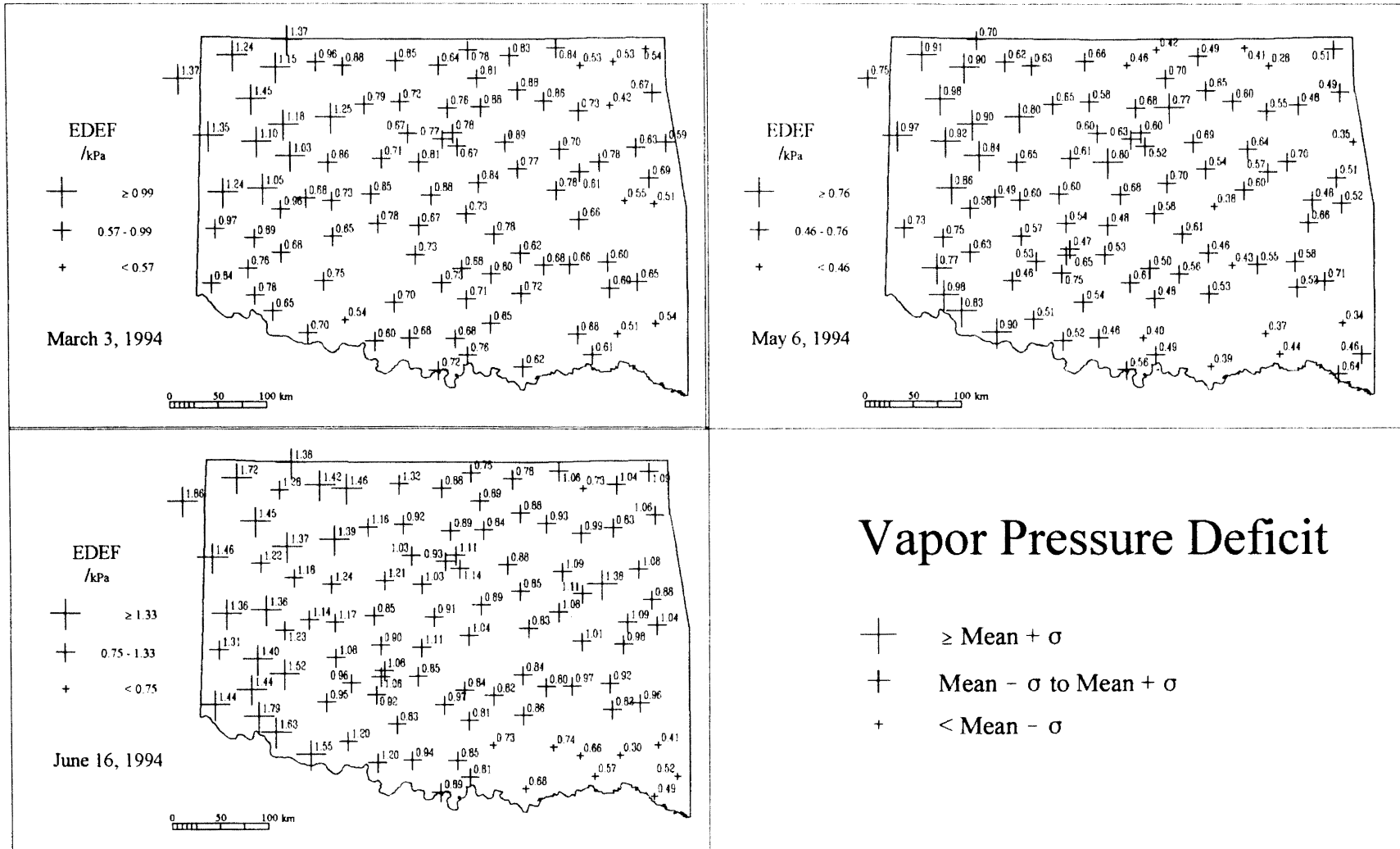


Figure 31. Daily Vapor Pressure Deficit at Mesonet Stations.

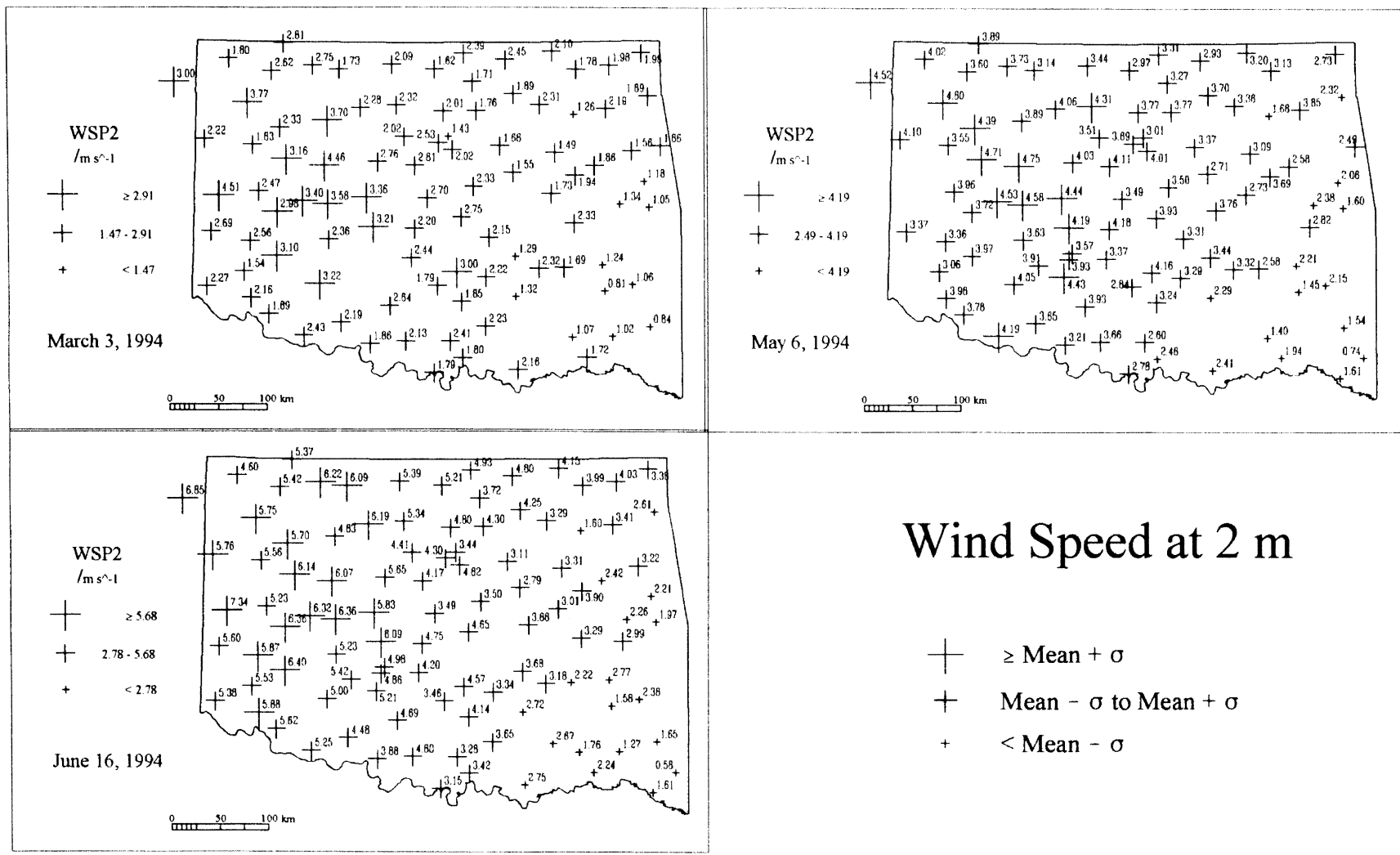
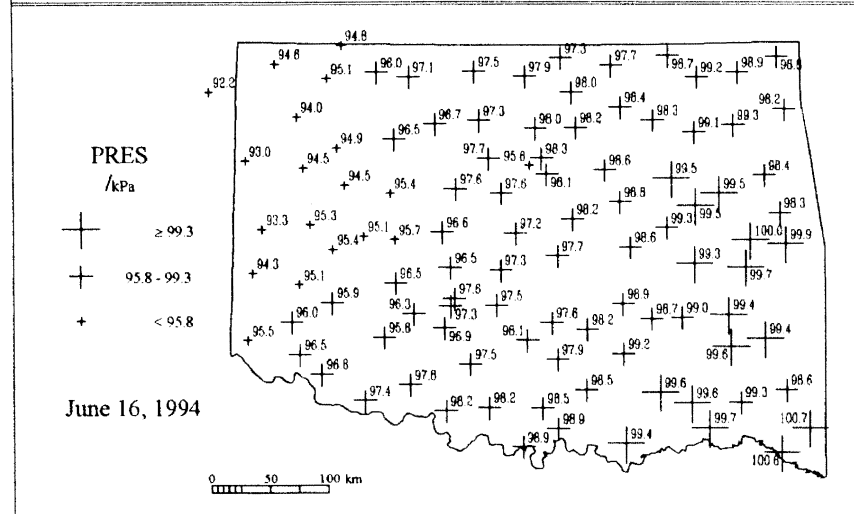
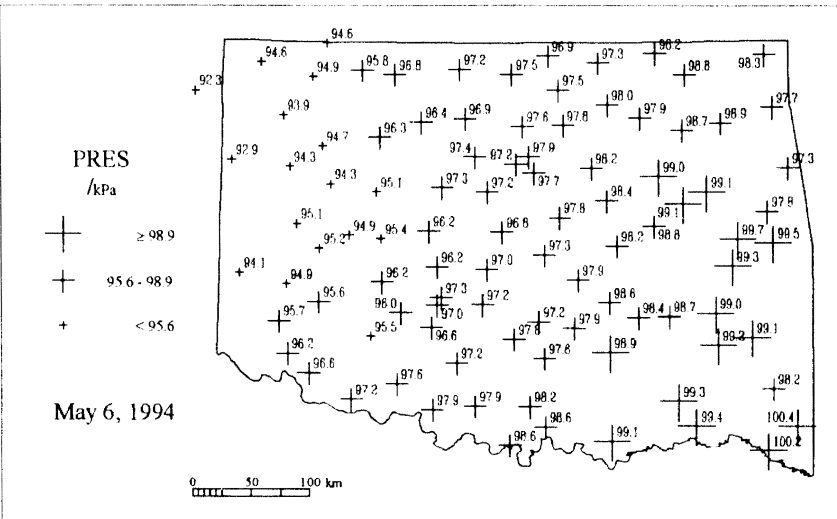
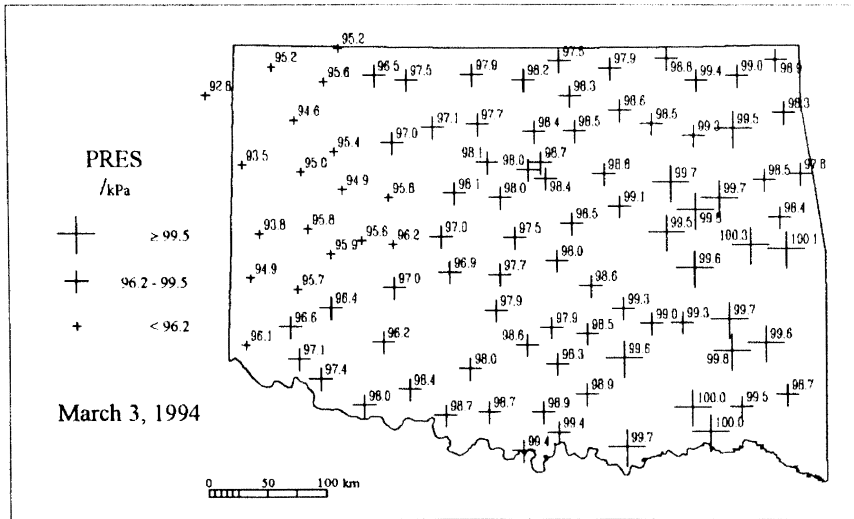


Figure 32. Daily Wind Speed at 2 m (Extrapolated from 10 m) at Mesonet Stations.



Air Pressure

- + ≥ Mean + σ
- + Mean - σ to Mean + σ
- + < Mean - σ

Figure 33. Daily Station Air Pressure at Mesonet Stations.

APPENDIX D—SEMI-VARIOGRAMS

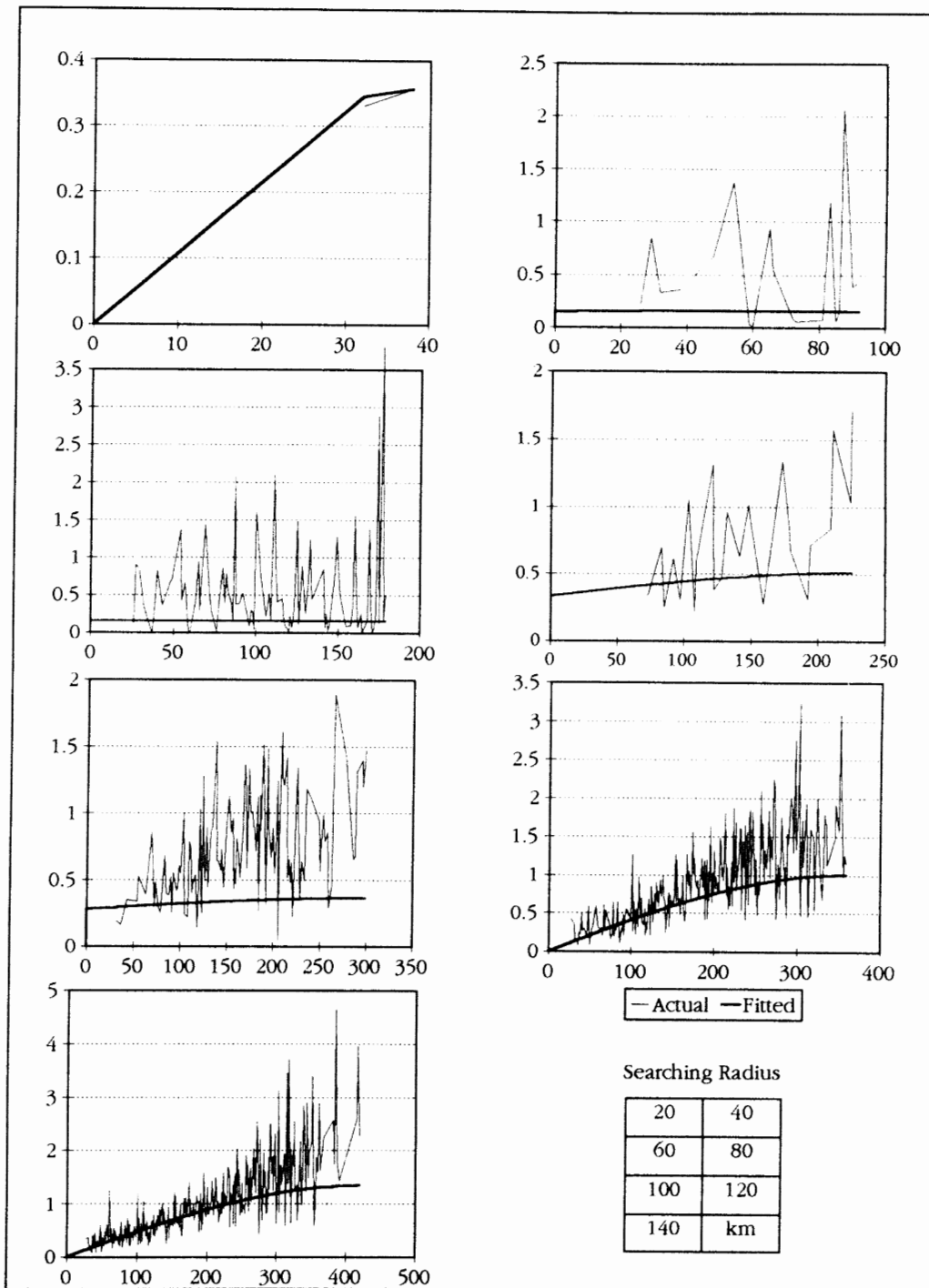


Figure 34. Actual and Fitted Variograms of Reference Evapotranspiration (Resolution = 1 km), May 6, 1994.

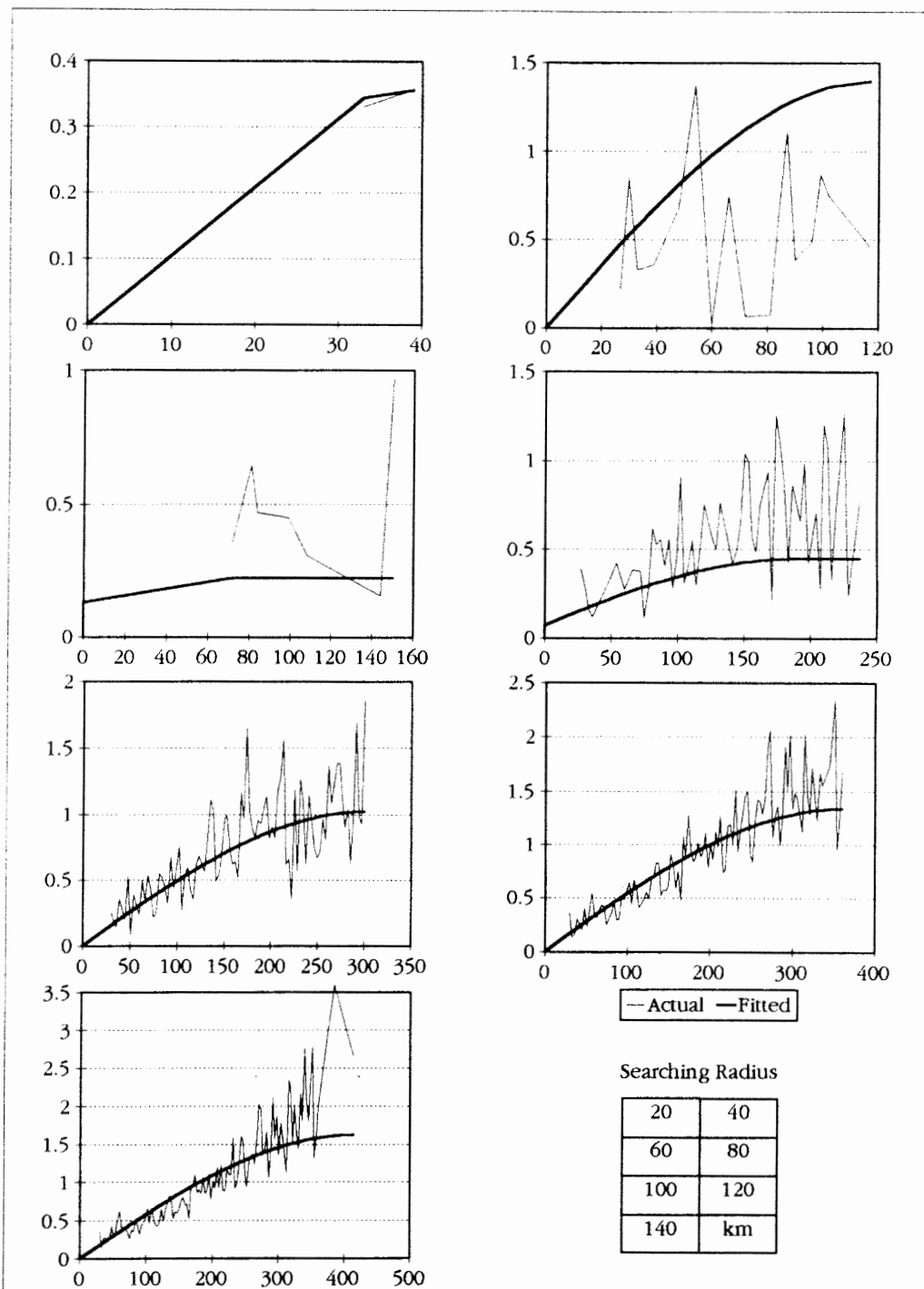


Figure 35. Actual and Fitted Variograms of Reference Evapotranspiration (Resolution = 3 km), May 6, 1994.

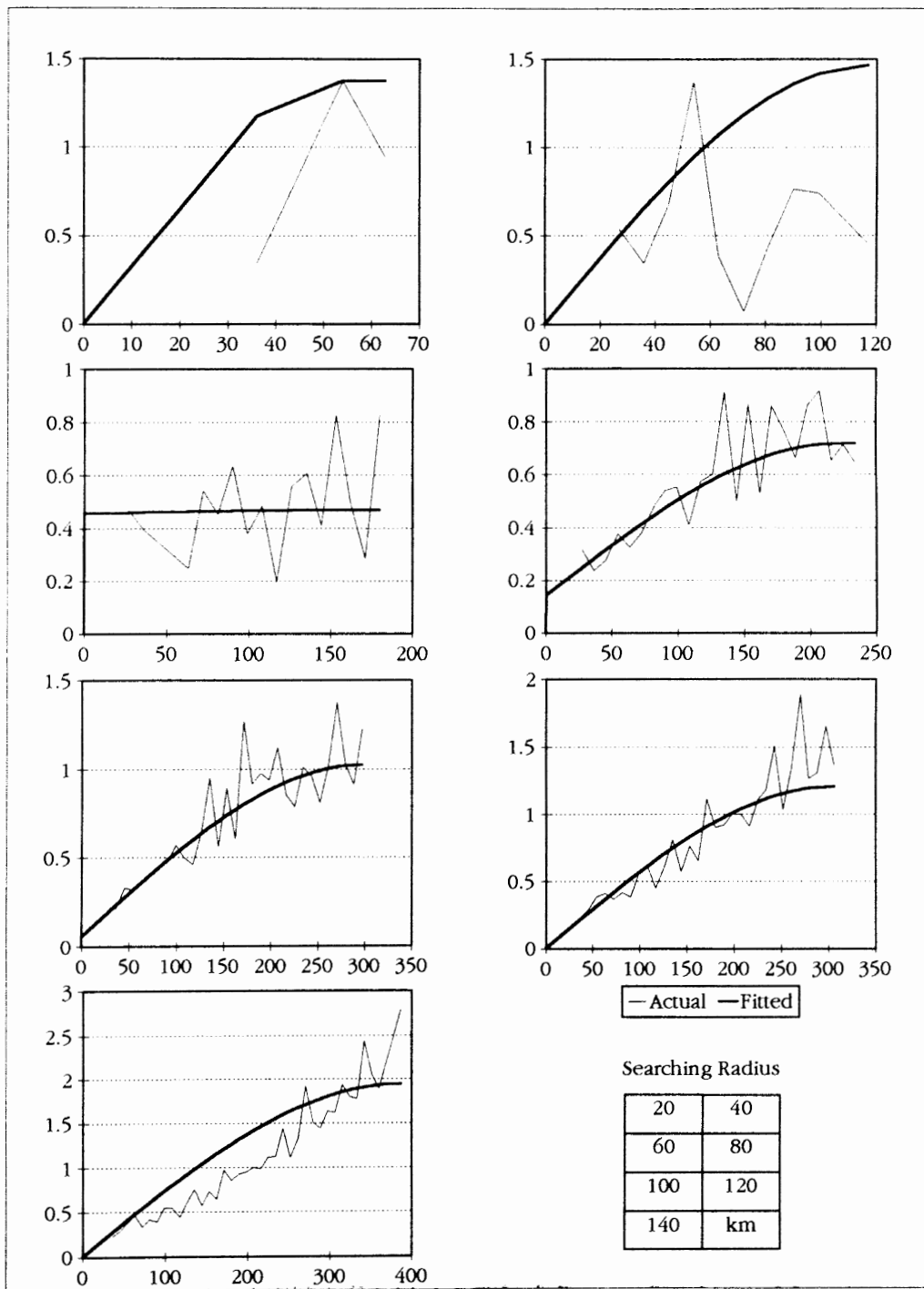


Figure 36. Actual and Fitted Variograms of Reference Evapotranspiration (Resolution = 9 km), May 6, 1994.

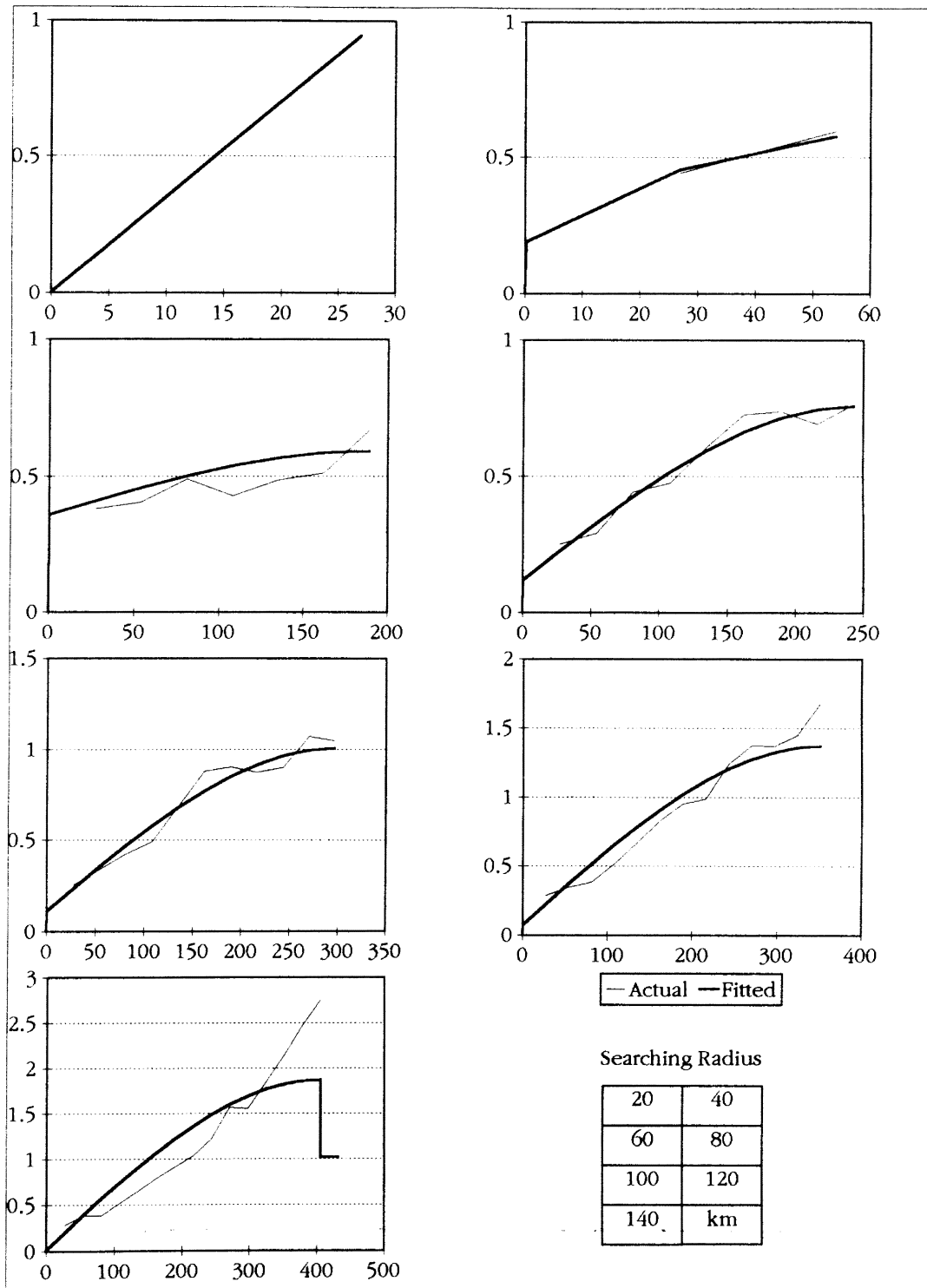


Figure 37. Actual and Fitted Variograms of Reference Evapotranspiration (Resolution = 27 km), May 6, 1994.

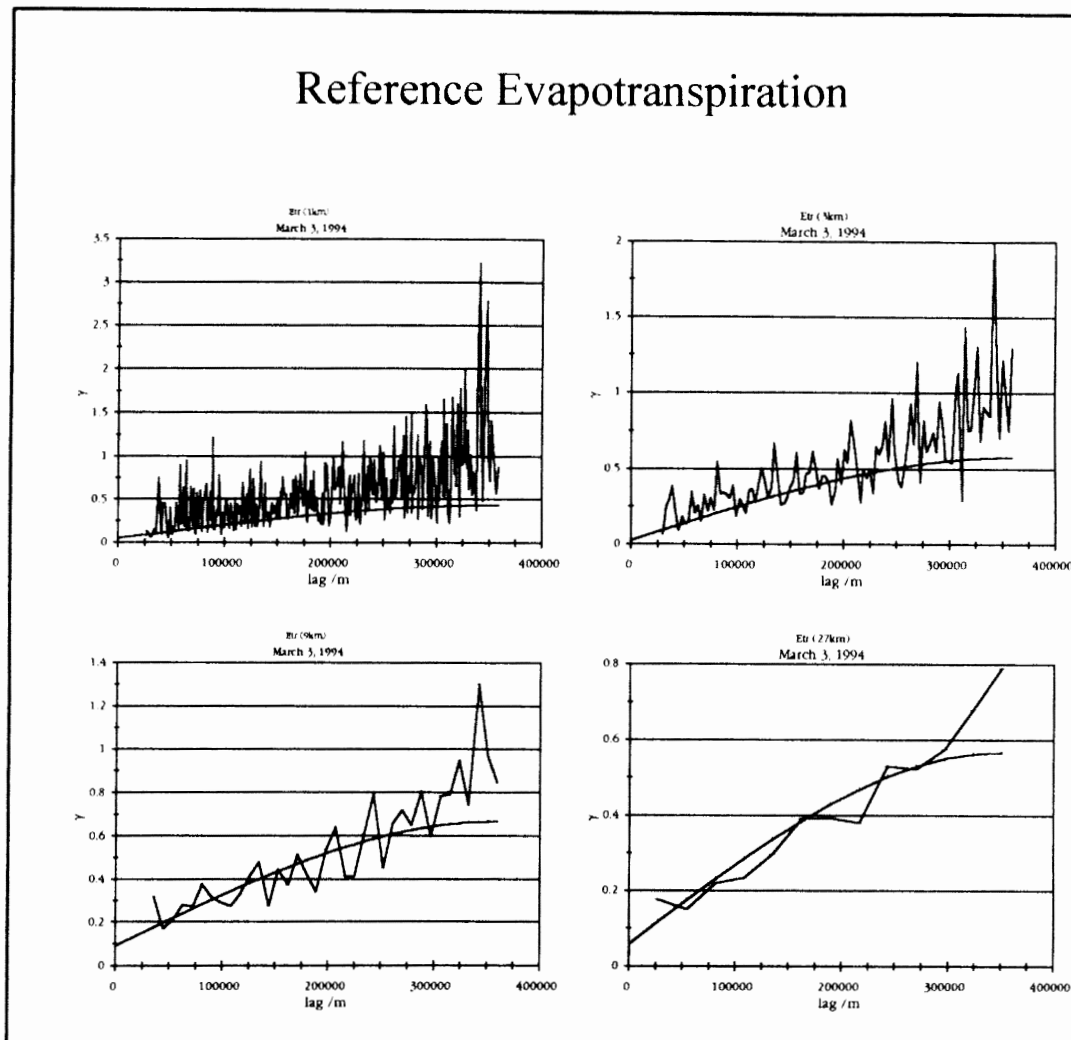


Figure 38. Actual and Fitted Variograms of Reference Evapotranspiration (Searching Radius = 120 km), March 3, 1994.

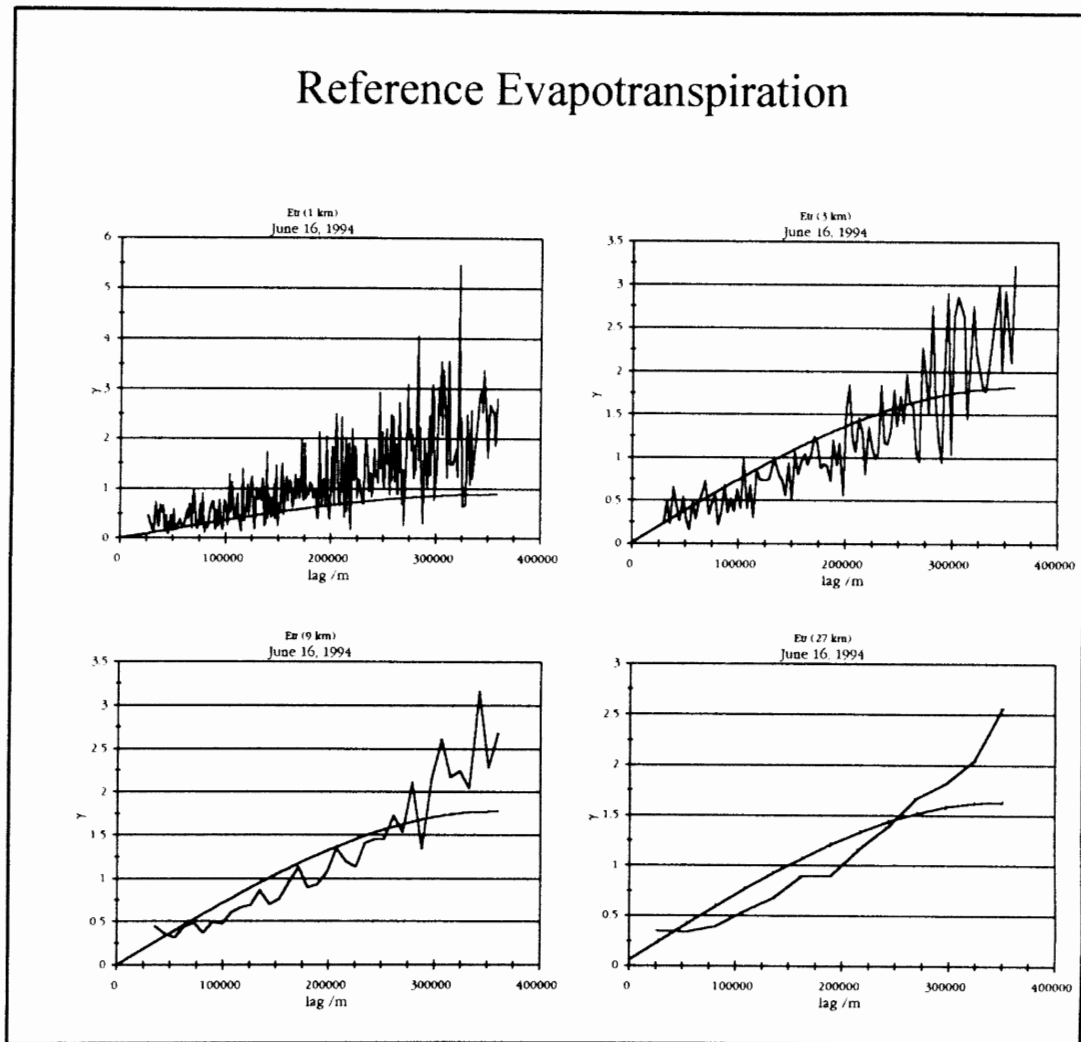


Figure 39. Actual and Fitted Variograms of Reference Evapotranspiration (Searching Radius = 120 km), June 16, 1994.

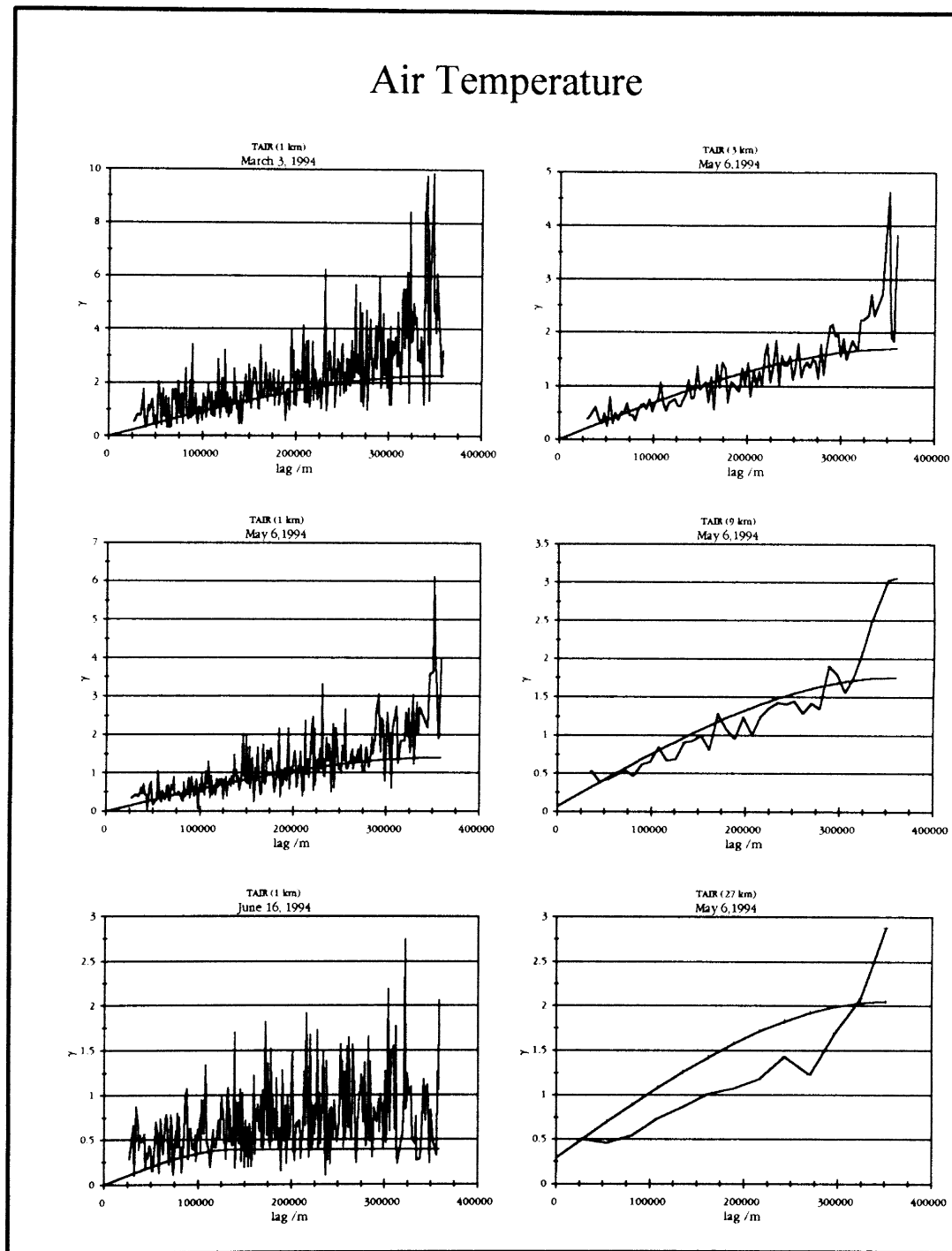


Figure 40. Actual and Fitted Variograms of Air Temperature (Searching Radius = 120 km).

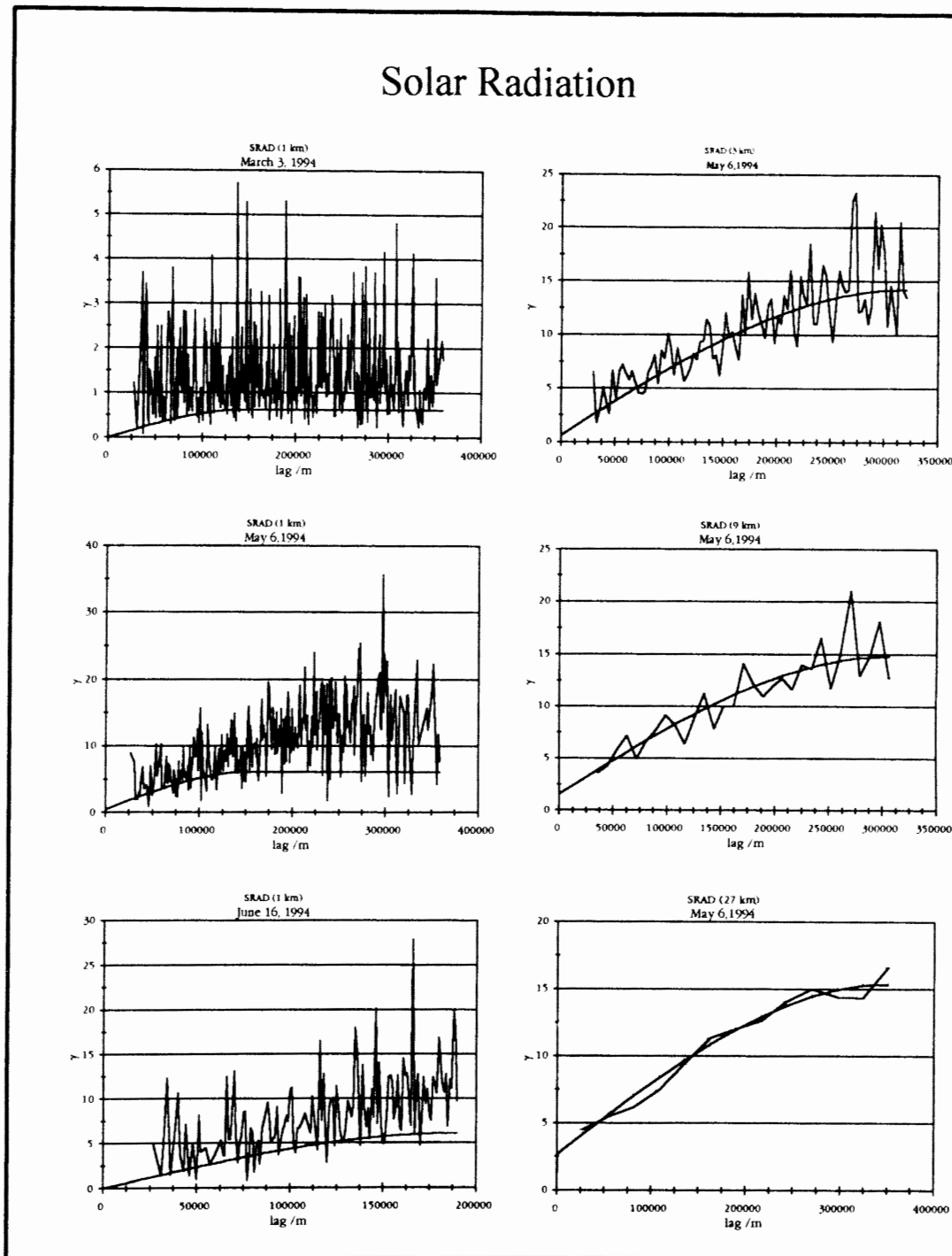


Figure 41. Actual and Fitted Variograms of Solar Radiation (Searching Radius = 120 km).

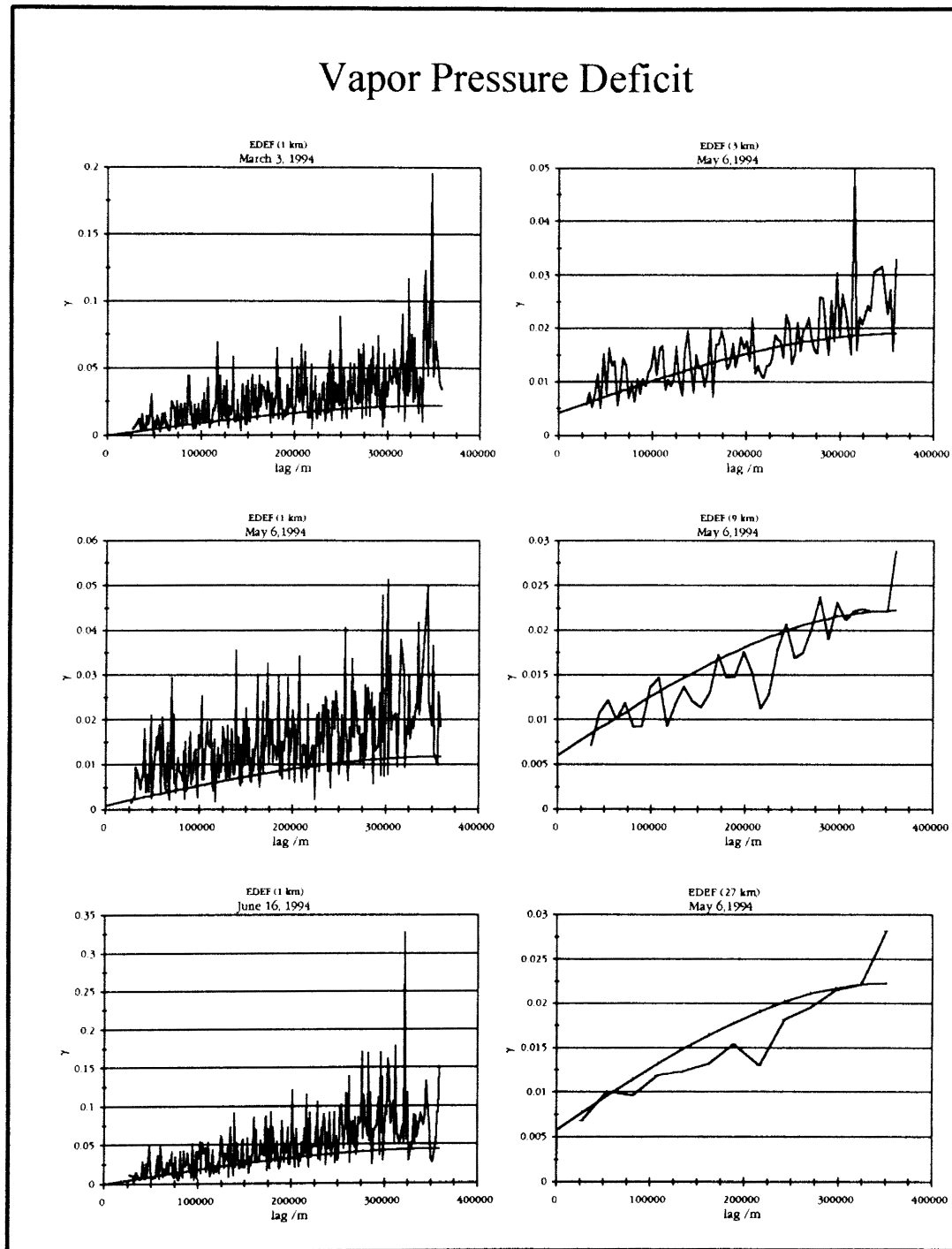


Figure 42. Actual and Fitted Variograms of Vapor Pressure Deficit (Searching Radius = 120 km).

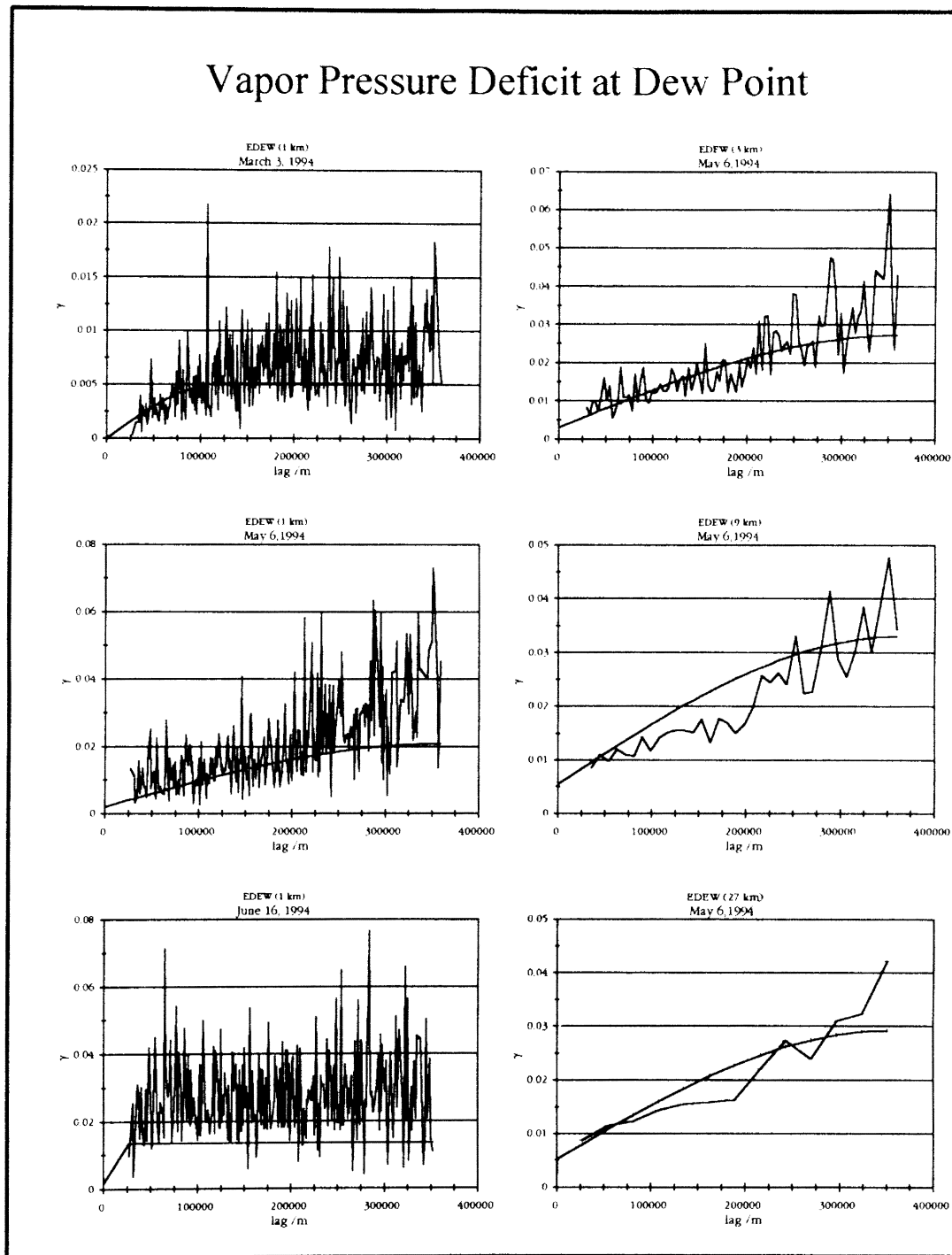


Figure 43. Actual and Fitted Variograms of Vapor Pressure Deficit at Dew Point (Searching Radius = 120 km).

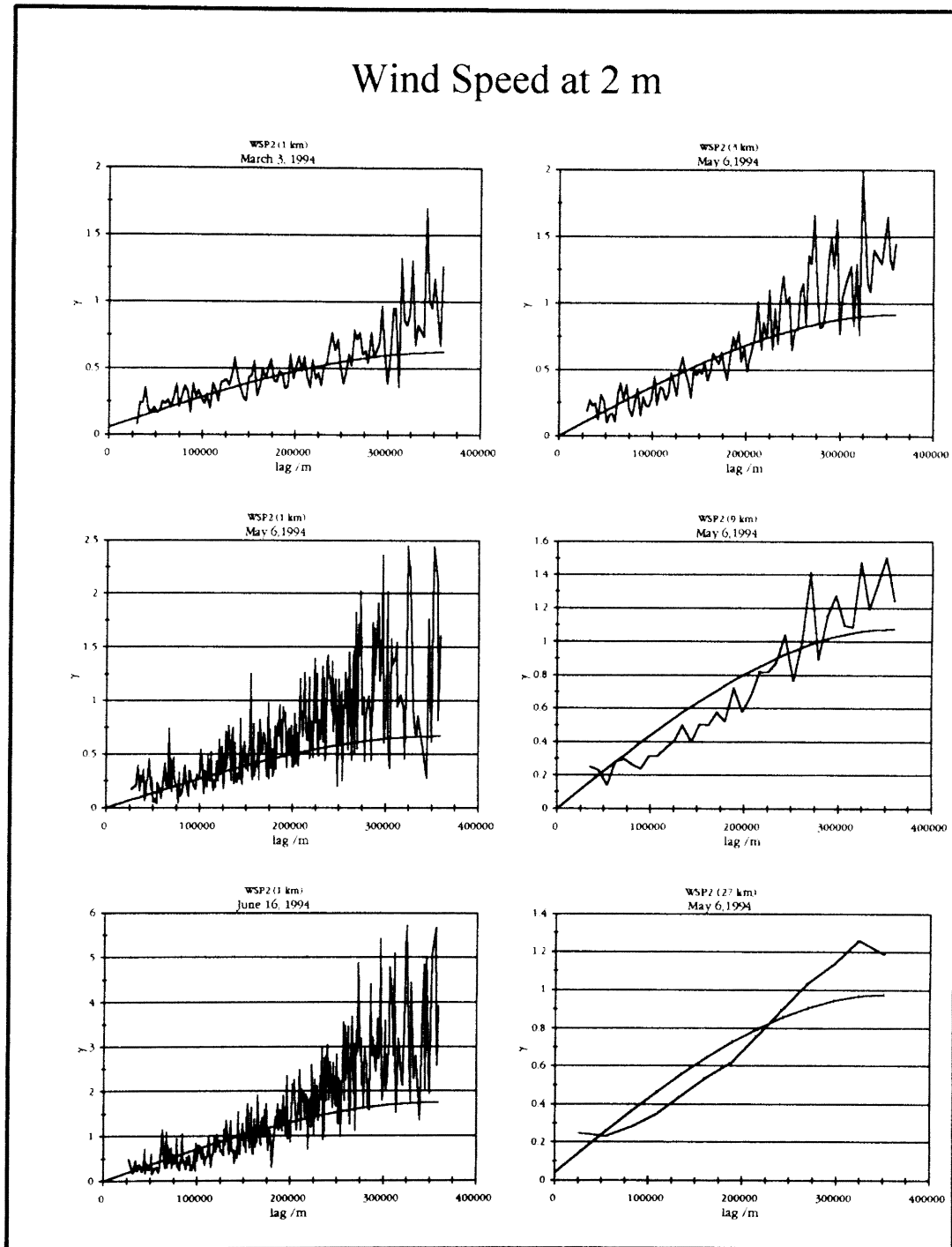


Figure 44. Actual and Fitted Variograms of Wind Speed at 2 m
—Extrapolated from 10 m (Searching Radius = 120 km).

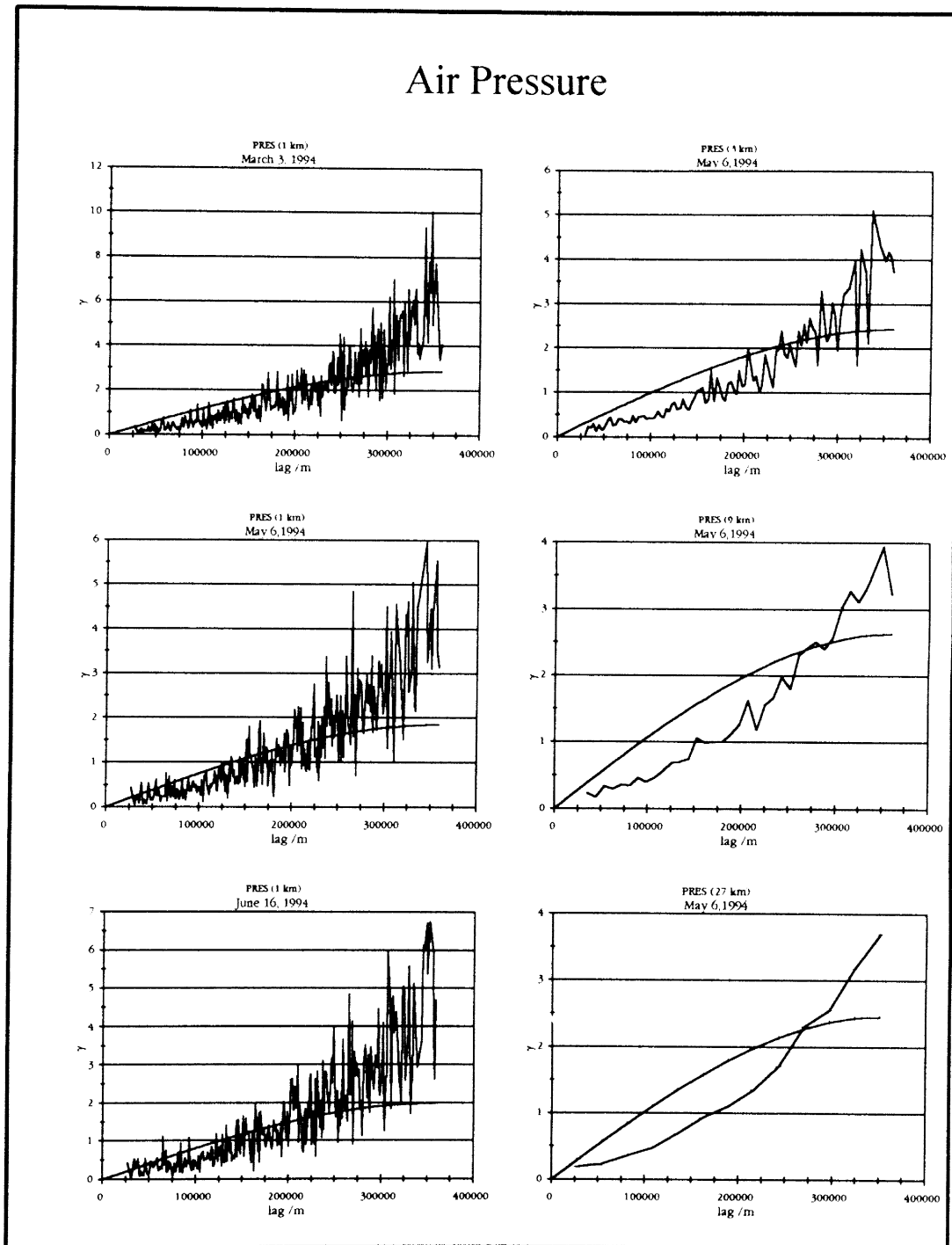


Figure 45. Actual and Fitted Variograms of Station Air Pressure (Searching Radius = 120 km).

APPENDIX E—CORRELATION ANALYSIS

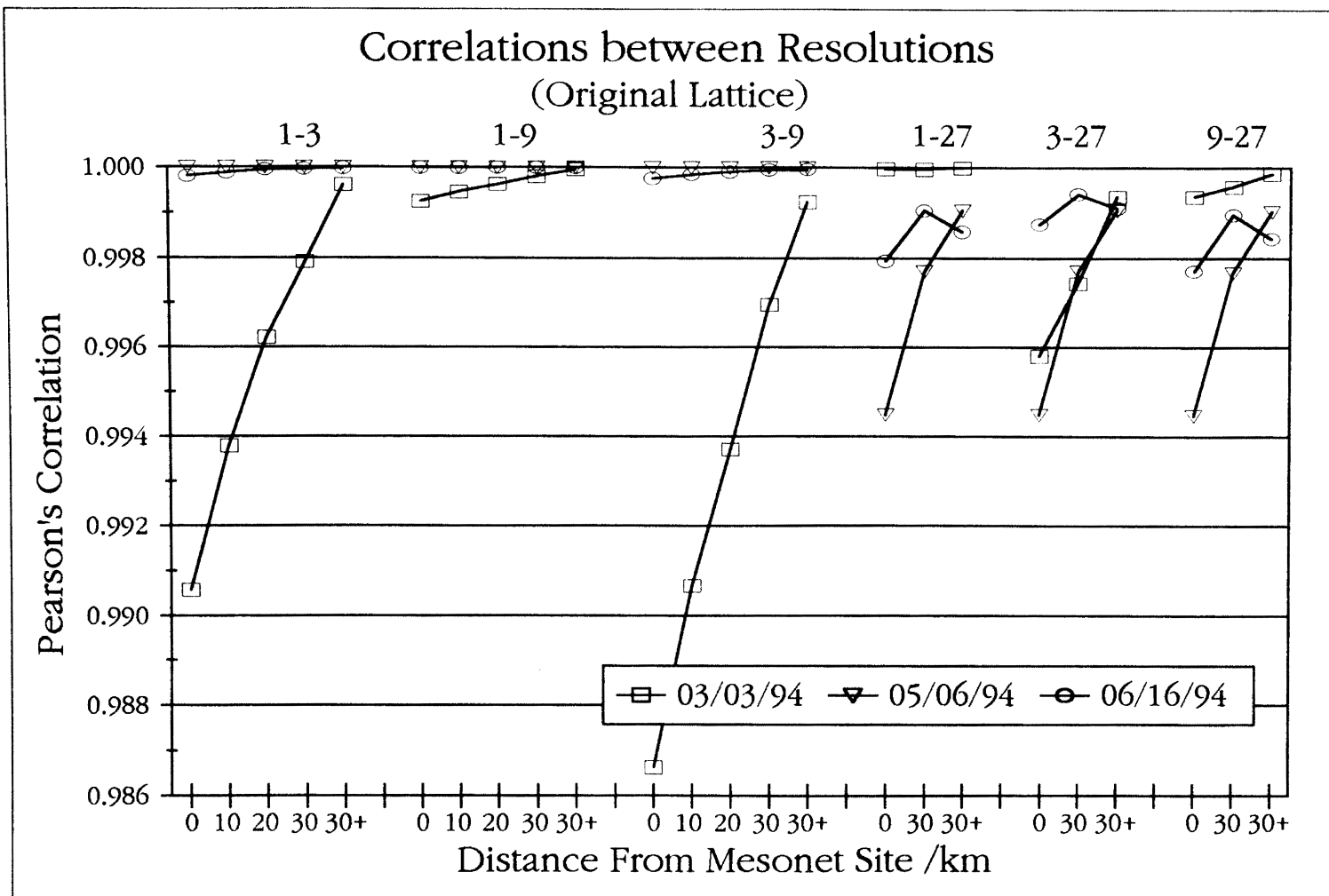


Figure 46. Correlation between Interpolation Results of Reference Evapotranspiration Using Various Resolutions in Kriging (Original Lattice).

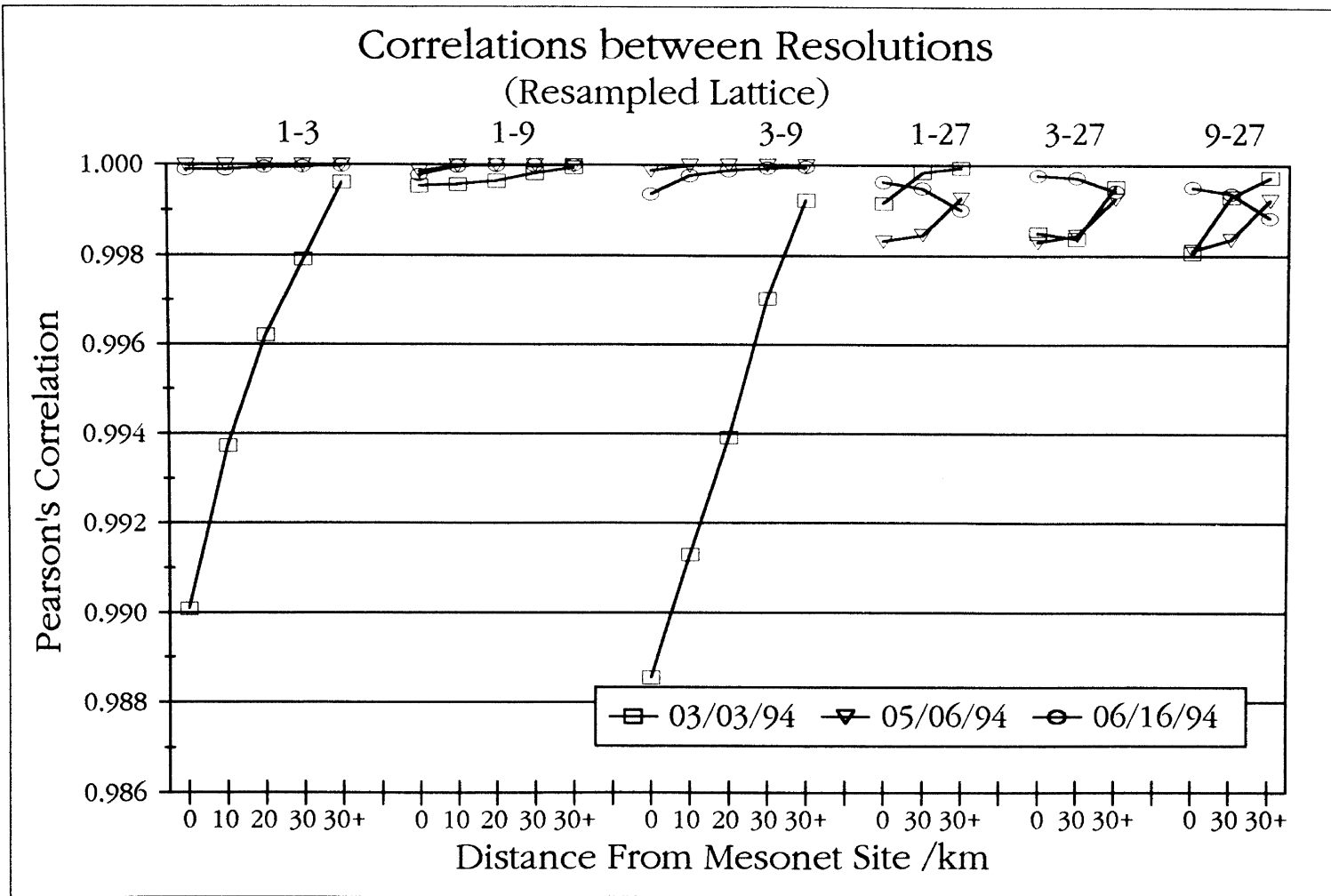


Figure 47. Correlation between Interpolation Results of Reference Evapotranspiration Using Various Resolutions in Kriging (Resampled Lattice).

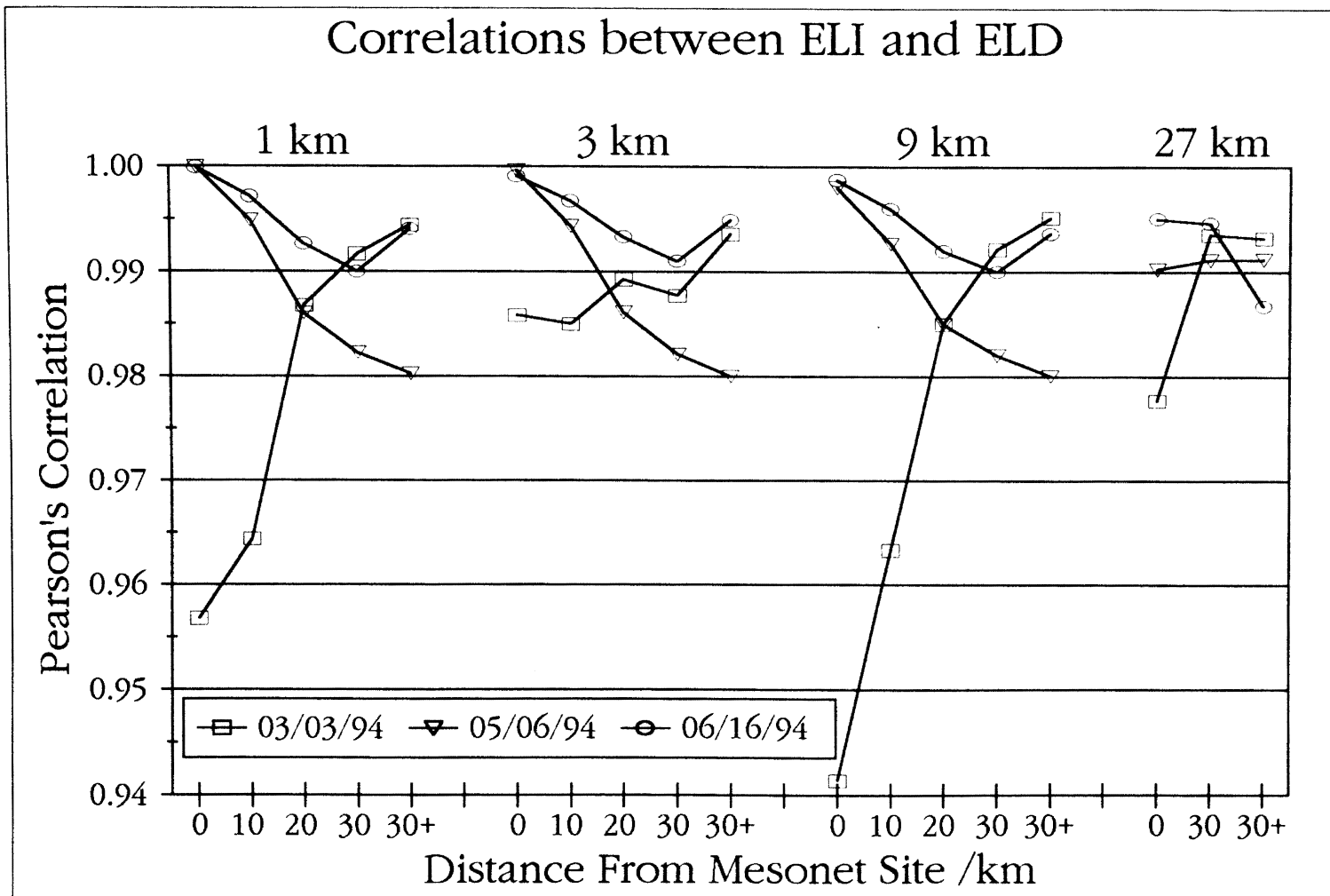


Figure 48. Correlation between Interpolation Results of Reference Evapotranspiration Using Kriging and Inverse Distance Weighting.

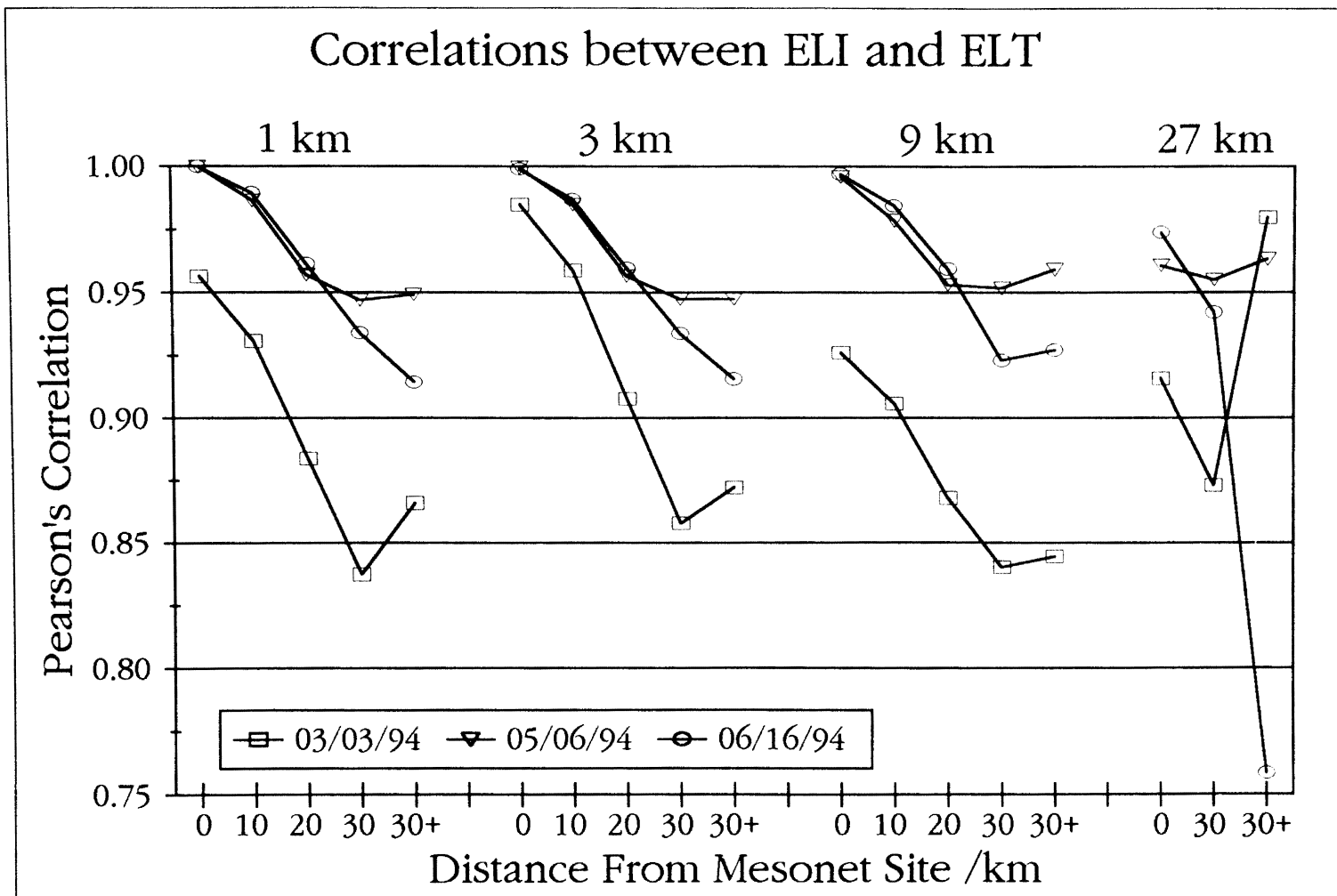


Figure 49. Correlation between Interpolation Results of Reference Evapotranspiration Using Kriging Thiessen Polygons.

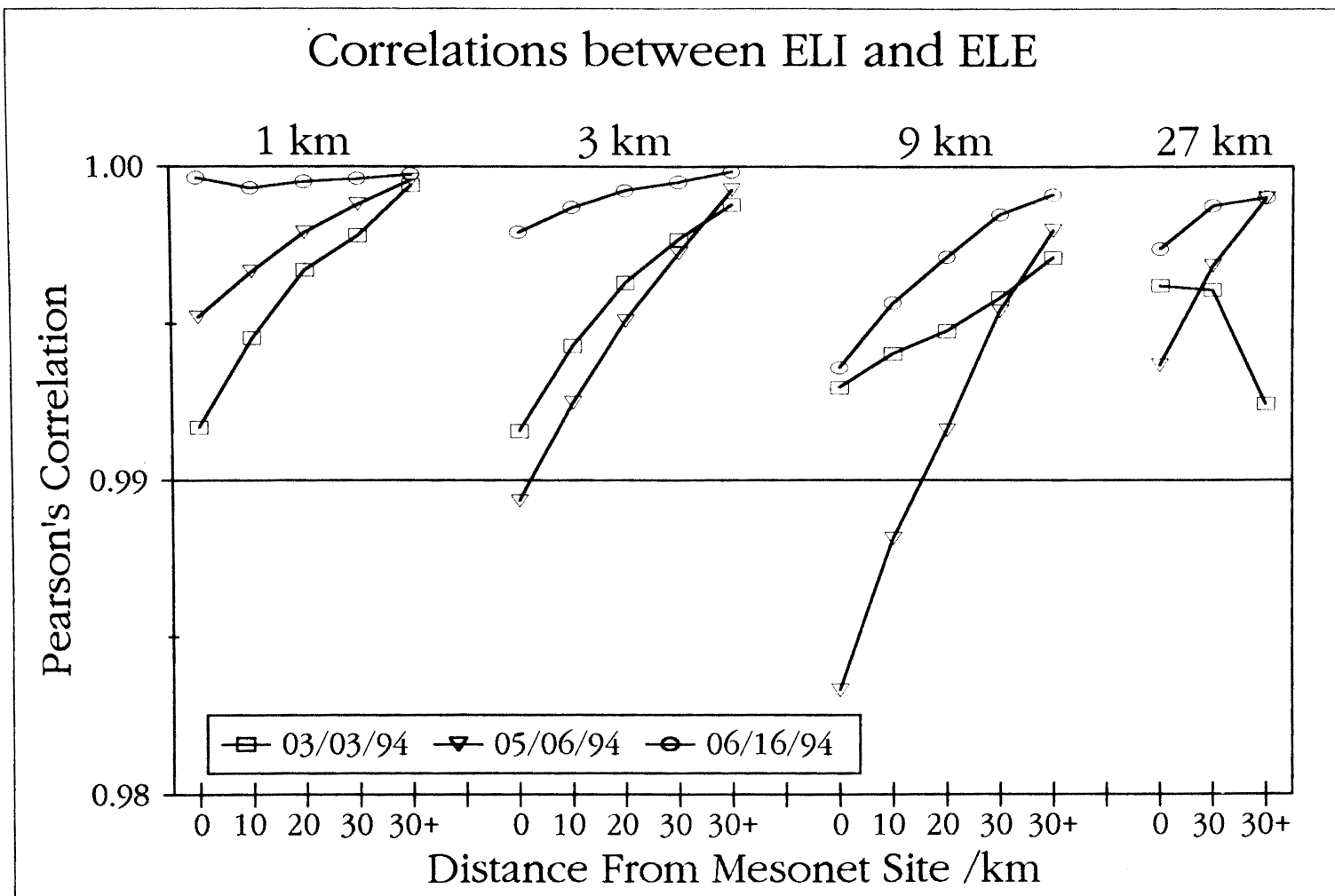


Figure 50. Correlation between Reference Evapotranspiration Surfaces Resulting from Point and Surface Meteorological Data.

APPENDIX F—DIFFERENCES BETWEEN VARIOUS SURFACES

TABLE XII
DIFFERENCES BETWEEN INTERPOLATION RESULTS
USING VARIOUS RESOLUTIONS
(ORIGINAL LATTICE)

		3 km	9 km	27 km
N		14,661	1,629	181
Paired T-test Scores				
March 3	1 km	(5.13)**	0.68	(1.67)
	3 km		1.45	0.40
	9 km			(0.53)
May 6	1 km	(23.07)**	8.23**	0.83
	3 km		8.23**	0.83
	9 km			0.79
June 16	1 km	0.70	(0.30)	(0.27)
	3 km		(0.23)	(0.27)
	9 km			(0.27)
Mean Difference ^a				
March 3	1 km	-2.9E-03	3.6E-04	-6.6E-04
	3 km		3.2E-03	1.9E-03
	9 km			-9.6E-04
May 6	1 km	-3.0E-06	2.2E-04	5.4E-03
	3 km		2.2E-04	5.5E-03
	9 km			5.2E-03
June 16	1 km	9.0E-05	-2.9E-05	-1.4E-03
	3 km		-1.1E-04	-1.1E-03
	9 km			-1.5E-03

TABLE XII (Continued)

		3 km	9 km	27 km
Maximum Absolute Difference ^a				
March 3	1 km	4.2E-01	1.2E-01	3.6E-02
	3 km		5.0E-01	2.6E-01
	9 km			1.0E-01
May 6	1 km	8.1E-05	4.6E-03	2.8E-01
	3 km		4.6E-03	2.8E-01
	9 km			2.8E-01
June 16	1 km	7.6E-02	1.7E-02	2.0E-01
	3 km		8.3E-02	1.6E-01
	9 km			2.1E-01
Mean Absolute Difference ^a				
March 3	1 km	4.7E-02	1.5E-02	3.2E-03
	3 km		6.3E-02	4.5E-02
	9 km			1.8E-02
May 6	1 km	1.0E-05	6.9E-04	7.0E-02
	3 km		7.0E-04	7.0E-02
	9 km			7.0E-02
June 16	1 km	1.2E-02	3.0E-03	5.6E-02
	3 km		1.5E-02	4.4E-02
	9 km			5.9E-02

** $p < .01$

^a Daily E_{tr} /mm

TABLE XIII
 T SCORES OF DIFFERENCE BETWEEN RESOLUTIONS
 BY DISTANCE FROM MESONET SITES
 (ORIGINAL LATTICE)

	0 km	0.1 - 10 km	10.1 - 20 km	20.1 - 30 km	> 30 km
March 3					
1 km / 3 km	0.18	-0.78	(3.21)**	(7.14)**	5.26**
1 km / 9 km	-0.18	-0.16	0.9	1	-1.84
3 km / 9 km	-0.13	0.14	1.55	1.38	-1.5
1 km / 27 km	-0.46			-1.74	-0.32
3 km / 27 km	-0.15			0.7	0.23
9 km / 27 km	0.13			-0.81	-0.38
May 6					
1 km / 3 km	-0.4	(4.60)**	(7.48)**	(15.56)**	(18.39)**
1 km / 9 km	0.05	2.02*	3.78**	4.98**	6.05**
3 km / 9 km	0.05	2.01*	3.78**	4.98**	6.05**
1 km / 27 km	0.89			0.22	0.09
3 km / 27 km	0.89			0.22	0.09
9 km / 27 km	0.89			0.18	0.04
June 16					
1 km / 3 km	-0.41	-0.93	(2.11)*	4.94**	8.24**
1 km / 9 km	0.33	0.09	-0.1	-0.7	-1.71
3 km / 9 km	0.32	0.1	0.01	-0.71	-1.75
1 km / 27 km	-0.83			0.21	2.08
3 km / 27 km	-0.83			0.2	2.07
9 km / 27 km	-0.83			0.21	2.08

* p < .05

** p < .01

TABLE XIV
 DIFFERENCES BETWEEN INTERPOLATION RESULTS
 USING DIFFERENT RESOLUTIONS
 (RESAMPLED LATTICE)

		3 km	9 km	27 km
N		14,661	1,629	181
Paired T-test Scores				
March 3	1 km	(5.13)**	0.68	(1.67)
	3 km		1.45	0.40
	9 km			(0.53)
May 6	1 km	(23.07)**	8.23**	0.83
	3 km		8.23**	0.83
	9 km			0.79
June 16	1 km	0.70	(0.30)	(0.27)
	3 km		(0.23)	(0.27)
	9 km			(0.27)
Mean Difference ^a				
March 3	1 km	-2.9E-03	3.6E-04	-6.6E-04
	3 km		3.2E-03	1.9E-03
	9 km			-9.6E-04
May 6	1 km	-3.0E-06	2.2E-04	5.4E-03
	3 km		2.2E-04	5.5E-03
	9 km			5.2E-03
June 16	1 km	9.0E-05	-2.9E-05	-1.4E-03
	3 km		-1.1E-04	-1.1E-03
	9 km			-1.5E-03

TABLE XIV (Continued)

Maximum Absolute Difference ^a				
March 3	1 km	4.2E-01	1.2E-01	3.6E-02
	3 km		5.0E-01	2.6E-01
	9 km			1.0E-01
May 6	1 km	8.1E-05	4.6E-03	2.8E-01
	3 km		4.6E-03	2.8E-01
	9 km			2.8E-01
June 16	1 km	7.6E-02	1.7E-02	2.0E-01
	3 km		8.3E-02	1.6E-01
	9 km			2.1E-01
Mean Absolute Difference ^a				
March 3	1 km	4.7E-02	1.5E-02	3.2E-03
	3 km		6.3E-02	4.5E-02
	9 km			1.8E-02
May 6	1 km	1.0E-05	6.9E-04	7.0E-02
	3 km		7.0E-04	7.0E-02
	9 km			7.0E-02
June 16	1 km	1.2E-02	3.0E-03	5.6E-02
	3 km		1.5E-02	4.4E-02
	9 km			5.9E-02

** p < .01

^a Daily E_{tr} /mm

TABLE XV
 T SCORES OF DIFFERENCE BETWEEN RESOLUTIONS
 BY DISTANCE FROM MESONET SITES
 (RESAMPLED LATTICE)

	0 km	0.1 - 10 km	10.1 - 20 km	20.1 - 30 km	> 30 km
March 3					
1 km / 3 km	0.19	-0.77	(3.21)**	(7.11)**	5.20**
1 km / 9 km	-0.11	-0.12	0.85	0.85	-1.59
3 km / 9 km	-0.11	0.15	1.57	1.4	-1.45
1 km / 27 km	0.44			-0.92	-0.59
3 km / 27 km	0.27			0.82	0.19
9 km / 27 km	0.36			-0.67	-0.47
May 6					
1 km / 3 km	0.34	(2.85)**	(3.60)**	-0.52	-0.12
1 km / 9 km	-0.51	-0.3	-1.75	3.20**	2.73**
3 km / 9 km	-0.56	-0.24	-1.53	3.28**	2.70**
1 km / 27 km	1.33			0.16	0.09
3 km / 27 km	1.33			0.16	0.08
9 km / 27 km	1.3			0.12	0.03
June 16					
1 km / 3 km	-0.24	-0.92	(2.08)*	5.11**	8.37**
1 km / 9 km	0.04	0.25	0.45	0.43	-0.88
3 km / 9 km	0.17	0.16	0.14	-0.45	-1.66
1 km / 27 km	0.69			0.33	2.06
3 km / 27 km	1.15			0.33	2.03
9 km / 27 km	0.48			0.3	2.08
* p < .05					
** p < .01					

TABLE XVI
DIFFERENCE BETWEEN INTERPOLATION RESULTS OF
KRIGING AND INVERSE DISTANCE WEIGHTING

	1 km	3 km	9 km	27 km
Paired T-test Scores				
March 3	11.41**	7.01**	1.11	0.82
May 6	11.47**	3.76**	1.20	0.01
June 16	37.00**	12.69**	4.05**	1.80
Mean Difference ^a				
March 3	4.2E-03	7.1E-03	3.9E-03	7.2E-03
May 6	6.2E-03	6.1E-03	5.8E-03	7.7E-05
June 16	1.8E-02	1.8E-02	1.8E-02	2.0E-02
Maximum Absolute Difference ^a				
March 3	9.7E-01	5.8E-01	1.0E+00	6.9E-01
May 6	6.8E-01	6.8E-01	6.7E-01	4.8E-01
June 16	6.0E-01	5.9E-01	6.0E-01	4.7E-01
Mean Absolute Difference ^a				
March 3	9.1E-02	9.1E-02	9.2E-02	8.3E-02
May 6	1.5E-01	1.5E-01	1.5E-01	1.2E-01
June 16	1.4E-01	1.3E-01	1.4E-01	1.2E-01

** p < .01

^a Daily E_r /mm

TABLE XVII
T SCORES OF DIFFERENCE BETWEEN KRIGING AND IDW BY
DISTANCE FROM MESONET SITES

	0 km	0.1 - 10 km	10.1 - 20 km	20.1 - 30 km	> 30 km
March 3					
1 km	0.23	1.01	14.56**	16.39**	(29.36)**
3 km	0.3	1.12	6.99**	6.91**	(11.16)**
9 km	0.21	0.23	1.73	0.82	(3.60)**
27 km	0.46			0.63	0.45
May 6					
1 km	0.44	20.04**	35.43**	-1.94	(40.59)**
3 km	0.82	7.57**	11.27**	-0.11	(14.38)**
9 km	1.4	2.11*	3.91**	-1.14	(4.60)**
27 km	1.47			-0.36	-1.5
June 16					
1 km	0.54	3.51**	10.48**	36.86**	31.76**
3 km	0.14	0.97	2.92**	13.31**	10.83**
9 km	0.64	0.58	1.64	3.82**	2.95**
27 km	1.19			1.02	1.35
*	p < .05				
**	p < .01				

TABLE XVIII
DIFFERENCES BETWEEN INTERPOLATION RESULTS
OF KRIGING AND THIESSEN POLYGONS

	1 km	3 km	9 km	27 km
Paired T-test Scores				
March 3	5.92**	1.18	0.20	0.47
May 6	0.75	0.29	0.04	1.07
June 16	2.13*	0.36	(0.25)	0.53
Mean Difference ^a				
March 3	6.8E-03	3.7E-03	2.2E-03	1.5E-02
May 6	6.2E-04	7.2E-04	2.8E-04	2.5E-02
June 16	2.2E-03	1.2E-03	-2.4E-03	1.6E-02
Maximum Absolute Difference ^a				
March 3	1.8E+00	1.8E+00	1.8E+00	1.8E+00
May 6	1.3E+00	1.2E+00	9.9E-01	8.3E-01
June 16	2.1E+00	2.1E+00	1.9E+00	1.5E+00
Mean Absolute Difference ^a				
March 3	2.9E-01	2.6E-01	3.0E-01	2.9E-01
May 6	2.3E-01	2.3E-01	2.3E-01	2.5E-01
June 16	2.9E-01	2.9E-01	2.9E-01	3.1E-01

* $p < .05$

** $p < .01$

^a Daily E_{tr} /mm

TABLES XIX

T SCORES OF DIFFERENCE BETWEEN KRIGING AND THIESSEN
POLYGONS BY DISTANCE FROM MESONET SITES

	0 km	0.1 - 10 km	10.1 - 20 km	20.1 - 30 km	> 30 km
March 3					
1 km	0.23	0.15	(2.23)*	(5.75)**	(4.40)**
3 km	0.25	0.20	0.30	(1.25)	(2.59)**
9 km	0.20	0.29	0.20	(0.94)	(0.17)
27 km	0.42			(1.02)	2.25
May 6					
1 km	0.38	(0.75)	2.10*	(0.28)	(5.46)**
3 km	0.42	0.18	0.93	0.10	(3.15)**
9 km	0.59	0.63	0.24	(0.87)	(0.07)
27 km	(0.16)			(1.17)	(0.22)
June 16					
1 km	0.54	0.84	(0.49)	(1.75)	(3.53)**
3 km	0.12	(0.03)	0.37	(0.56)	(1.02)
9 km	0.86	0.70	(0.03)	(0.09)	0.33
27 km	(0.04)			(1.14)	1.59
*	p < .05				
**	p < .01				

TABLE XX
 DIFFERENCE BETWEEN INTERPOLATION RESULTS
 USING POINT AND SURFACE
 METEOROLOGICAL DATA

	1 km	3 km	9 km	27 km
Paired T-test Scores				
March 3	5.59**	8.93**	(3.31)**	(1.11)
May 6	33.15**	9.90**	3.22**	1.18
June 16	(33.05)**	(4.54)**	(0.90)	(0.16)
Mean Difference ^a				
March 3	9.1E-04	4.8E-03	-5.6E-03	-5.2E-03
May 6	5.9E-03	8.2E-03	1.1E-02	8.4E-03
June 16	-3.8E-03	-1.9E-03	-2.2E-03	-9.3E-04
Maximum Absolute Difference ^a				
March 3	3.4E-01	4.2E-01	2.4E-01	2.3E-01
May 6	3.5E-01	4.8E-01	5.4E-01	2.9E-01
June 16	1.4E-01	2.4E-01	4.7E-01	2.4E-01
Mean Absolute Difference ^a				
March 3	4.2E-02	4.8E-02	5.2E-02	4.8E-02
May 6	4.9E-02	7.8E-02	1.1E-01	7.7E-02
June 16	3.4E-02	4.0E-02	7.8E-02	5.9E-02

** p < .01

^a Daily E_{tr} /mm

TABLES XXI

T SCORES OF DIFFERENCE BETWEEN USING POINT AND SURFACE
METEOROLOGICAL DATA BY DISTANCE FROM MESONET SITES

	0 km	0.1 - 10 km	10.1 - 20 km	20.1 - 30 km	> 30 km
March 3					
1 km	0.41	2.63**	(0.30)	2.74**	35.25**
3 km	(0.07)	0.90	3.90**	12.06**	5.08**
9 km	(0.38)	(0.65)	(1.11)	(2.97)**	(6.18)**
27 km	(0.58)			(0.70)	(0.77)
May 6					
1 km	0.38	13.42**	25.52**	12.49**	19.06**
3 km	0.54	5.51**	8.56**	2.96**	(1.53)
9 km	0.74	1.66	3.43**	0.05	(1.63)
27 km	1.13			0.51	0.12
June 16					
1 km	(0.56)	(15.08)**	(17.40)**	(23.74)**	(16.13)**
3 km	(0.80)	(4.43)**	(3.28)**	0.83	1.19
9 km	(0.66)	(0.75)	(0.84)	0.59	1.48
27 km	(0.59)			0.29	1.28

*p < .05

**p < .01

APPENDIX G—SPATIAL PATTERN OF DIFFERENCES BETWEEN SURFACES

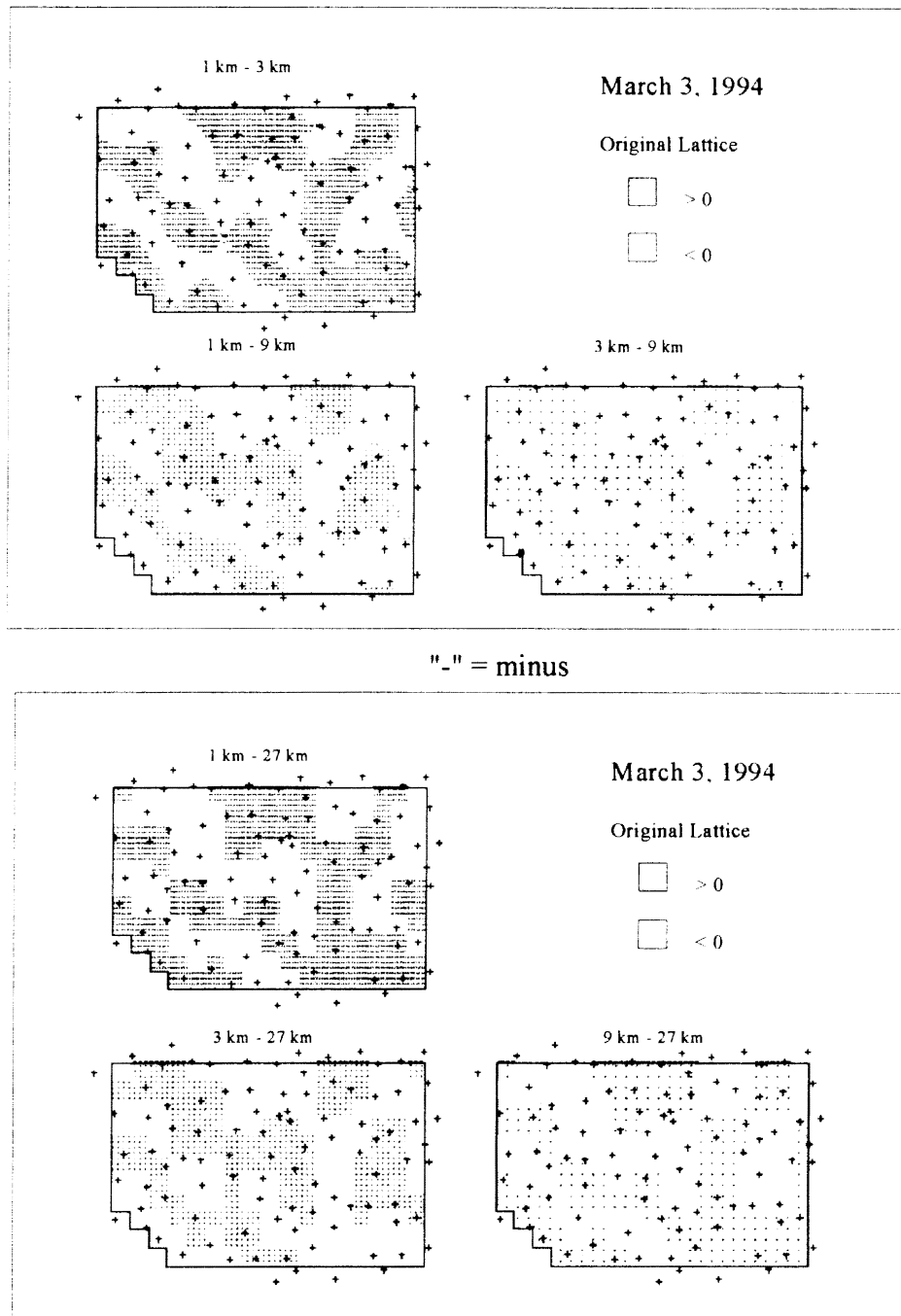


Figure 51. Spatial Pattern of the Difference between Interpolation Results of Various Resolutions (Original Lattice), March 3, 1994.

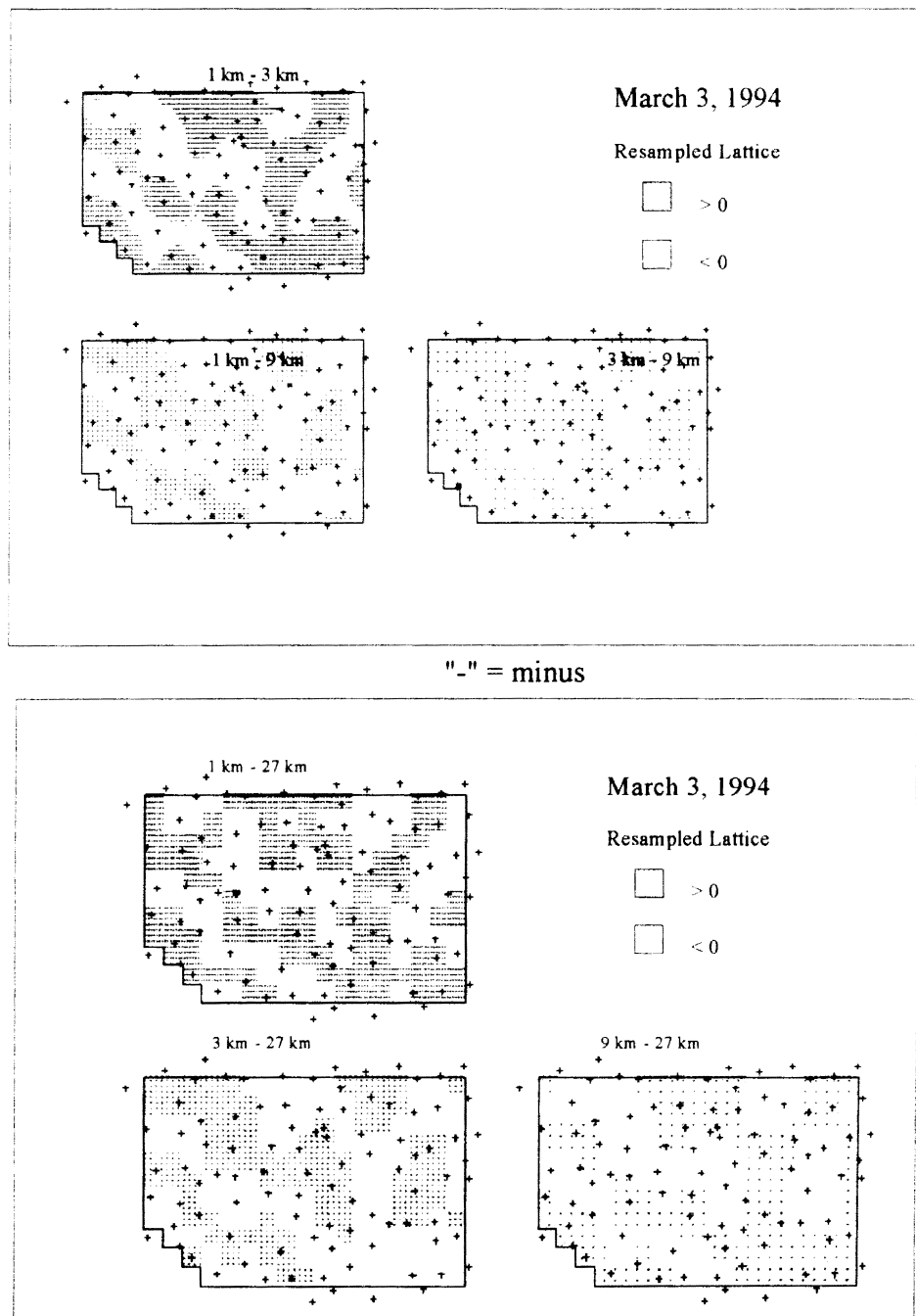
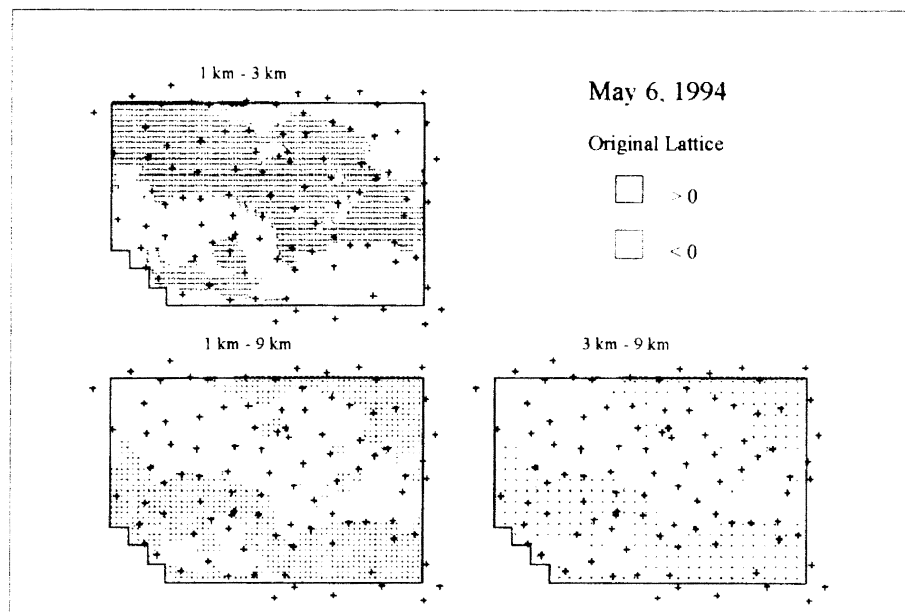


Figure 52. Spatial Pattern of the Difference between Interpolation Results of Various Resolutions (Resampled Lattice), March 3, 1994.



"-" = minus

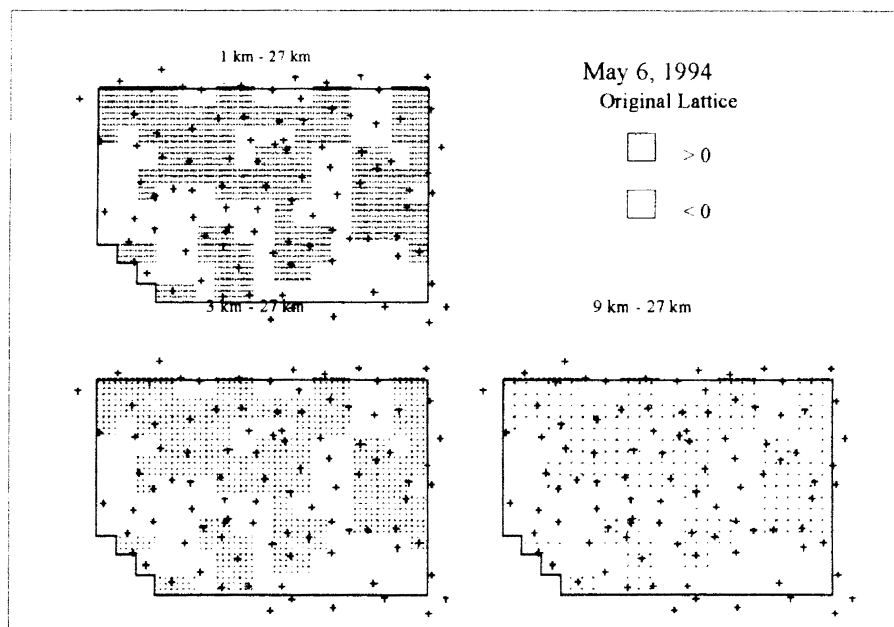


Figure 53. Spatial Pattern of the Difference between Interpolation Results of Various Resolutions (Original Lattice), May 6, 1994.

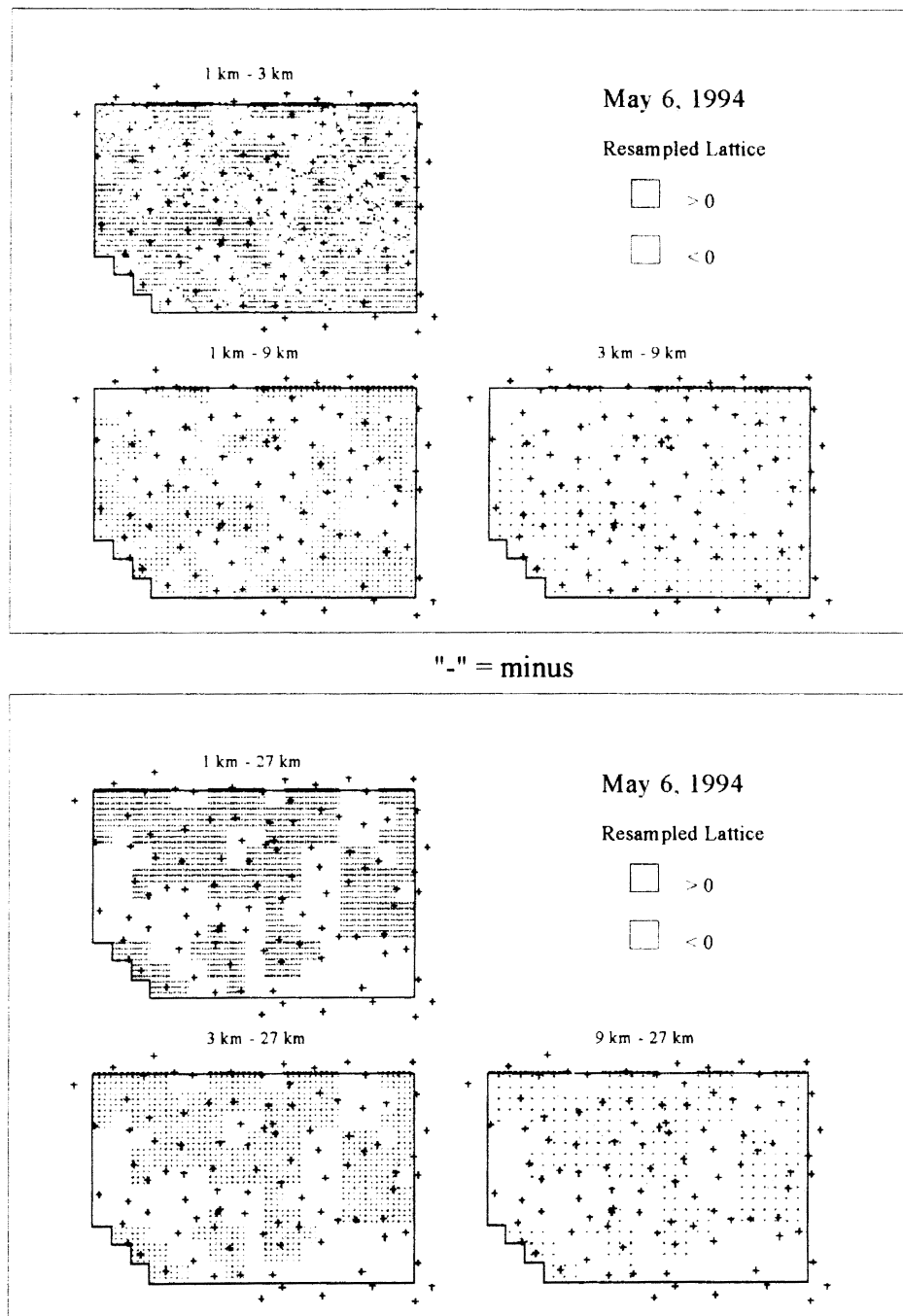


Figure 54. Spatial Pattern of the Difference between Interpolation Results of Various Resolutions (Resampled Lattice), May 6, 1994.

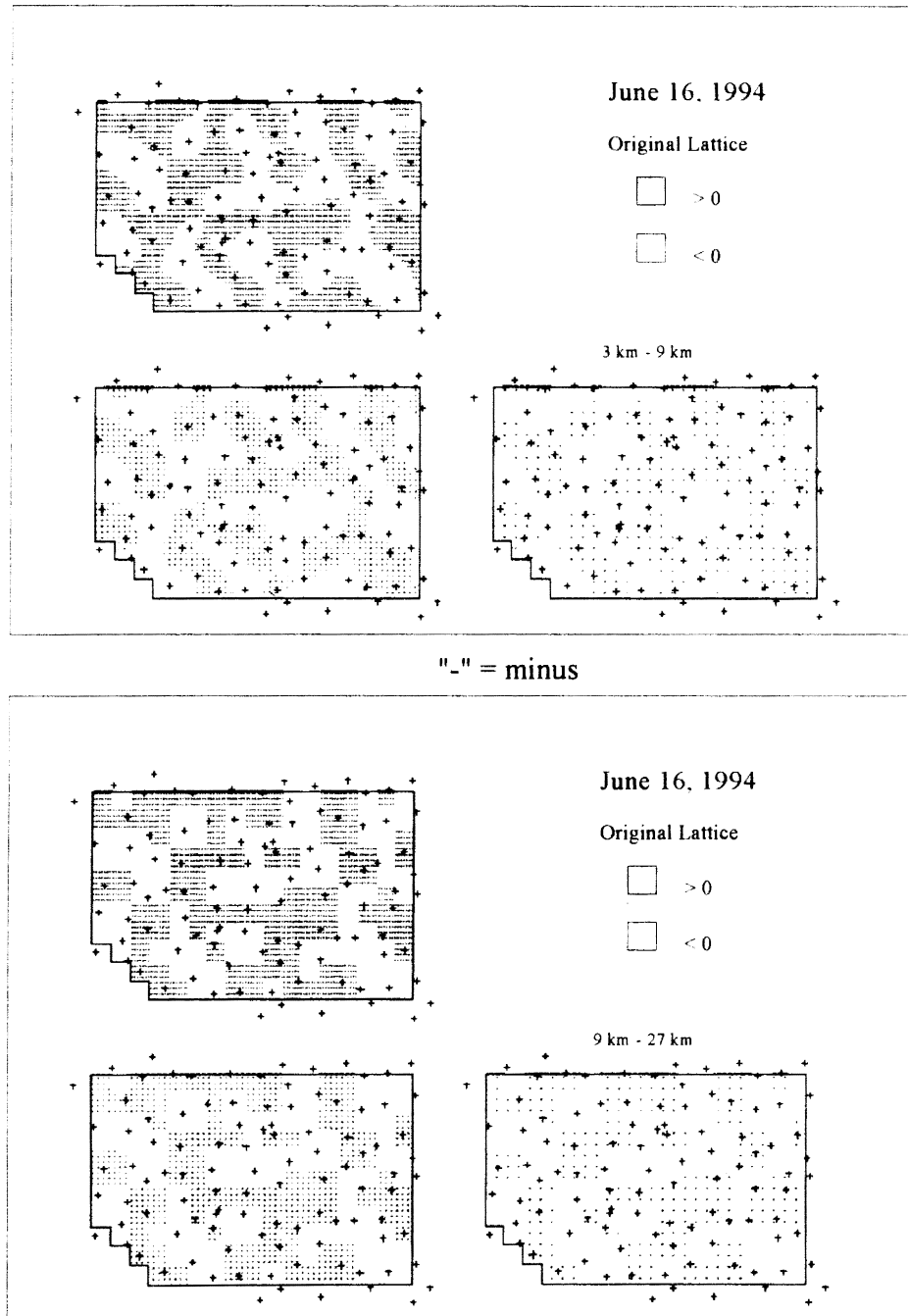


Figure 55. Spatial Pattern of the Difference between Interpolation Results of Various Resolutions (Original Lattice), June 16, 1994.

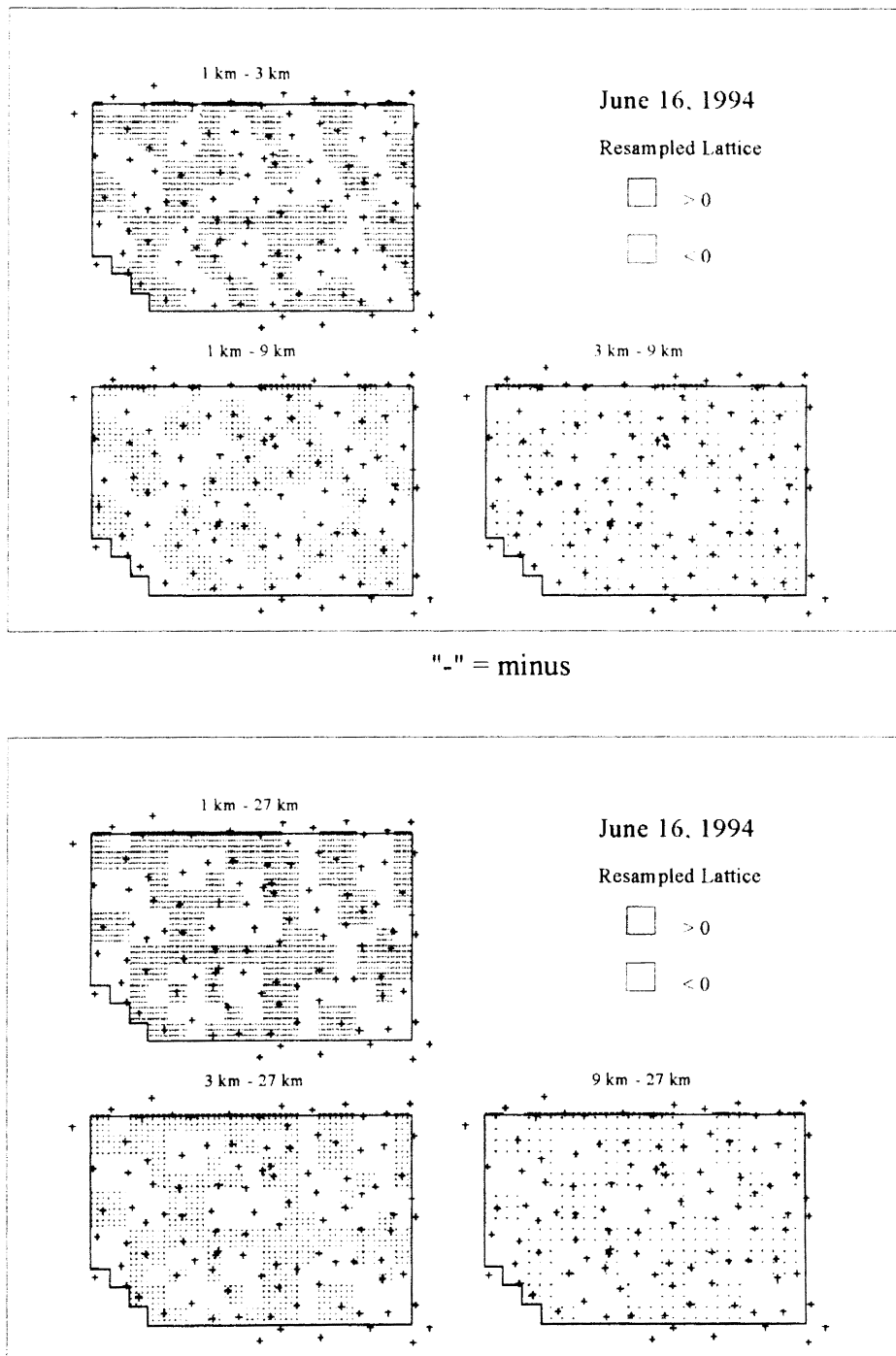


Figure 56. Spatial Pattern of the Difference between Interpolation Results of Various Resolutions (Resampled Lattice), June 16, 1994.

VITA

Oi-Ming Daniel Yuen

Candidate for the Degree of

Master of Science

Thesis: ESTIMATING REGIONAL REFERENCE EVAPOTRANSPIRATION
FROM MESO-RESOLUTION ZERO-DIMENSIONAL
METEOROLOGICAL DATA

Major Field: Geography

Biographical:

Personal Data: Born in Hong Kong, October 15, 1962, the son of Shui-Lan Yuen and Wai-Sing Yuen.

Education: Matriculated from Wah Yan College, Kowloon, Hong Kong, in July, 1982; graduated from Grantham College of Education with Teacher Certificate in July, 1985; received Bachelor of Science Degree in Geography from Bemidji State University, Minnesota in November, 1991; completed requirements for the Master of Science Degree at Oklahoma State University in December, 1994.

Professional Experience: Integrated science teacher in TWGHs Yow Kam Yuen Prevocational School, 1986 to 1989; integrated science and geography teacher in Pok Oi Hospital Chan Kai Memorial School, 1991 to 1992; graduate research assistant in Oklahoma State University, Department of Geography, 1992 to 1994.

Professional Memberships: Association of American Geographers, American Society for Photogrammetry and Remote Sensing, Gamma Theta Upsilon